Spring 2018

PERFORMANCE BASED EVALUATION OF CRACKING IN ASPHALT CONCRETE USING VISCOELASTIC AND FRACTURE PROPERTIES

Mirkat Tamire Oshone
University of New Hampshire, Durham

PERFORMANCE BASED EVALUATION OF CRACKING IN ASPHALT CONCRETE USING VISCOELASTIC AND FRACTURE PROPERTIES

BY

MIRKAT TAMIRE OSHONE

B.S. Civil Engineering, Mekelle University, 2005

DISSERTATION

Submitted to the University of New Hampshire

in Partial Fulfillment of

the Requirements for the Degree of

Doctor of Philosophy

in

Civil Engineering

May, 2018

This dissertation has been examined and approved in partial fulfillment of the requirements for the degree of Doctor of Philosophy in Civil Engineering by:

Dissertation Director, Jo Sias Daniel, Professor of Civil and Environmental Engineering

Dissertation Co-director, Eshan V. Dave, Assistant Professor of Civil and Environmental Engineering

Majid Ghayoomi, Assistant Professor of Civil and Environmental Engineering

David J. Mensching, Asphalt Pavement Engineer, Federal Highway Administration

Geoffrey M. Rowe, President, Abatech, Inc.

On DATE MAY 7, 2018

Original approval signatures are on file with the University of New Hampshire Graduate School.

DEDICATION

To Girma, who loved and supported me in everything I have ever done or gone through.

ACKNOWLEDGEMENTS

First and foremost, I would like to extend my special thank you to Dr. Daniel who have been the best advisor/mentor anyone could ever ask for. She has created a comfortable working environment that contributed immensely to my professional growth. I will always be indebted for the many opportunities she has provided me throughout my study. My special appreciation also goes to my co-advisor, Eshan Dave, for his unwavered support and contribution to my study. Thank you for enthusiastically supporting my ideas and helping me to develop them. I would also like to thank my dissertation committee members, Dr. Majid Ghayoomi, Dr. David Mensching, Dr. Geoff Rowe, Dr. Leslie McCarthy for their willingness to take part and contribute to the dissertation. Your comments and suggestions have been invaluable. It was an honor to have you in my committee and hope will get a chance to collaborate with you in the future.

Thanks also goes to my previous and current research mates at UNH, Eric Caron, Ashton Congalton, Christopher DeCarlo, Mohamed Elshaer, Katie Haslett, Christopher Jacques, Jayne Knott, Rasool Nemati, Chibuike Ogbo, Sonja Pape, Yaning Qiao, Reyhaneh Rahbar-Rastegar, Runhua Zhang and Yuefeng Zhu for your friendship and the wonderful discussions. It was a pleasure to have been working with you and I wish you all the best. I would also like to thank the Graduate Christian Fellowship and the Ethiopian community at NH for their friendship and great memories: you have been family-away-from-family. Special thanks goes to Ginny Teeter who have showed us incredible love and support.

This dissertation would not have been possible without the fund and support provided by the following entities and would like to acknowledge their contribution. I want to thank Rhode Island, New Hampshire and Minnesota Department of Transportations for providing research materials and funding the projects. I would also like to thank the Department of Civil and Environmental Engineering for Teaching Assistantship in the Fall of 2014 and 2015, and the spring 2013 semesters and PhD Civil and Environmental Engineering Summer Graduate Fellowship in 2015. I would also like to thank the UNH Graduate School for Summer Teaching Assistant Fellowship in 2016, the Dissertation Year Fellowship for 2017/2018 and a number of travel grants through the years. My thank you is also extended to North East Transportation Training and Certification Program for the honor I received in 2014. I am also grateful to Michelle Mancini, Kristen Parenteau and Kelly Shaw for all their help.

Words cannot express my appreciation to my family. Thank you dad and mom for instilling in me the love for education at a very young age and supporting me in every possible way to reach my goal since then. My sisters, Hiwi, Adi and Meazi and my one and only brother Rediet for inspiring and influencing my journey. You have always been there for me when I needed your support. I'm grateful for my in laws; thank you for your incredible love and support. And most of all my appreciation goes to my husband, Girma, for unconditionally loving, supporting and encouraging me: you made this journey possible. All the Glory to God who has been with me through everything. Thank you God for your grace, everlasting love, protection and guidance since childhood. None of this would be possible without you.

TABLE OF CONTENTS

LIST OF TABLES

LIST OF FIGURES

ABSTRACT

PERFORMANCE BASED EVALUATION OF CRACKING IN ASPHALT CONCRETE USING VISCOELASTIC AND FRACTURE PROPERTIES

by

Mirkat Tamire Oshone

University of New Hampshire, May, 2018

Cracking is one of the major distresses encountered in pavements. Pavements that fail prematurely due to cracking precipitate lower ride quality, elevate the chance of road accidents, and cause agencies to spend considerable amount of public funds on pavement maintenance and rehabilitation. As part of the concerted endeavor to ensure high performing pavements, extensive research is being undertaken throughout the United States to develop more effective and efficient performance based materials selection and specification procedures as well as mechanistic-empirical (M-E) methods for pavement cracking performance evaluation. However, agencies have been hesitant to introduce the methods to their specifications, pavement evaluation protocols and design procedures for reasons related to complexity and uncertainty associated to precisions and accuracy of these methods.

This dissertation contributes to the ongoing performance based specifications and design efforts by addressing known gaps related to linear viscoelastic and fracture characterization of asphalt concrete. Overarching goals of this dissertation research has been enhancement of performance property determination processes and increased confidence in asphalt pavement performance

predictions. Specific research contributions include, a simple and robust method is provided to determine phase angle from stiffness data and BBR low temperature specification parameters, stiffness (S) and relaxation properties (m-value), from DSR measurement for linear viscoelastic characterization of asphalt concrete. The ability of dynamic modulus and phase angle master curve parameters to capture the changes in mixture properties is investigated. Finally, increased understanding is achieved regarding fracture properties of asphalt mixtures as it relates to the effect of mix variables and number of replicates to be tested to obtain representative measurement to help agencies make informed decision during mix design and production.

CHAPTER 1

INTRODUCTION

The traffic and environmental loading on a pavement is non-uniform due to daily and seasonal variation in amount of loading, loading rate, temperature, and moisture within the pavement structure. The material properties for the different layers of the pavement also vary with the changing temperature, moisture conditions and aging level. Due in part to these complexities, empirical relationships have been widely implemented for the design and evaluation of pavement performance in the United States. However, due to the rapid advancement in the technology of bituminous materials (e.g., recycled materials and modifiers), increase in heavy traffic volume and changing climatic conditions, the use of these empirical relationships to predict performance may or may not be adequate and would be a potential for lower reliability. Therefore, there is a pressing call to develop simple and reliable performance based approaches for material specification and pavement design instead of empirical based relationships for pavement performance evaluation to ensure longevity of pavements. Nevertheless, a great deal of research has to be carried out to refine and increase the accuracy of these approaches before the transition is realized.

It is known that improving the cracking performance of pavements lies at the forefront of the priorities of several state agencies. As part of the concerted endeavor to address the exigent problem, extensive research is being undertaken throughout the United States to develop more

effective and efficient pavement cracking performance evaluation methods to ensure high performing pavements. A Federal Highway Administration (FHWA) study on the importance of the Long-Term Pavement Performance (LTPP) program highlights the benefits of adopting performance based pavement evaluation methods in terms of increased pavement life. Current developed performance based pavement evaluation methods use parameters determined based on mechanical and/or engineering properties of asphalt mixture to evaluate mixes during design and production. The reliability of the methods (index parameters or performance prediction models) largely depends on the material characterization method used to determine these engineering properties and its accuracy. During development of the methods researchers strive to balance accuracy and complexity so that agencies and contractors are encouraged to adapt them to their performance based decision making.

During the last three decades, several attempts have been made to develop performance based pavement evaluation methods that describe the fatigue and thermal cracking of properties of asphalt concrete. The parameters are commonly determined by performing linear viscoelastic characterization and fracture tests. Complex modulus and phase angle are key parameters used in mechanistic response and performance models to characterize the linear viscoelastic properties of asphalt concrete. Fracture tests are widely implemented to characterize the thermal cracking properties of asphalt concrete. This study aims to simplify, refine and increase the accuracy and understanding in relation to parameters determined based on complex modulus, phase angle and fracture energy measurements so as to provide effective and efficient pavement cracking performance evaluation methods. The introduction of simple and reliable ways to determine the parameters, increased accuracy achieved, and a better understanding obtained from the study will

provide increased confidence for agencies to implement the methods to their pavement design procedure and performance evaluation protocol.

1.1 Statement of Problem

To ensure the longevity of pavements, there is a need to shift from empirical to performance based pavement evaluation methods. While several efforts have been made to develop different pavement cracking performance evaluation methods, a lot of work has to be undertaken to understand, simplify and reduce uncertainties associated to linear viscoelastic and fracture characterization to increase agencies confidence to implement the methods as a tool for performance based decision making.

1.2 Objectives

The primary objectives of this dissertation are:

1. To provide simple and robust methods to determine key material inputs such as phase angle and BBR low temperature specification parameters (S and m-value) for linear viscoelastic characterization of asphalt concrete during performance based material selection and pavement design. This will result in enormous practical use for owner agencies as well as contractors by drastically reducing time and effort otherwise required for material characterization.
2. To relate dynamic modulus and phase angle master curve parameters to changes in mixture properties caused by aging, addition of rejuvenator, use of recycled material and change in binder performance grade.
3. To gain a better understanding on the effect of mix variables on thermal cracking performance of asphalt concrete to provide guidance to mix specifiers and producers on

changes they should consider making on the composition of asphalt mixture to achieve specification requirements.

4. To establish a practical number of replicate tests that are required to obtain accurate and representative asphalt concrete fracture energy from the DCT fracture test.

1.3 Structure of Work

The form of this dissertation is a series of technical papers that have been published or that are currently in review. The dissertation includes eight chapters and the tasks undertaken in each chapter are expected to contribute to the fulfilment of the dissertation objective as presented in Figure 1. The author of this dissertation is the primary author of all technical chapters. Chapter 1 gives introduction to the problem, significance, objective and contribution of the dissertation as it relates to performance based material selection and design of asphalt concrete. Chapter 2 presents a literature review done in relation to linear viscoelastic and fracture characterization of asphalt binder and mixture.

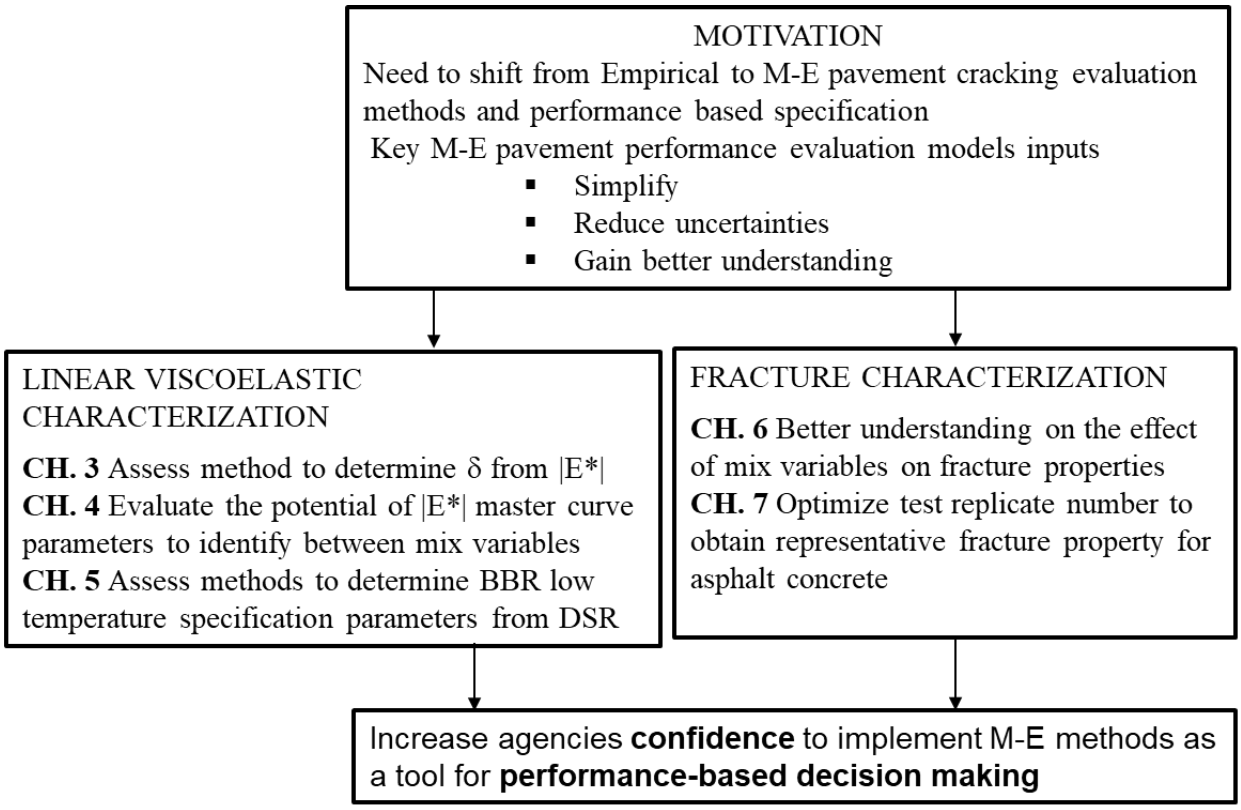

Figure 1. 1 Dissertation structure

Table 1.1 is presented to show the range of materials included in the study. More detail on the mixtures are presented in each individual chapter.

Table 1.1 Study mixture information

Mix variables	Chapter #				
	Chapter 3	**Chapter 4**	**Chapter 5**	**Chapter 6**	**Chapter 7**
	36 mixtures	29 mixtures	22 mixtures	171 mixtures	23 mixtures
Total binder content	4.7-6.8%	4.7-6.1%	4.7-6.1%	4-7%	4-6%
Effective binder content	4.2-6.3%	4.2-5.7%	4.2-5.7%	4-6.5%	4-5.5%
Asphalt film thickness	-	-	-	5.5-10%	7-10%
Air void	3-9%	5.3-7.7%	5.3-7.7%	3-10%	3-5%
Recycled asphalt pavement content	20-40%	0-50%	20-40%	0-40%	10-30%
Nominal maximum aggregate size	9.5, 12.5, 19mm	9.5, 12.5, 19mm	9.5, 12.5, 19mm	9.5, 12.5, 19mm	9.5, 12.5mm
Binder high temperature grade	58-64	52-70	52-58	52-64	52-64
Binder low temperature grade	-28	-22 to - 34	-28 to - 34	-22 to -34	-22 to -34
PG spread (PGHT-PGLT)	86 to 92	86 to 92	86	86 to 98	86 to 98
Voids in the mineral aggregate	14-16.5	14-16.5	14-16.5	13-16	13-16
Rejuvenator amount	-	0-12.5	-	-	-

Chapter 3 presents a technical paper accepted for publication by the Association of Asphalt Paving Technologists and Journal of Road Materials and Pavement Design, entitled “Prediction of Phase Angles from Dynamic Modulus Data and Implications on Cracking Performance Evaluation”. This part of the dissertation evaluates a fundamental relationship approach to determine the phase angle via the slope of the log-log of stiffness. The study by Rowe (2009) investigated this relationship and concluded the validity of the relationship to large set of modified and unmodified binders, asphalt mixes and some other polymers. This paper extends the previous research to a larger set of asphalt mixtures and evaluates the reliability of the relationship to asphalt mixtures. In the study

phase angle determined from slope of log-log stiffness master curve was compared to lab measurement and phase angle determined using Hirsch model. Moreover, the effect of measured and predicted phase angle on mixture Black Space diagram, S-VECD fatigue analysis and LVECD pavement fatigue performance evaluation is assessed.

Chapter 4 comprises a study undertaken to investigate the ability of dynamic modulus and phase angle master curve parameters to capture the changes in mixture properties caused by aging, addition of rejuvenator, use of recycled material and change in binder grade. Evaluated master-curve parameters are the mixture Glover-Rowe (G-R) parameter which relates $|E^*|$ and ϕ in Black space, and master-curve shape parameters (log of the inflection point frequency ($-\beta/\gamma$), log of the distance between the glassy modulus and the inflection point modulus (γ), $-\beta/\gamma$ vs γ and lower and upper asymptotes of the sigmoidal form of the master curve). The effect of the changes in the parameters on performance due to variation in the mixture variables is described qualitatively. This paper is accepted for publication in the proceeding of the International Society for Asphalt Pavements conference.

Chapter 5 presents a technical paper accepted for publication by the Association of Asphalt Paving Technologists and Journal of Road Materials and Pavement Design, entitled "Assessment of Various Approaches to Determining Binder Bending Beam Rheometer Low Temperature Specification Parameters from Dynamic Shear Rheometer Test". In this study the applicability of determining low temperature Bending Beam Rheometer (BBR) specification parameters, S and m-value, from Dynamic Shear Rheometer (DSR) testing is assessed for twenty-two neat and extracted and recovered binders from mixtures with a wide set of variables. Different methods proposed by previous researchers were employed and the robustness of the methods is explored by comparing estimated values from DSR with measured S and m-values from BBR testing.

Finally, a simple equation is developed to enable estimation of BBR specification parameters from a single point measurement of shear modulus and phase angle.

Chapter 6 presents a technical paper accepted for publication by the Transportation Research Record: Journal of the Transportation Research Board, entitled “Effect of Mix Design Variables on Thermal Cracking Performance Parameters of Asphalt Mixtures”. The study identified mix design variables that potentially affect the thermal cracking performance properties of asphalt mixtures. Databases developed by Minnesota Department of Transportation (MnDOT) with data from 90 mixtures and University of New Hampshire (UNH) containing data for 81 mixtures were used to determine the statistical significance and correlation between common mix design variables, including recycled asphalt amount, mix volumetric properties and binder grade, to the fracture energy and mix G-R values.

Chapter 7 provides the results of a study to establish a practical number of replicate tests that are required to obtain accurate and representative asphalt mixture fracture energy from DCT fracture test. The study strives to reduce measurement variability to an acceptable level and enable producers and agencies to be confident when they reject or accept mixes based on measurements from the test. The manuscript for this study is to be submitted to special issue of the ASTM International Journal of Testing and Evaluation with a title, “Increasing Precision and Accuracy in Fracture Energy Measurement by Optimizing the Number of Test Replicates for Disk-shaped Compact Tension Test (ASTM D7313)”.

Chapter 8 presents concluding remarks that emphasize the work done in this dissertation to simplify and increase the accuracy associated to performance based pavement cracking evaluation

methods. Moreover, further gaps in the current performance evaluation methods are identified and suggested for future work. Chapter 10 provides a master reference list.

CHAPTER 2: LITERATURE REVIEW

To fulfill the objective of the dissertation, the literature review presented in this chapter summarizes research articles on the topic of linear viscoelasticity, linear viscoelastic characterization of asphalt binder and asphalt concrete, fatigue cracking and low temperature cracking tests and performance evaluation methods. The purpose of the literature review is to inform regarding tests and parameters used for linear viscoelastic and fracture characterization of asphalt binder and concrete. Additional relevant literature to each chapter is available in each technical paper.

2.1 Viscoelasticity

Viscoelastic materials exhibit time and temperature dependent properties. The time dependency comes from a continual response of material due to increasing strain over time during load application, referred as strain creep, or decaying when imposed to deformation over time, referred as stress relaxation. Due to temperature dependency viscoelastic materials behave as an elastic solid at low temperature and as viscous fluid at high temperature. It is a common practice to use viscoelastic material models to explain these varied responses due to varying time and temperature. Such models combine springs and dashpots in different arrangements or use mathematical equations to explain the constitutive properties of viscoelastic materials. The constitutive properties are usually represented by either relaxation modulus, E(t) or creep compliance, D(t). Representation using relaxation modulus is commonly used for strain prescribed condition, Equation 2.1, and creep compliance is used for stress prescribed condition, Equation 2.2.

$$E(t) = \frac{\sigma(t)}{\varepsilon} \quad [2.1]$$

$$D(t) = \frac{\varepsilon(t)}{\sigma} \quad [2.2]$$

where;

$\sigma(t)$ = Stress at time t

ε = Applied strain

$\varepsilon(t)$ = Strain at time t

σ = Applied stress

2.2 Viscoelastic Models for Asphalt Concrete

2.2.1 Generalized Models

The generalized Maxwell and Kelvin models are the most commonly used viscoelastic models in asphalt concrete. In the models springs and dashpots are combined as shown in Figure 2.1 to explain the complex response of viscoelastic materials. The spring represents the elastic response whereas the dashpot represents the viscous response of a material. The generalized Maxwell and Kelvin model can be expressed in the form of Prony series for strain and stress-imposed conditions respectively. Current developed pavement evaluation method employs these models for asphalt concrete material characterization.

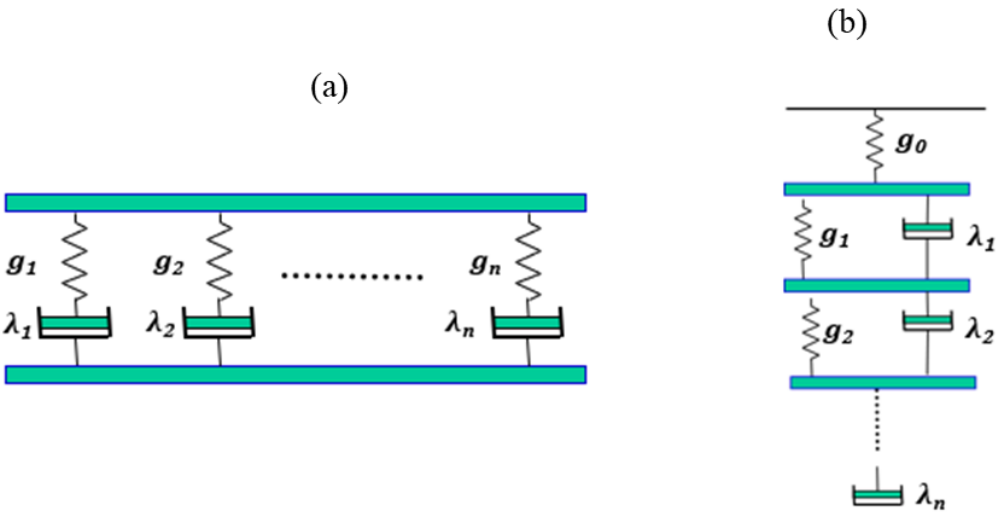

Figure 2. 1 (a) Generalized Maxwell model (b) Generalized Kelvin model

2.2.2 CAM Model

As part of the Strategic Highway Research Program (SHRP), Christensen and Anderson (1992) developed a fitting equation for asphalt binder shear modulus and phase angle that enable to determine the values at a certain frequency. Later Christensen, Anderson and Marasteanu (Marasteanu et al.,1999) proposed a modified version of the equation, Equation 2.3-2.5. The fitting parameters are the glassy modulus that represents a purely elastic modulus and cross over frequency of asphalt binder that corresponds to frequency where the phase angle of asphalt binder is 45°.

$$G^*(\omega) = G_g\left[1 + (\frac{\omega_c}{\omega})^{\beta}\right]^{-1/\beta} \quad [2.3]$$

$$\phi(\omega) = \frac{90}{\left[1 + (\frac{\omega}{\omega_c})^{\beta}\right]} \quad [2.4]$$

$$\beta = ln\left(\frac{G_g}{2}\right)/ln\left(G^*(\omega_c)\right) \quad [2.5]$$

where;

$G^*(\omega)$ = Complex shear modulus

G_g = Glassy modulus

ω_c = Cross over frequency

ω = Reduced frequency

β = Fitting parameter

ϕ(ω) = Phase angle

2.2.3 Standard Logistic /Generalized Logistic Functions

Rowe (2009b) presented sigmoidal form equations (Standard logistic /Generalized logistic) that can be applied to fit shifted dynamic modulus and phase angle points as shown in Equations 2.5 to 2.9. Each of the regression coefficients (δ, α, β, λ) are related to the shape of the sigmoid fit to the master curve as detailed by Mensching et al. (2017). The Williams-Landel-Ferry functional form is developed to fit the time-temperature shift factors. Representation in terms of dynamic modulus and phase angle master curves helps to understand stiffness, elastic and viscous components of asphalt concrete as a pavement is exposed to different temperatures and traffic speed.

Standard logistic- $log|E^*| = \delta + \frac{\alpha}{1+e^{[\beta+\gamma(logw)]}}$ [2.5]

Standard logistic- $\phi = 90 \times \frac{d\ logE^*}{d\ log\ w} = -90 \times \alpha\gamma \frac{e^{[\beta+\gamma(logw)]}}{\left[1+e^{[\beta+\gamma(logw)]}\right]^2}$ [2.6]

Generalized logistic- $log|E^*| = \delta + \frac{\alpha}{(1+\lambda e^{[\beta+\gamma(logw)]})^{1/\lambda}}$ [2.7]

Generalized logistic- $\phi = 90 \times \frac{d\ logE^*}{d\ log\ w} = -90 \times \alpha\gamma \frac{e^{[\beta+\gamma(\log w)]}}{\left[1+\lambda e^{[\beta+\gamma(\log w)]}\right]^{1+1/\lambda)}}$ [2.8]

$$log_{10}^{\alpha_T} = \frac{C_1(T-T_0)}{C_2+(T-T_0)} \quad [2.9]$$

where;

(δ, α, β, λ) = fitting coefficients;

C_1 & C_2 = model coefficients;

T = test temperature;

T_0 = reference temperature.

2.3 Linear Viscoelastic Characterization of Asphalt Mixtures

Asphalt mixtures manifest a more complex viscoelastic behavior due to the combination of the viscoelastic asphalt binders and the aggregate skeleton. Researchers have shown that asphalt mixtures demonstrate linear viscoelastic properties within a small strain level (<100 micro strain) and limited number of cycles (Airey et al., 2004; Gardner et al., 1967). Yet, some studies argue that nonlinear viscoelastic behavior can appear at strain levels as low as 40 micro strain (Sayegh, 1967). For materials that exhibit linear viscoelastic behavior, the relationship between stress and strain depends on loading frequency, temperature and time. The stress strain relationship can be represented by the Boltzmann principle which describes the effect of combined load to be equal to

the sum of the effects of the individual loads (Findley, Lai, and Onaran, 1976). This principle can be applied to obtain the linear viscoelastic response of materials to a given load. Equations 2.10 and 2.11 describe the constitutive relationship between stress and strain expressed by the Boltzmann superposition integrals corresponding to an applied strain history and an applied stress history, respectively.

$$\sigma(t) = \int_0^t E(t-\zeta)\frac{d\varepsilon}{d\zeta}d\zeta \quad [2.10]$$

$$\varepsilon(t) = \int_0^t D(t-\zeta)\frac{d\sigma}{d\zeta}d\zeta \quad [2.11]$$

where;

E(t) = relaxation modulus

D(t) = creep compliance

ζ = integral variable

t = time.

2.3.1 Relaxation Modulus

The relaxation modulus of linear viscoelastic materials is given by Equation 2.12. It is commonly represented by the generalized Maxwell model (Prony series forms) comprising a spring and a series of N Maxwell elements in parallel. Researchers have shown that viscoelastic representation is better achieved using the relaxation function as compared to others (Lakes, 1999).

$$E(t) = E_e + \sum_{i=1}^{N} E_i e^{-t/\tau_i} = E_g - \sum_{i=1}^{N} E_i(1 - e^{-t/\tau_i}) \quad [2.12]$$

where;

E(t) = relaxation modulus

τ_1 = relaxation time

E_e = equilibrium modulus

E_g = glassy Modulus

2.3.2 Creep Compliance

The creep compliance, D(t) of linear viscoelastic materials is commonly represented by the generalize Voigt model. The model is composed of a spring and a group of N-1 Kelvin elements in series. The analytical expression is given by Equation 2.13.

$$D(t) = D_e - \sum_{i=1}^{N} D_i e^{-t/\tau_i} = D_g + \sum_{i=1}^{N} (1 - D_i e^{-t/\tau_i}) \quad [2.13]$$

where;

D(t) = creep compliance

τ_i = retardation time

E_e = equilibrium compliance

E_g = glassy compliance

Currently several pavement evaluation models use the Generalized Maxwell model for relaxation and generalized Kelvin model for creep representation (Bozkurt and Buttlar, 2002). These representations are particularly advantageous because the models are interchangeable. Different methods (exact interconversion, approximate interconversion methods (Quasi-elastic approximation, power law based interrelationship (Leaderman, 1958), interrelationship by Christensen (1982), interrelationships by Denby (1975)) can be employed to interconvert creep

compliance properties expressed using the generalized Kelvin model to relaxation modulus properties expressed using the generalized Maxwell model.

2.3.3 Complex Modulus

Performing test to determine relaxation modulus in the laboratory is challenging due to the need to apply a sudden load that results in a constant strain level. Due to this, complex modulus is commonly implemented for linear viscoelastic characterization of asphalt mixtures. Complex modulus is expressed as a function of storage and loss modulus, Equations 2.14 to 2.16.

$$E^* = E' + iE'' \quad [2.14]$$

$$E' = |E^*|\cos\phi \quad [2.15]$$

$$E'' = |E^*| \sin\phi \quad [2.16]$$

where;

E^* = complex modulus

E' = storage modulus

E'' = loss modulus

ϕ = phase angle

The relaxation spectrum is presented as a function of storage and loss modulus in the frequency domain as shown in Equations 2.17 and 2.18.

$$E'(\omega) = \sum^{n} g_i \ (\omega\lambda_i)^2/(1 + (\omega\lambda_i)^2) \quad [2.17]$$

$$E''(\omega) = \sum^{n} g_i \ \omega\lambda_i/(1 + (\omega\lambda_i)^2) \quad [2.18]$$

where the *n* relaxation modes are defined by their relaxation strength g_i and their relaxation times λ_i.

Complex modulus which is a measure of the stiffness is determined by dividing stress amplitude by the strain amplitude (Equation 2.19). At a smaller strain rates, asphalt mixtures exhibit linear viscoelastic properties meaning the stress strain relationship remains constant. During tests to determine complex modulus of asphalt material to ensure the response is in the linear viscoelastic range limiting values are set to the prevailing strains on the specimen. During sinusoidal load application a purely elastic response component in a material is described by the simultaneous occurrences of stress and strain whereas in a purely viscous material the strain response lags behind the stress by 90 degrees. Phase angle, which describes the relative proportions of elastic and viscous response is determined for viscoelastic material from the time lag between peak stress and peak strain (Equation 2.20). These are illustrated in Figure 2.2.

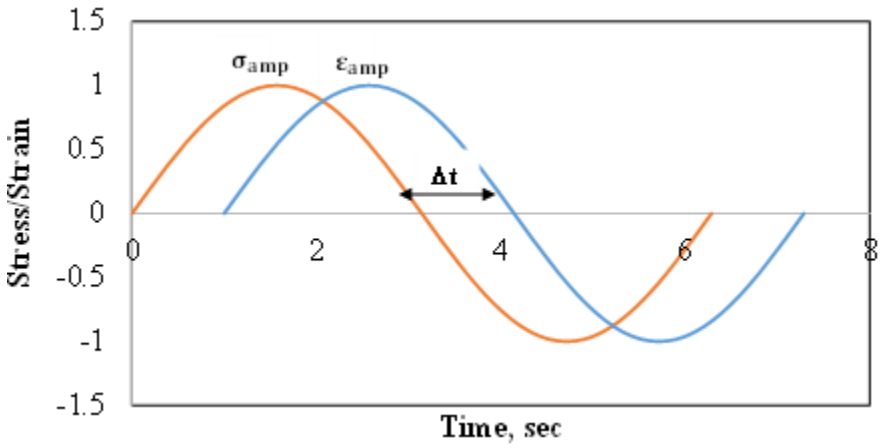

Figure 2. 2 Stress strain plot during complex modulus testing

$$|E^*| = \frac{\sigma_{amp}}{\varepsilon_{amp}} \qquad [2.19]$$

$$\phi = 2\pi f \Delta t \quad [2.20]$$

where;

σ_{amp} = amplitude of applied sinusoidal stress

ε_{amp} = amplitude of sinusoidal strain response

f = stress and strain frequency

Δt = Time lag between stress and strain at a given frequency and temperature

2.4 Time-temperature Superposition Principle

When asphalt mixtures are in the linear viscoelastic range, they generally exhibit thermorheologically simple properties. Though different researchers have demonstrated the existence of linear viscoelastic properties for small strain level (<100 micro strain) (Airey et al., 2004; Gardner et al., 1967), Chehab et al. (2002) and Gibson (2006) in their work showed that the thermologically simple behavior could be exhibited in asphalt mixtures at large strain as well.

Since asphalt mixture exhibits thermorheologically simple properties when tested in the linear viscoelastic range, the time–temperature superposition principle can be employed to horizontally shift results measured at different temperatures along time or frequency axis to construct a master curve for the full characterization of material behavior (Van der Poel 1955, Ferry 1980). The amount of shift along the time or frequency axis to a reference temperature is called the time-temperature shift factor. The complex modulus test (dynamic modulus and phase angle) has been one of the methods in use for linear viscoelastic characterization of asphalt mixtures in undamaged states since the 1950s (Heukelom et al., 1964; Van der Poel, 1955). This test is straightforward

and easy to adopt for the characterization of asphalt mixes in the small strain region. By combining the master curve with the shift factor, it is possible to predict the linear viscoelastic behavior of asphalt mixtures over a wide range of frequency and temperature conditions. The process of time-temperature superposition is illustrated in Figure 2.3 using dynamic modulus data measured at three temperatures.

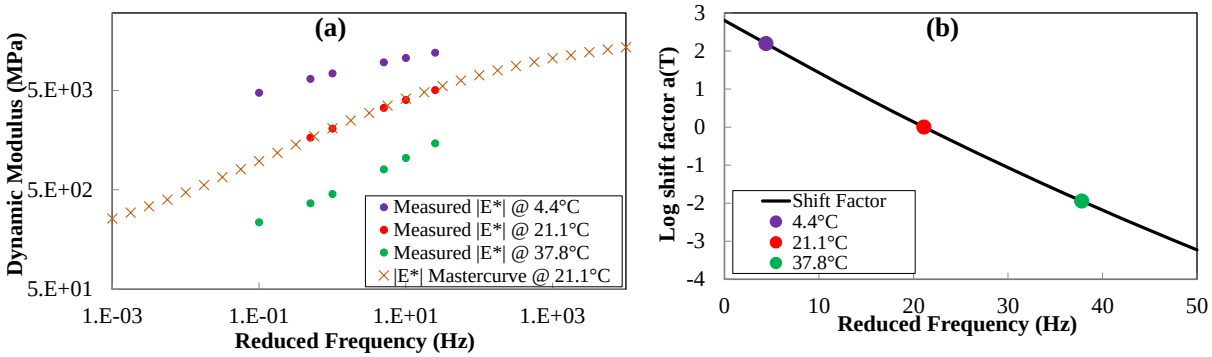

Figure 2.3(a) Dynamic modulus master curve construction using the time temperature superposition principle (b) time-temperature shift factors

2.5 Binder Tests for Linear Viscoelastic Characterization

The current binder grading system, Superpave performance grading, which is widely implemented in the United States uses different test for full characterization of asphalt binders at a wide range of pavement service temperature. These tests are the Bending Beam Rheometer (BBR), used for low temperature characterization, and Dynamic Shear Rheometer (DSR), used for intermediate and high temperature binder characterization. The details on the tests are discussed below.

2.5.1 Dynamic Shear Rheometer

DSR testing is used to measure binder shear complex modulus |G*| and phase angle (ϕ). |G*| is determined by dividing the maximum shear stress to maximum strain. It is a measure of the total resistance of binder to applied strain. ϕ is the time lag between the applied stress and resulting

strain. During DSR testing the specimen is sheared by applying a torque at a specific loading frequency to the top plate while the bottom plate is kept fixed (Pavement Interactive, 2011; ASTM-D7175, 2006). The test is performed on RTFO residues. The Superpave binder grading system uses limiting values set based on binder |G*| and ϕ values to ensure the performance of binders at intermediate and high temperatures. The rutting performance of binders is evaluated based on the |G*|/sinϕ value. The temperature that results in a |G*|/sinϕ value equivalent to 2.20 kPa is specified as the high temperature performance grade of binder. A binder that meets this requirement is expected to have good rutting performance in the field. The limit is set based on the dissipated energy to deform asphalt binder during oscillatory application of shear load. The work done to cause permanent deformation is calculated as the dissipated energy to cause damage. The dissipated energy concept informs that the |G*|/sinϕ is proportional to the dissipated energy to cause unrecoverable deformation implying an increase in |G*|/sinϕ is associated to better rutting performance. A maximum limit is set for |G*| sinϕ to ensure the fatigue performance of asphalt mixture. This is achieved due to the low stiffness and increased ability of the binder to dissipate energy by recovering.

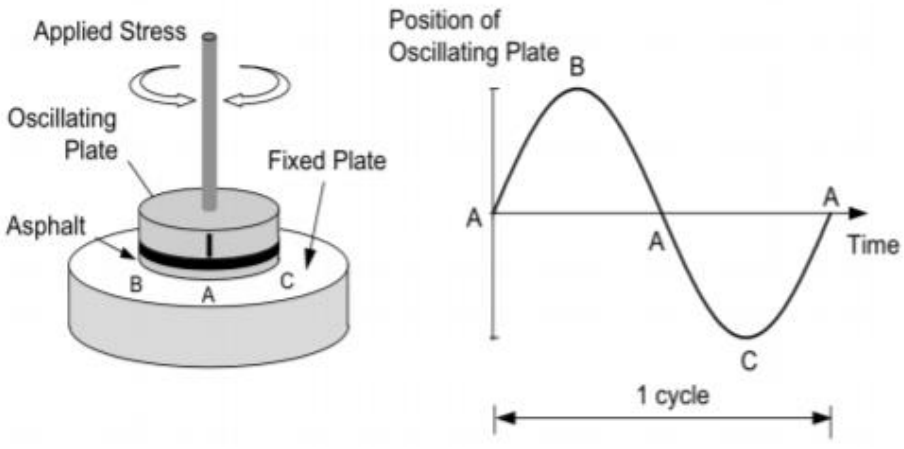

Figure 2.4 DSR test on an asphalt binder specimen (NHI,2000)

During the development of Superpave binder grading system, compliance error associated to DSR measurement below 5ºC introduced error on the absolute values of the dynamic moduli and relaxation modulus (Christensen and Anderson 1992). The error arised due to the higher stiffness of sample as compared to the instrument which caused the applied strain to be lower than the command strain meaning part of the applied torque deforms the instrument rather than the sample resulting in a considerable error in the test result.

The idea of applying compliance correction to be able to measure low temperature properties of asphalt binder is initiated by Schroter et al. (2006). Later a 4mm DSR approach is developed by Sui et al. (2010) and Farrar et al. (2015) to determine the low temperature rheological properties of asphalt binder as low as -40ºC and up to 60ºC. This is achieved by applying a compliance correction to DSR measurements. Figure 2.5 presents the difference between measurement values with and without compliance correction.

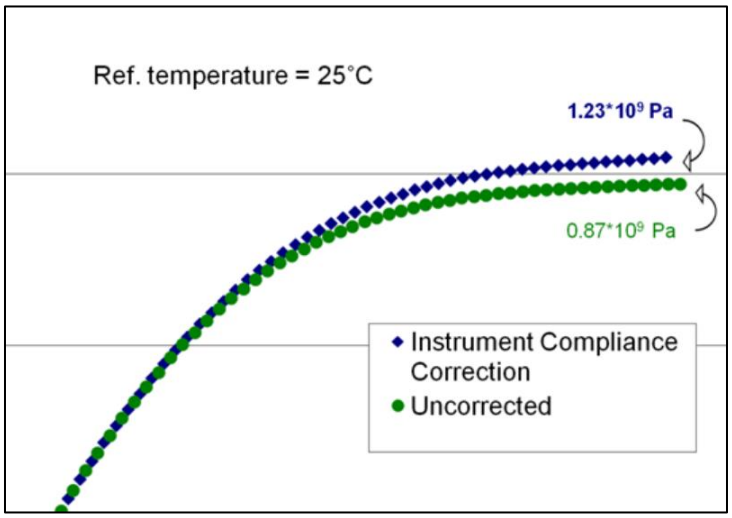

Figure 2.5 Corrected and uncorrected data from 4mm DSR, Sui et al., 2010

Due to the ability of the 4mm DSR to measure the low temperature properties of asphalt binder, it is now in consideration to use it as an alternative to BBR test. This is particularly attractive due to

the small amount of binder required to perform DSR testing as compared to BBR. This is particularly significant when it is required to determine the low temperature properties of extracted and recovered binders or asphalt emulsion residues. This alternative method reduces solvent needed as well as effort required to obtain required test material. Sui et al. (2011) showed that there is a good correlation between S and m values determined from BBR and estimated using DSR. Figure 2.6 is shown to illustrate the strong relationship between estimated and measured values.

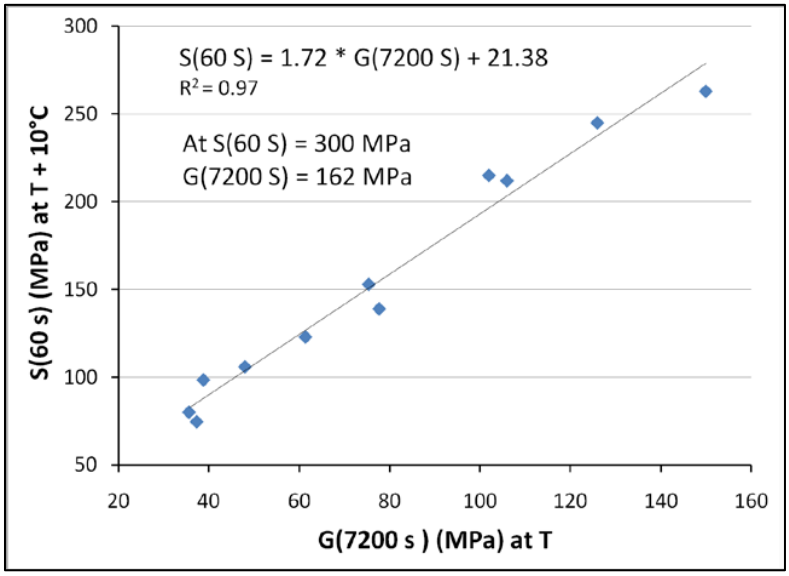

Figure 2.6 Correlation between BBR m(60s) and 4mm DSR m (7200 s) (Sui et al., 2011)

Monismith and Tsai (2005) performed tests other than dynamic shear test of binders using DSR. The equipment was used to perform static creep and repeated creep tests to determine time till failure, strain at failure, strain corresponding to 100 cycles and 5% strain (Reinke & Glidden, 2004).

2.5.2 Bending Beam Rheometer

BBR is used to determine the low temperature Superpave binder grading system specification parameters, stiffness (S) and relaxation properties (m-value), to specify the low temperature grade of asphalt binder. The test is performed on a simply supported PAV aged asphalt sample beam by applying a load at the center of the beam and measuring the deflection as a function of time. The beam geometry and deflection measurements are used to determine the stiffness and relaxation properties. Creep stiffness is calculated using Equation 2.21 at 8, 15, 30, 60, 120 and 240 seconds of loading time. The slope of the creep stiffness curve is used to determine the relaxation properties. A higher creep stiffness value is associated with high thermal stress and due to this a limiting value of 300MPa is specified. On the other hand, since higher value of m indicates ability to relax stress, a value higher than 0.3 is required to ensure good performance of asphalt mixtures at low temperature.

$$S(t) = A + B(\log(t) + C[\log(t)]^2 \tag{2.21}$$

where;

S(t) = Creep stiffness

P = Applied load

L = Distance between beam supports

H = Beam thickness

δ(t) = deflection as a function of time

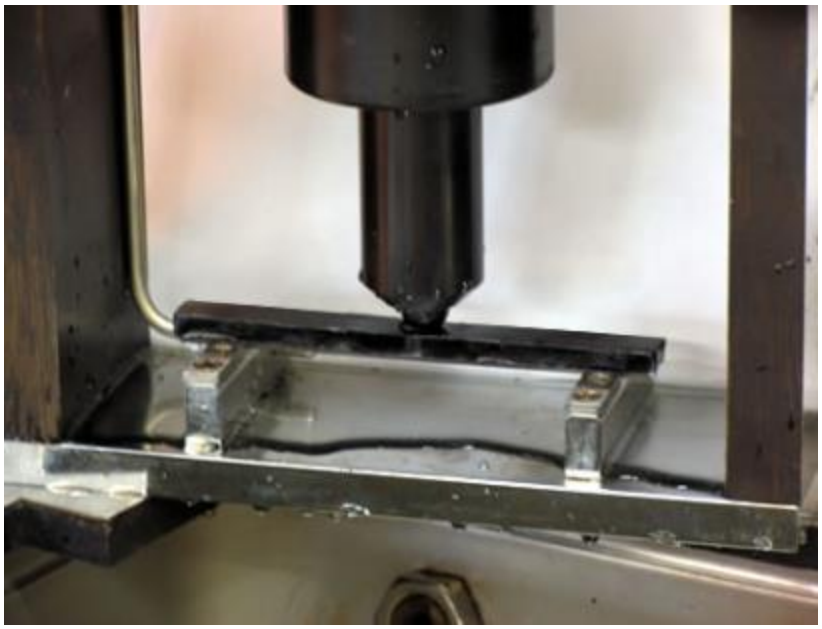

Figure 2.7 BBR testing (Pavement Interactive, 2011)

Based on an extensive experimental work, Al-Qadi et al. (2007) made modifications to the original BBR test and came up with a method that allowed performing the test on crack sealant to understand their behavior at low temperature. The method is referred as Crack Sealant Bending Test. An extended Bending Beam Rheometer test method was also introduced by Yee et al. (2006). The method employs reversible aging theory to consider the effect of storage time on low temperature properties of asphalt concrete. The finding from the study resulted in a potential method that enabled researchers to estimate creep stiffness and m-value. This is achieved by determining the double logarithmic shift rate, μ, which remains the same with changes in conditioning and loading times with the exception at short loading times and high stiffness.

Marasteanu et al. (2009); Marasteanu et al. (2012); Clendennen and Romero (2013); Romero and Jones (2013) extended the Bending Beam Rheometer test originally developed for binders to characterize the low temperature properties of asphalt mixtures, Figure 2.8. The test is carried on

thin beams by applying a three point loading to obtain the creep compliance curves which are used to determine low temperature specification parameters, S and m-value. Initially researchers were concerned regarding the ability of this small size specimens being a representative of the actual mix. Later Velasquez et al. (2009) studied the potential effect of specimen size, loading time and temperature on the output of the test. The finding from the study indicated that characterization done at intermediate temperature was not affected by the specimen size whereas differences were observed at low and high temperatures.

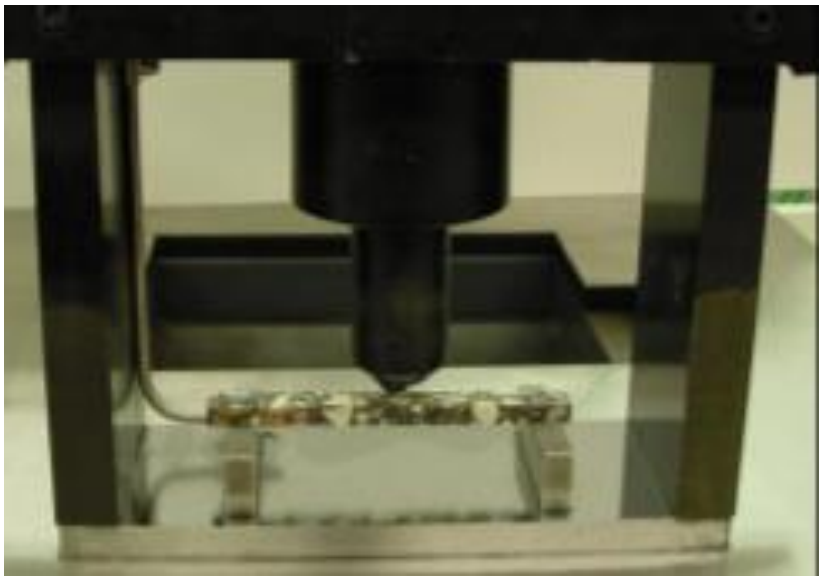

Figure 2.8 Bending Beam Rheometer test for asphalt mixture beam

2.6 Mixture Tests for Linear Viscoelastic Characterization

2.6.1 Complex Modulus Testing

Complex modus test procedure is provided in AASHTO TP 62, Standard Method of Test for Determining Dynamic Modulus of Hot-Mix Asphalt Concrete Mixture using Asphalt mixture performance tester (AMPT). The test is performed on three cylindrical specimens at different temperatures (4.4°, 21.1°, and 37.8° C) and a range of frequencies (0.1, 0.5, 1.0, 5.0, 10, and 25

Hz) to develop master curves using time-temperature superposition principle. The test is performed in unconfined compression state. Four LVDTs with a 70 mm gage length measure deformations. Dynamic modulus and phase angle are calculated from measured stresses and strains.

2.7 Low Temperature Cracking of Asphalt Concrete

Low temperature cracking (non-load associate cracking) is a critical mode of distress in asphalt pavements built in cold climates (Jung and Vinson 1994). The main cause for low temperature cracking is repeated heating and cooling of a pavement due to daily or seasonal temperature changes. In cold climates as the temperature drops, the pavement starts to contract subsequently causing tensile thermal stress to build up. When this stress exceeds the tensile strength, crack starts to propagate in a pavement along the transverse direction. These cracks allow water to penetrate into the underlying layers compromising the pavement structure. Moreover, moving vehicles force water and fine materials to be impelled through the cracks weakening the underlying layers (Marasteanu et al., 2007). In the current Superpave specification, the low temperature PG grade of binder is specified to ensure the low temperature cracking performance of asphalt pavements.

Previous researchers have shown the significant role binder parameters such as stiffness, relaxation property, viscosity and penetration play for the low temperature cracking performance of asphalt mixtures (McLeod, 1972, Kandhal et al., 1988, Jung and Vinson, 1994, Oshone et al., 2018). However, other researchers have shown that only binder test is not sufficient to ensure good performance in the field since it doesn't account for mixture properties such as aggregate type and gradation, recycled material type and amount and others. Thus, in recent years advancements have been made to develop tests that give better indication of asphalt concrete performance in the field.

From such test fracture energy determined from DCT test and Black Space developed based on stiffness and relaxation properties are discussed below.

2.7.1 Disk-Shaped Compact Tension Test

The Disc-Shaped Compact Tension test was developed at University of Illinois to evaluate the low temperature fracture properties of asphalt mixtures based on fracture energy measured on laboratory and field produced specimens. The test follows a standard fracture test configuration. Information on DCT test development can be found in Wagoner et al. (2005c). The test is carried out on a cylindrically-shaped asphalt concrete specimen following the test procedure on ASTM D7313 -13. The test specimen is conditioned to a recommend standard test temperature of 10°C warmer than the PG low temperature value for a minimum of 2 hours. The test is performed by applying a tensile load on the specimen at a constant CMOD rate of 1mm/min until the post peak load level is reduced to 0.1kN. From the test, the fracture energy of the specimens is determined by computing the area under the load displacement curve normalized by the ligament length times the thickness of the specimen (Johanneck et al. 2015)

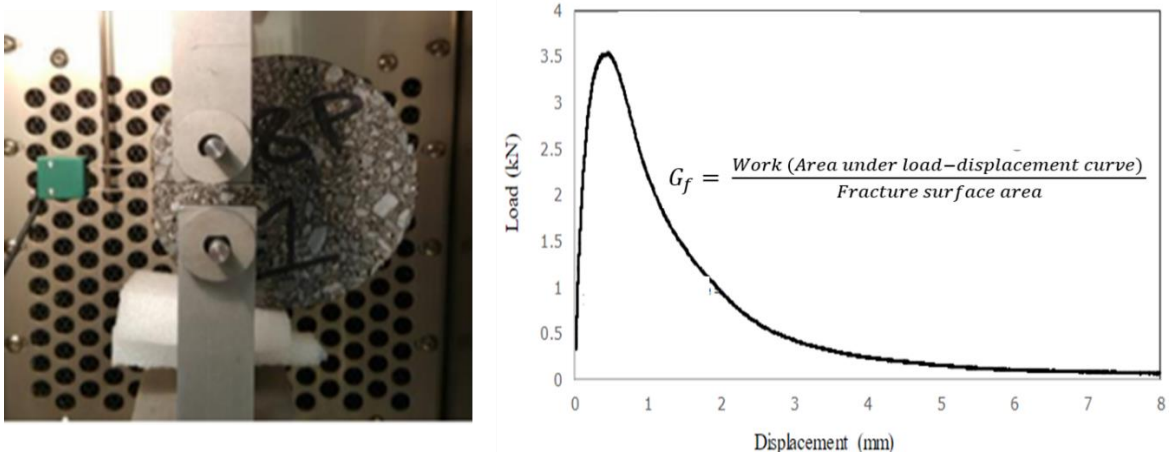

Figure 2.9 DCT test configuration and fracture energy determination from load-displacement curve

In an effort to address the problem associated with low temperature cracking states such as, Minnesota, Illinois and Iowa has taken the initiative to incorporate DCT test as one of the requirements in their low temperature performance-based specification. This is achieved by setting a threshold limit of fracture energy determined from DCT test to ensure the low temperature performance of asphalt mixtures. However, in recent years concerns were raised regarding the ability of fracture energy to differentiate between mixes with recycled asphalt pavement (RAP) and recycles asphalt shingles (RAS) (Al-Qadi et al. 2009, Al-Qadi et al., 2015, Behnia et al., 2011, Bahia et al., 2016).

2.7.2 Mixture Black Space

In the past decades, various researchers have tried to describe non-load associated cracking using an index parameter (Clark, 1958; Doyle, 1958; Kandhal, 1977; Glover et al., 2005). Recently the Glover Rowe (G-R) parameter modified from the Glover parameter (Anderson et al., 2011) was identified to describe the non-load associated cracking properties of asphalt mixtures. The parameter is determined from the |G*| and ϕ of binders at 15ºC and a frequency of 0.005 rad/s using Equation 2.22. A value of 180 kPa and 450 kPa were set as a limit to indicate onset non-load associated cracking and significant cracking problem respectively. Sample binder Glover-Rowe Black space diagram is shown in Figure 2.9 (Mensching et al., 2015).

$$Mix\ G-R\ paramter = \frac{G^{*}(cos\emptyset)^{2}}{sin\emptyset} \qquad (2.22)$$

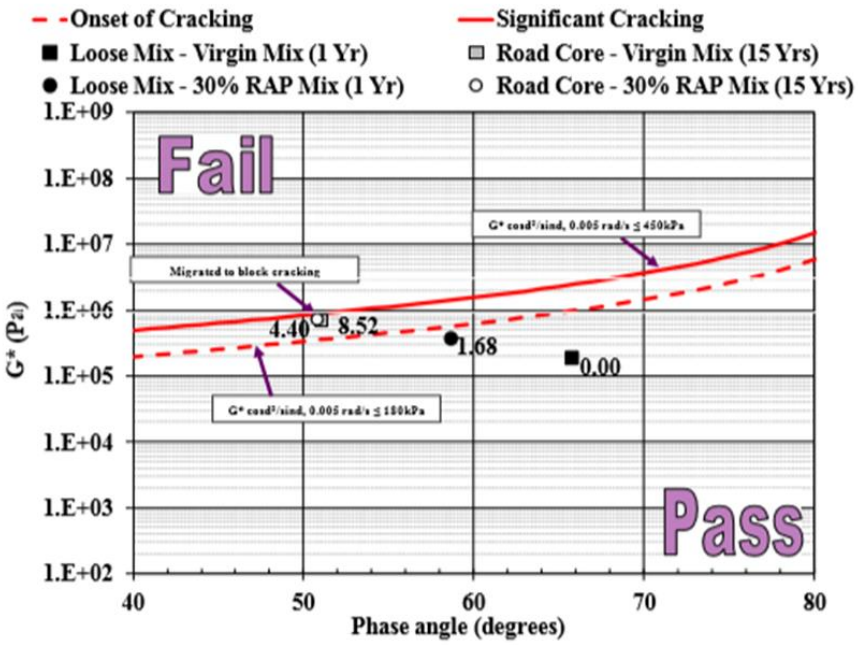

Figure 2.10 Sample binder Glover-Rowe Black Space diagram (Mensching et al., 2015)

2.8 Fatigue Cracking of Asphalt Mixture

Fatigue is the principal structural distress that is prevalent in asphalt pavements. Generally, fatigue cracking initiates at the bottom of the asphalt layer and propagates upward to the surface of the pavement layer under repeated traffic load applications. The application of heavy vehicle loading induces tensile stresses and strains due to bending of the AC layers which causes cracks to form. The cracks are a series of longitudinal and/or interconnected cracks and are commonly referred to as bottom-up fatigue cracking. Fatigue cracking gives an indication to structural failure and the cracks allow moisture infiltration and creates potholes which cause uncomfortable rides, accidents and agencies to spend a considerable amount of money on maintenance. Inadequate structural design (weak surface course, base, subbase or subgrade material: thin surface course, base, subbase or subgrade), excessive loading, poor drainage and poor construction (inadequate compaction) could attribute to the fatigue failure of pavements.

2.8.1 S-VECD Fatigue testing

S-VECD fatigue testing is developed to determine the damage characteristics of asphalt mixtures during a sinusoidal load application. The test procedure in available in AASHTO TP 107, Proposed Standard Method of Test for Determining the Damage Characteristic Curve of Asphalt Concrete from Direct Tension Cyclic Fatigue Tests using Asphalt mixture performance tester (AMPT). Four replicate specimens are recommended to be tested at four different peak to peak on specimen strains to get a range of N_f values. The test temperature is determined based on the binder type. The test is conducted by pulling the specimen constantly in crosshead-controlled mode until failure. The test setup allows homogenous state of stress in the test specimen throughout the load application. Failure is defined based on Reese's approach as the cycle where the specimen phase angle starts decreasing sharply instead of increasing.

2.8.2 S-VECD based Fatigue Evaluation

The S-VECD model is built based on the concepts of elastic-viscoelastic correspondence principle for modeling the viscoelastic behavior of the material with pseudo strains (ε^R), the continuum damage mechanics-based work potential theory for modeling the effects of microdamage on the macro-response of asphalt concrete and the time temperature superposition principle for combining the effects of time and temperature on material response. The approach based on Schapery (1990) is adopted to develop a constitutive relationship for asphalt mixtures by Daniel et al. (2002) and Underwood et al. (2010). The key functions necessary to develop this model include the relationships shown in Equations 2.23 to 2.25.

The pseudo strain energy density function,

$$W^R = f(\varepsilon^R, S) \qquad [2.23]$$

The stress-pseudo strain relationship,

$$\sigma = \frac{\partial W^R}{\partial \varepsilon^R} \quad [2.24]$$

The damage evolution law,

$$\frac{ds}{dt} = \left(-\frac{\partial W^R}{\partial S}\right)^{\alpha} \quad [2.25]$$

where;

σ = stress

α = damage evolution rate

ε^R = pseudo strain

S = internal state variable

A study by Sabouri et al. (2014) presented energy-based failure criterion, G^R (the rate of change of average released pseudo strain energy per cycle), to characterize the rate of damage accumulation during load application. A relationship is developed between the released pseudo strain energy which causes damage and the number of cycles to failure using S-VECD approach, Equation 2.26. The equation demonstrates that if damage is accumulating faster, material failure will occur sooner. The study showed that a unique relationship exists between the two terms for different mixtures. The test interpretation in terms of these parameters normalizes temperature and loading frequency variation and delivers a unique mixture characterization.

$$G^R = \frac{\frac{1}{2}\int_0^{N_f} \left(\varepsilon_{0,ta}^R\right)_i^2 (1-F_i)}{N_f^2} \quad [2.26]$$

where;

$(\varepsilon_{0,ta}^{R})_i$ = pseudo strain amplitude at cycle i;

F_i = pseudo stiffness at cycle i;

N_f = No of cycles to failure.

The S-VECD based fatigue life prediction equation is shown in Equation 2.27. The equation requires the critical tensile strain at the bottom of the AC layer and dynamic modulus inputs to predict the fatigue life of pavements in terms of number of cycles to failure. Additionally, the equation requires the traditional fatigue coefficients k_1 and k_2 obtained from S-VECD analysis.

$$N_f = K_1 \left(\frac{1}{\varepsilon_t}\right)^{K_2} (|E^*|)^{K_2} \quad [2.27]$$

where;

ε_t = tensile strain at the critical location;

|E| = stiffness of the material.

2.8.3 Layered Viscoelastic Pavement Analysis for Critical Distresses (LVECD)

Eslaminia et al. (2012) developed Layered Viscoelastic Pavement Analysis for Critical Distresses (LVECD) program based on the S-VECD model, G^R failure criterion and layered viscoelastic moving load analysis. The program evaluates the fatigue performance of mixtures in the pavement structure. The program performs the prediction using layer material properties, structure, traffic and climate inputs. A layered viscoelastic structural model is used to determine the structural response of a pavement. The linear viscoelastic characterization for the asphalt layer is performed by producing dynamic modulus master curve, shift factor function, and prony series from

measured dynamic modulus data. The S-VECD model coefficients Alpha, a, b, Initial C, Gamma and Delta are used to represent the damage growth in the asphalt pavement and to determine the N_f using Equations 2.2.8 and 2.29 respectively. The unbound layers are modeled as linear elastic in the program. The climate information is obtained from Enhanced Integrated Climate Model (EICM) database available in the LVECD program and a one-year temperature is averaged and is used for pavement performance analysis.

$$C(S) = e^{-as^b} \tag{2.28}$$

$$Secant\ G^R = \gamma N_f^{\delta} \tag{2.29}$$

The output from LVECD fatigue analysis includes the predicted pseudo stiffness (C) as a contour along the cross section at any given time. The term C is a damage parameter and ranges from 1 (undamaged material) to 0 (fully broken material). The parameter gives a good representation of surface material condition as exposed to traffic loading in which the repeated load application creates micro cracks and decrease the material stiffness by decreasing the effective area. As cracks develop more and more due to load application, the material integrity is compromised and the C value approaches to 0. The other output from LVECD fatigue analysis is the N/N_f ratio defined as the damage distribution factor, where N is the number of cycles at a given time and N_f is the number cycles at failure. When the damage factor becomes 1.0, the asphalt element is considered to be completely cracked.

CHAPTER 3: PREDICTION OF PHASE ANGLES FROM DYNAMIC MODULUS DATA AND IMPLICATIONS ON CRACKING PERFORMANCE EVALUATION

3.1 Introduction

Asphalt binders exhibit aspects of both elastic and viscous behaviors, and therefore they are considered viscoelastic materials. Viscoelastic materials are some of the most common materials that we encounter and are frequently used for many engineering applications. The mechanical properties of viscoelastic materials are temperature, frequency, loading history and time dependent. Most often the creep and flow behavior is small and can be neglected in engineering computations. However, asphalt binders and mixtures need to be fully characterized to capture the viscoelastic behavior to understand the performance of pavement structures. Viscoelastic materials exhibit both elastic and viscous characteristics during load application. The elastic component of the response is described by the storage modulus and the viscous component of the response is the loss modulus. It is important to accurately measure both components of the response, however the complex nature of the mechanical behavior presents experimental difficulties and uncertainties during material characterization.

Asphalt mixtures manifest a more complex viscoelastic behavior due to the combination of the viscoelastic asphalt binders and the aggregate skeleton. Researchers have shown that asphalt mixtures demonstrate linear viscoelastic properties within a small strain level (<100 micro strain) and limited number of cycles (Airey et al., 2004; Gardner et al., 1967). Yet, some studies argue that nonlinear viscoelastic behavior can appear at strain levels as low as 40 micro strain (Sayegh, 1967). For materials that exhibit linear viscoelastic behavior, the relationship between

stress and strain depends on loading frequency and temperature and can be fully described using complex modulus (dynamic modulus and phase angle); this test is straightforward and when asphalt mixtures are in the linear viscoelastic range, they generally exhibit thermorheologically simple properties. The time–temperature superposition principle can then be employed to horizontally shift results measured at different temperatures along time or frequency axis to construct a master curve for the full characterization of material behavior (Van der Poel, 1955). The amount of time or frequency shift is called the time-temperature shift factor. By combining the master curve with the shift factor, it is possible to predict the linear viscoelastic behavior of materials over a wide range of frequency and temperature conditions.

The complex modulus test has been one of the methods in use for linear viscoelastic characterization of asphalt mixtures in undamaged states since the 1950s (Heukelom et al., 1964; Van der Poel, 1955). This is achieved by determining two fundamental viscoelastic properties, namely, dynamic modulus ($|E^*|$) and phase angle (ϕ). Based on comparative studies, Elseifi et al. (2006) concluded that inclusion of a viscoelastic constitutive model into pavement design methods leads to improved accuracy. Currently, different structural and performance mechanistic models use dynamic modulus and phase angle master curves for linear viscoelastic characterization of asphalt mixtures at a required range of temperature, strain rates, and stress states. Specific applications include the determination of various parameters including binder or mix rheological parameters - such as R-Value (Christensen et al., 1992), Glover-Rowe (G-R) parameter (Rowe et al., 2014; King et al., 2012), inflection point frequency, mixture Black Space plots (Mensching et al., 2015), C1 and C2 parameter in Williams Landel Ferry (WLF) equation (Rowe et al., 2009b); Kaelble, 1985), lower and upper asymptote of mix master curves with a sigmoidal form. The application also extends to fatigue characterization and

performance prediction models such as Simplified Viscoelastic Continuum Damage (S-VECD) and Layered Viscoelastic Pavement Analysis for Critical Distresses (LVECD).

The mechanistic analysis of pavements greatly depends on the material characterization method and its accuracy. In recent years, significant advances have been made in specimen fabrication and testing equipment resulting in increased precision of the test data and lower variability associated with |E*| measurements. Moreover, well-developed and robust |E*| prediction equations such as Witczak model (Andrei et al., 1999), Hirsch model (Christensen et al., 2003) and others are available and have been successfully used by researchers. The long term pavement performance (LTPP) program has also employed these models to determine |E*|. While it is known that the accurate measurement of phase angle is very important for determining the elastic and viscous components, the measurement of phase angle in the laboratory still remains a challenge due to the need to accurately capture time based data with existing measurement technology. The variability mostly arises from the large amount of inherent noise in the deformation measurement signal. In addition, the calibration aspect is also complex. Generally, a testing device is evaluated using a solid fixture for a zero phase lag response. However, standards of materials with a known stiffness and intermediate values of phase angle (typical of that found in asphalt mixtures) are not available. The accuracy further depends upon many other factors (e.g., adjustments for equipment compliance that have been made, details of displacement transducer design). Moreover, a large amount of historic data exists with |E*| measurements but with no accompanying phase angle measurements. For example, the LTPP database is populated with measured and predicted |E*| data but lacks phase angle. This prohibits the use of these data for rheological and performance evaluation. Further, it inhibits their use for verification of rheological parameters and linkage of historic data to field performance data.

Several researchers have developed relationships between phase angle and modulus for asphalt mixtures. Bonnaure et al. (1977) developed a relationship that was limited to binder stiffness (S_b) values greater than 5 MPa and less than 2 GPa (when S_b is greater than 2GPa the mixture phase angle (ϕ_m) is taken to be zero). The relationship used the binder stiffness (S_b) volume of binder (V_b) in the prediction and is as follows, Equation 3.1.

$$\phi_m = 16.36 \times V_b^{0.352} exp\left[\frac{log_{10}S_b - log_{10}\ 5\times10^6}{log_{10}S_b - log_{10}\ 2\times10^9} \times 0.974\, V_b^{-0.172}\right] \quad [3.1]$$

During the SHRP project Tayebali et al. (1994) developed several relationships linking the phase angle to mix stiffness, an example of which is shown in Equation 3.2.

$$\phi_o = 260.096 - 17.172Ln(S_o) \quad [3.2]$$

where ϕ_0 is the mixture phase angle and S_0 is the mixture stiffness. This relationship was developed from a study of fatigue properties. The subscript to the parameters denotes that the initial condition is used. The preceding two relationships for bituminous mixtures are empirical in nature with derived constants from regression analysis.

The Hirsh model was originally developed in the late 1960s based on the modified law of mixtures. The law states that the property of a composite material can be treated as a combination of the properties of its components assuming the influence of each component is proportional to its volume fraction. Christensen et al., (2003) developed a calibrated phenomenological model based on the Hirsch model that links the phase angle to binder properties and mixture volumetrics, as follows (Equation 3.3, 3.4, 3.5).

$$|E^*|_{mix} = Pc \cdot \left[4{,}200{,}000 \cdot \left(1 - \frac{VMA}{100}\right) + 3 \cdot |G^*|_{binder} \cdot \left(\frac{VFA \cdot VMA}{10{,}000}\right)\right] +$$

$$(1 - Pc) \cdot \left[\frac{1 - \frac{VMA}{100}}{4{,}200{,}000} + \frac{VMA}{3 \cdot VFA \cdot |G^*|_{binder}}\right]^{-1} \quad [3.3]$$

where the contact area Pc is defined as;

$$Pc = \frac{\left(20 + \frac{VFA \cdot 3 \cdot |G^*|_{binder}}{VMA}\right)^{0.58}}{650 + \left(\frac{VFA \cdot 3 \cdot |G^*|_{binder}}{VMA}\right)^{0.58}} \quad [3.4]$$

and:

$$\phi = -21(\log Pc)^2 - 55 log Pc \quad [3.5]$$

where;

VFA = voids filled with asphalt

VMA= percent voids in the mineral aggregate

G_b^* = complex shear modulus of the binder

It is generally accepted that asphalt mixtures are best modeled with a viscoelastic solid model represented by a sigmoidal shape. The only model format that describes this shape to some extent is that of the Hirsch model whereas the other equations are clearly limited.

The concept of predicting the phase angle from the slope of the complex modulus versus frequency was first suggested by Booij et al. (1982). Christensen et al. (1992) used the same concept in the development of the Christensen Anderson binder model phase angle calculation. Rowe (2009a) presented equations using a similar basis for sigmoidal forms that can be applied to asphalt mixture analysis, as follows, Equations 3.6 to 3.9. The equations can be applied to either the analysis of master curves that contain |E*| and phase angle data or just |E*| data alone. The work conducted by Booij et al. (1982); Christensen et al. (1992) and more recently by Rowe (2009a) demonstrates that the phase angle response can be determined from a mathematical understanding of the dependency on the stiffness (either |G*| or |E*|) versus the

frequency (ω) using regression parameters for a sigmoidal model. Each of the regression coefficients (δ, α, β, λ) are related to the shape of the sigmoid fit to the master curve as detailed by Mensching et al. (2017). This results in a method to determine the phase angle from just dynamic modulus vs. frequency data, when it is available.

Standard logistic- $log|E^*| = \delta + \frac{\alpha}{1+e^{[\beta+\gamma(logw)]}}$ [3.6]

Standard logistic- $\phi = 90 \times \frac{d\ logE^*}{d\ log\ w} = -90 \times \alpha\gamma \frac{e^{[\beta+\gamma(logw)]}}{\left[1+e^{[\beta+\gamma(logw)]}\right]^2}$ [3.7]

Generalized logistic- $log|E^*| = \delta + \frac{\alpha}{(1+\lambda e^{[\beta+\gamma(logw)]})^{1/\lambda}}$ [3.8]

Generalized logistic- $\phi = 90 \times \frac{d\ logE^*}{d\ log\ w} = -90 \times \alpha\gamma \frac{e^{[\beta+\gamma(\mathrm{logw})]}}{\left[1+\lambda e^{[\beta+\gamma(\mathrm{logw})]}\right]^{1+1/\lambda)}}$ [3.9]

This paper evaluates a fundamental relationship approach to determine the phase angle via the slope of the log-log of stiffness curve (from now on referred as the slope method). The study by Rowe (2009a) investigated this relationship and concluded the validity of the relationship to large set of modified and unmodified binders, asphalt mixes and some other polymers. This paper extends the previous research to a larger set of asphalt mixtures and evaluates the reliability of the relationship to asphalt mixtures. Phase angles predicted using the slope method are compared to laboratory measurements to assess the validity of the relationship for various mixtures. Further comparisons are made with the Hirsh model, the slope method, and laboratory measured phase angle values. Finally, the implication on rheological parameters and pavement fatigue performance predictions due to the use of predicted phase angle values as opposed to lab measured values is assessed.

3.2 Research Approach and Materials

3. 2.1 Materials and Testing

Three sets of independent data were used for this study; two from specimens fabricated and tested by the research team as part of ongoing projects and the third from the LTPP database. The first set of specimens includes two 9.5mm nominal maximum aggregate size (NMAS) (C-9.5mm and L-9.5mm) and one 12.5mm NMAS (C-12.5mm) laboratory produced mixtures. The aggregates and binders were obtained from Rhode Island Department of Transportation (RIDOT) and specimens were fabricated to replicate a range of acceptable as-built field conditions in terms of asphalt binder and air void content. The low, optimum and high levels of asphalt and air void content combinations for the three mixtures resulted in 27 specimen conditions overall. The second set test specimens were plant produced materials obtained from New Hampshire Department of Transportation (NHDOT) projects. These included 12.5mm and 19mm NMAS mixtures containing various amounts of RAP and RAS and a virgin mixture. The last set includes three mixtures from Vermont, New Jersey and North Carolina LTPP sections. Overall, the wide selection of mixtures used in this study covers a range in as-built conditions, NMAS, laboratory versus plant production, virgin and modified binder (V), and % RAP and RAS; this provides a platform for comparing the potential effects of these parameters on the phase angle predictions. Mixture information is summarized in Table 3.1.

Table 3.1 Continuous PG grades and mixture gradations

Rhode Island (RI) Mixtures				
Mixture Label	**AC Level**	**AV Level**	**NMAS, mm**	**Binder**
L-9.5mm	5.9, 6.3, 6.8%	4, 7, 9%	9.5	PG 64-28
C-9.5mm	5.9, 6.3, 6.8%	4, 7, 9%	9.5	PG 64-28V
C-12.5mm	5.2, 5.6, 6.1%	4, 7, 9%	12.5	PG 64-28V
New Hampshire (NH) Mixtures				
Mixture Label	**%Total Binder Replacement (%RAP/%RAS)**	**AV Level**	**NMAS, mm**	**Binder**
NH-12.5mm, 20%RAP	18.9 (18.9/0)	7.7	12.5	PG 58-28
NH-12.5mm, 30%RAP	28.3 (28.3/ 0)	6.8	12.5	
NH-12.5mm, RAP/RAS	18.5 (7.4/11.1)	7.4	12.5	
NH-19mm, 20%RAP	20.8 (20.8/0)	6.1	19	
NH-19mm, 30%RAP	31.3 (31.3/ 0)	6.3	19	
NH-19mm, RAP/RAS	20.4 (8.2/12.2)	6.0	19	
Virgin Mixture	0 (5.9% ac	4.4	12.5	PG 58-28
Mixtures from LTPP				
Mixture Label	**SHRP ID**	**|E*| Link**	**VFA**	**VMA**
NC Mixture	1992	807	55.1	21.4
NJ Mixture	1033	715	76.4	14.4
VT Mixture	1682	1110	72.4	14.5

Specimens fabricated and tested by the research team were compacted using a Superpave gyratory compactor and then cut and cored to test specimen dimensions of 100 x 150mm and 100 x 130mm for dynamic modulus and fatigue testing, respectively. Complex modulus (E*) testing was performed following the test procedure provided in AASHTO T 342 (2015) in load-controlled uniaxial compression mode. Testing was done at three temperatures (4.4°C, 21.1°C & 37.8°C) and six loading frequencies (25, 10, 5, 1, 0.5 and 0.1Hz) on three replicate specimens using an Asphalt Mixture Performance Tester (AMPT). Axial deformation was measured using four LVDTs with a 70 mm gauge length. Strain amplitudes during tests were limited to 50 to 75 micro-strain to ensure the test response remains in linear viscoelastic range. The resulting stress and strain of the final six cycle of each loading series were used to calculate the dynamic modulus and phase angle of the mixtures. Dynamic modulus is determined by dividing peak to

peak specimen stress to strain, Equation 3.10, and phase angle is obtained from the time lag between peak to peak strain and stress, Equation 3.11.

$$|E^*| = \frac{\sigma_{amp}}{\varepsilon_{amp}} \quad [3.10]$$

$$\phi = 2\pi f \Delta t \quad [3.11]$$

where;

σ_{amp} = amplitude of applied sinusoidal stress

ε_{amp} = amplitude of sinusoidal strain response

f = stress and strain frequency

Δt = average time lag between stress peak and strain peak at given frequency and temperature

Cyclic fatigue testing using the AMPT was carried out on specimens following the test procedure in AASHTO TP 107 (2014). Four specimens were tested at four different peak to peak on specimen strains to cover the appropriate range of number of cycles to failure.

3.2.2 Dynamic Modulus and Phase Angle Master Curve Construction from Measured Data

In this study the RHEA^{TM} software (Rowe et al., 2001) is used to construct |E*| and ϕ master curves from measured |E*| and ϕ data points using the time temperature superposition principle. For tests performed in the linear viscoelastic range, the time temperature superposition principle allows test isotherms to be shifted to a required temperature at a reduced frequency. The shifting in the RHEA^{TM} software is done following the work done by Gordon et. al (1994). The storage modulus, representing the elastic behavior, and loss modulus, representing the viscous behavior, are shifted separately. Then the shifting from the two components is averaged to produce the final shift factor. In the absence of phase angle data, the shifting in the program is done only once using the dynamic modulus component. The same shift factors are applied to the corresponding phase angle measured points to produce phase angle master curves. The

five parameter generalized sigmoidal model (Richards curve) was used to fit the dynamic modulus and phase angle master curves, Equations 3.8 and 3.9.

The |E*| and ϕ master curve construction process is illustrated in Figures 3.1 and 3.2. Figure 3.1 shows lab measured |E*| isotherms at test temperatures 4.4, 21.1 and 37.8°C and loading frequencies 25, 10, 5, 1, 0.5 and 0.1Hz. The isotherms are shifted horizontally to a reduced frequency to construct |E*| master curve at a reference temperature of 21.1°C, Figure 3.2(a). The shifted points are fitted with a generalized logistic equation, Figure 3.2(a). The time–temperature shift factors are shown in Figure 3.2(b). The same shift factors, Figure 3.2(b) are applied to measured phase angle points to construct phase angle master curves, Figure 3.2(c). The measured phase angle master curve is fitted with a generalized logistic equation, Figure 3.2(c).

To determine mixture phase angle using the slope method, first the |E*| master curve is constructed using average measured |E*| data from replicates and |E*| values deviating from the mean by one standard deviation. This is done to account for some degree of variability that exists during |E*| measurement. The sample standard deviation for each replicate at each test temperature and frequency was calculated to obtain the high and low range of measured |E*|. For each set of measured data (average, average + 1 standard deviation and average - 1 standard deviation), independent time-temperature shifting was conducted and this yielded three master curves for |E*|. These are labelled as “Measured”, “Measured High Range” and “Measured Low Range” Figure 3.2a.

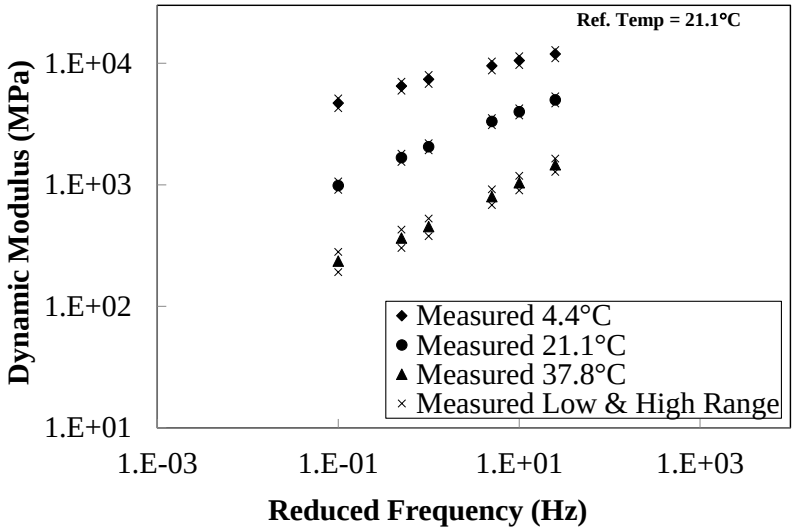

Figure 3. 1 Measured |E*| Raw Data

3.2.3 Phase angle Prediction from Slope of log-log |E| Master curve*

Using the fitting sigmoidal logistic function, 28 |E*| master curve points were computed at 5 equally spaced points per decade on logarithmic scale over a frequency range of 0.001 to 10000 Hz. Figure 3.3(a) shows the points determined in this manner for average |E*|, low, and high range |E*|. The unfitted master curve points which correspond to the unfitted phase angle points in Figure 3.2(b) are also shown in Figure 3.3(a). The phase angle points, Figure 3.3(b) are determined from the slope of the log-log |E*| master curve of Figure 3.2(a) using Equation 9. Figure 3.3 (b) shows the predicted phase angle from average, low and high range. The measured unfitted and fitted curves are shown to allow visual comparison between measured and predicted phase angle points Figure 3.3 (b).

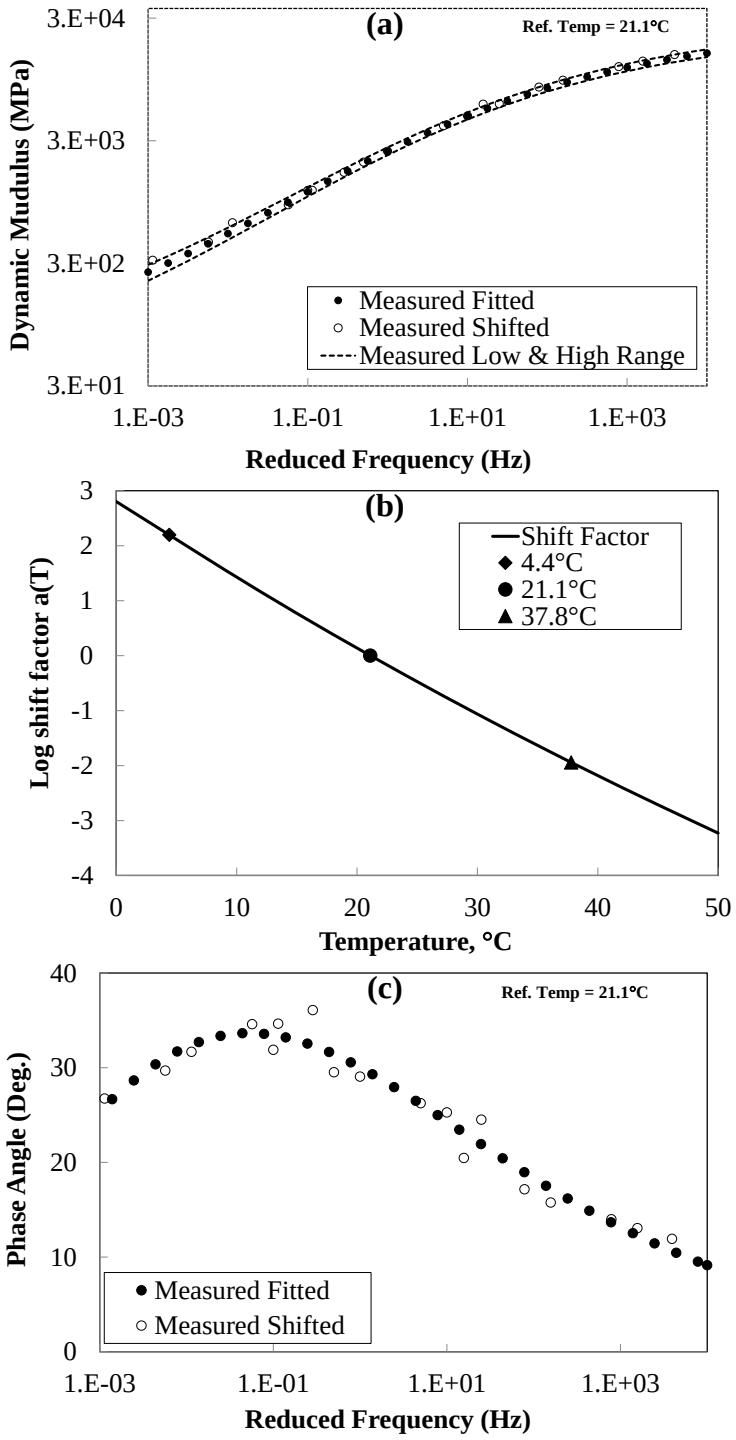

Figure 3. 2 a) |E*| Master curves (b) time-temperature shift factors (c) phase angle master curves

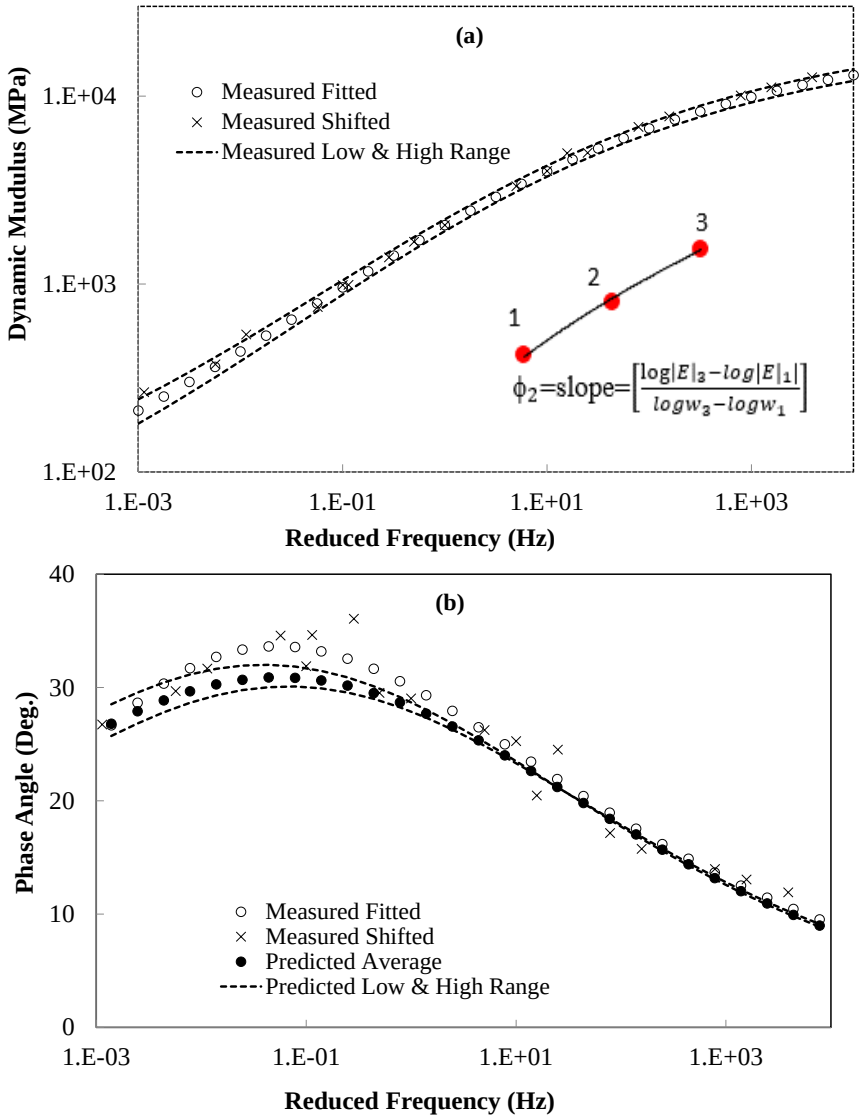

Figure 3. 3 |E*|master curves (b) measured and predicted phase angle master curves

3.2.4 Phase angle Prediction using Hirsch Model

In this portion of the study, the Hirsch model is used to determine phase angle from binder shear modulus |G*| and mix volumetrics (Equation 3.5) to allow comparison to the slope method prediction and lab measurements. The lab measured |G*| binder values were used for the NH virgin mixture. However, the |G*| values back calculated using Equation 3.3 and 3.4 are used for the LTPP mixtures because the binder shear modulus values were not available. The back calculated shear modulus is then used in Equation 3.5 to determine the phase angle. It should be noted that for the phase angle prediction done in this manner, the compounding

error from each model could contribute to the differences or similarities observed during Hirsch, slope method and lab measurement comparison for the LTPP mixtures.

3.2.5 Statistical Analysis

Statistical analysis is performed to examine the accuracy of the phase angle estimation from slope of log-log |E*| master curve. First, the Pearson linear correlation coefficient is used to measure the strength of linear association between the 28 measured and predicted data points corresponding to each mixture condition. Next, a linear relationship is fitted to the points and the equation of the fitted line is generated to allow comparison on a unity plot (x=y). Further statistical analysis is employed by calculating the root mean square error (RMSE) between measured and predicted phase angle points. RMSE complements the correlation coefficient because it provides the difference in measurements between each measured and predicted points. The RMSE for individual mixtures is normalized by dividing the total RMSE by the number of points.

3.2.6 Impact on Pavement Performance Evaluation

3.2.6.1 Mixture Black Space Diagram

Mixture Black space diagrams assess the stiffness and relaxation capability of mixtures from a plot of |E*| versus phase angle. A recent study by Mensching et al. (2017) evaluated the correlation between certain Black Space points to low temperature cracking performance based on the Glover-Rowe (G-R) binder cracking parameter. The G-R parameter correlates binder Black Space points to non-load associated cracking (Rowe et al., 2014; King et al., 2012). The temperature and frequency combinations evaluated for mixture Black Space points were 15°C and 0.005, 5, and 500 rad/s. For this study the Black Space points are generated using measured and predicted phase angle data to evaluate the relative location of the points.

3.2.6.2 Pavement Fatigue Life Evaluation, S-VECD and LVECD

In recent studies the S-VECD approach (Underwood et al., 2012) has been used to evaluate the fatigue performance of various mixtures using uniaxial cyclic fatigue testing. In this approach, two relationships are developed to characterize the fatigue performance of the mixtures and are used in subsequent modeling and pavement performance prediction. The damage characteristic curve (C versus S) is represented by the reduction in the pseudo secant modulus (material integrity) and accumulated damage during cyclic loading. The curve is fitted with an exponential function, Equation 3.12. This relationship shows how the stiffness, or integrity, of the material changes as micro cracks grow during continued load applications.

The fundamental energy based failure criterion, G^R (the rate of change of the average released pseudo strain energy), is plotted versus the number of cycles to failure and demonstrates that if damage is accumulating faster, material failure will occur sooner. The curve from this relationship is fitted with Equation 3.13. The fitting parameters a, b, γ and s in Equations 3.12 and 3.13 are referred to as damage model coefficients. Both relationships require dynamic modulus and phase angle master curves for the linear viscoelastic characterization of the asphalt mixtures.

$$C = e^{-aS^b} \quad [3.12]$$

$$N_f = \gamma(G^R)^s \quad [3.13]$$

where;

a, b, γ and s = fitting parameters

The LVECD program employs a finite element structural analysis for pavement response computation and pavement fatigue performance prediction based on the S-VECD approach (Eslaminia et al. 2012). The fatigue coefficients from S-VECD analysis are used in the model to determine the fatigue performance of the study mixtures in a pavement structure in terms of number of failure points. Failure of an element is defined when the ratio of applied loading

cycles to the failure loading cycle is equal to 1 ($N/N_f = 1$), in which case the asphalt element is considered completely cracked. A spatial distribution plot from LVECD analysis displays the ratio of N/N_f for the matrix of 11 by 101 finite element nodes producing a total of 1111 nodes along the pavement cross section. For this study the number of failure points were tallied to compare relative fatigue performance.

For this study, S-VECD analysis and LVECD pavement simulations were performed using both measured and predicted phase angles. The S-VECD approach was used to analyze the fatigue test results and determine the damage characteristics curves (C versus S and G^R versus N_f) for the study mixtures. One of the required inputs to the S-VECD analysis is phase angle measurement of mixtures at three temperatures and six frequencies for linear viscoelastic characterization of mixtures. The phase angle prediction from the stiffness data was used to obtain these values. The fatigue coefficients obtained from SVECD analysis using predicted and measured phase angle values are used in the LVECD to compute the fatigue performance of the mixtures in a pavement structure. A typical pavement structure and traffic were used in the analysis. Fatigue cracking performance evaluation in terms C versus S and G^R versus N_f as well as number of failure points determined using the predicted and measured phase angle values for the mixtures were compared. This is done to assess the potential effect of predicted phase angle on the damage characteristic curves and fatigue performance prediction and further gauge the accuracy of the prediction approach in the context of pavement performance estimates.

3.3 Result and Discussion

The results from statistical analysis, rheological indices and pavement performance evaluation are discussed in this section. Results for all of the mixtures evaluated are summarized in tabular form and example figures for two cases were chosen for illustration. The two cases represent

the best and worst examples, from the perspective of match between measured and predicated phase angles.

Figure 3.4 demonstrates the |E*| master curve fitted with the generalized logistic equation for Measured (Mean), Measured High Range (Mean + 1 Standard deviation) and Measured Low Range (Mean – 1 Standard deviation). Comparing all Rhode Island and New Hampshire Mixtures, the L-9.5mm 6.8AC 7AV mixture exhibited the lowest variability (Figure 3.4a) whereas the C-12.5mm 6.1AC 7AV showed the highest variability (Figure 3.4b) in |E*| measurement among replicates. For most of the mixtures the coefficient of variation (COV) between replicates is within the allowable range of the specification (below 7% when three replicates are tested). Therefore, for these mixes the effect on phase angle prediction due to dynamic modulus measurement variation is expected to be minimal. However, a COV as high as 11% is observed for some mixes and this high deviation in dynamic modulus measurements among replicates could impact the accuracy of phase angle prediction.

3.3.1 Comparison of Measured and Predicted Phase Angle

Figure 3.5 shows the different measured and predicted phase angle master curves. The actual measured phase angle values are shown along with the logistic curve fitted to the measured points to illustrate the variability in phase angle measurements and its influence on the shape of the fitted logistic curve. Throughout the study, the statistical and other comparisons are done using fitted measured phase angle values as opposed to predicted. So, it should be noted that the fitting might magnify or reduce the differences between measured and predicted values.

The phase angle master curve predicted from the measured |E*| curve is shown in Figure 3.5. The mixtures presented represent the best and worst match between measured and predicted values. The L-9.5mm 5.9AC 7AV and NH-12.5mm, 30%RAP mixtures had the lowest differences among the Rhode Island and New Hampshire mixtures, respectively, Figure 3.5 (a)

and (b). The C-12.5mm 6.1AC 7AV and NH-19mm, RAP/RAS mixtures exhibited the largest differences between measured and predicted values, Figure 3.5(c) and (d). The difference between measured and predicted values appears to be higher at the peak phase angle, which corresponds to higher testing temperature or lower loading frequency. As it can be seen from actual phase angle measurements, the variability in lab measurements is usually higher at this location as well. While a number of factors related to the prediction could contribute to this observed difference, phase angle measurements corresponding to this location (high temperature or low loading frequency) are less reliable as well. Therefore, the error that is present during lab measurement should be incorporated during model verification. It has to be noted that at both best and worst scenarios, the measured and predicted phase angle master curves have comparable shape and peak at similar frequencies. This is further quantified by computing the inflection point frequency for both curves, shown in Figure 3.6. Overall, the inflection points match very well which is indicated by the high R^2 value (0.98) and low average RMSE (0.02Hz).

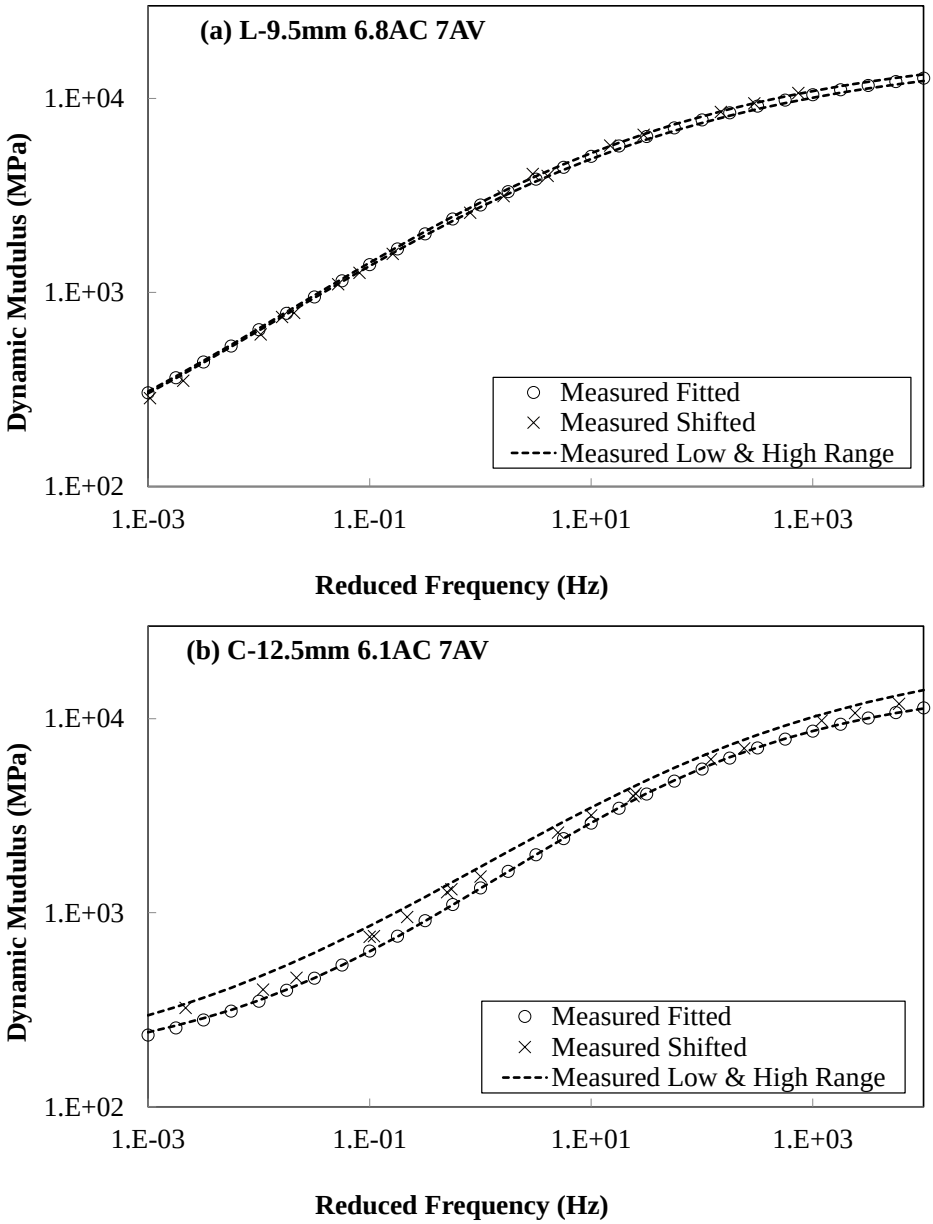

Figure 3. 4 |E*| Master Curves (a) L-9.5mm 6.8AC 7AV (b) C-12.5mm 6.1AC 7AV.

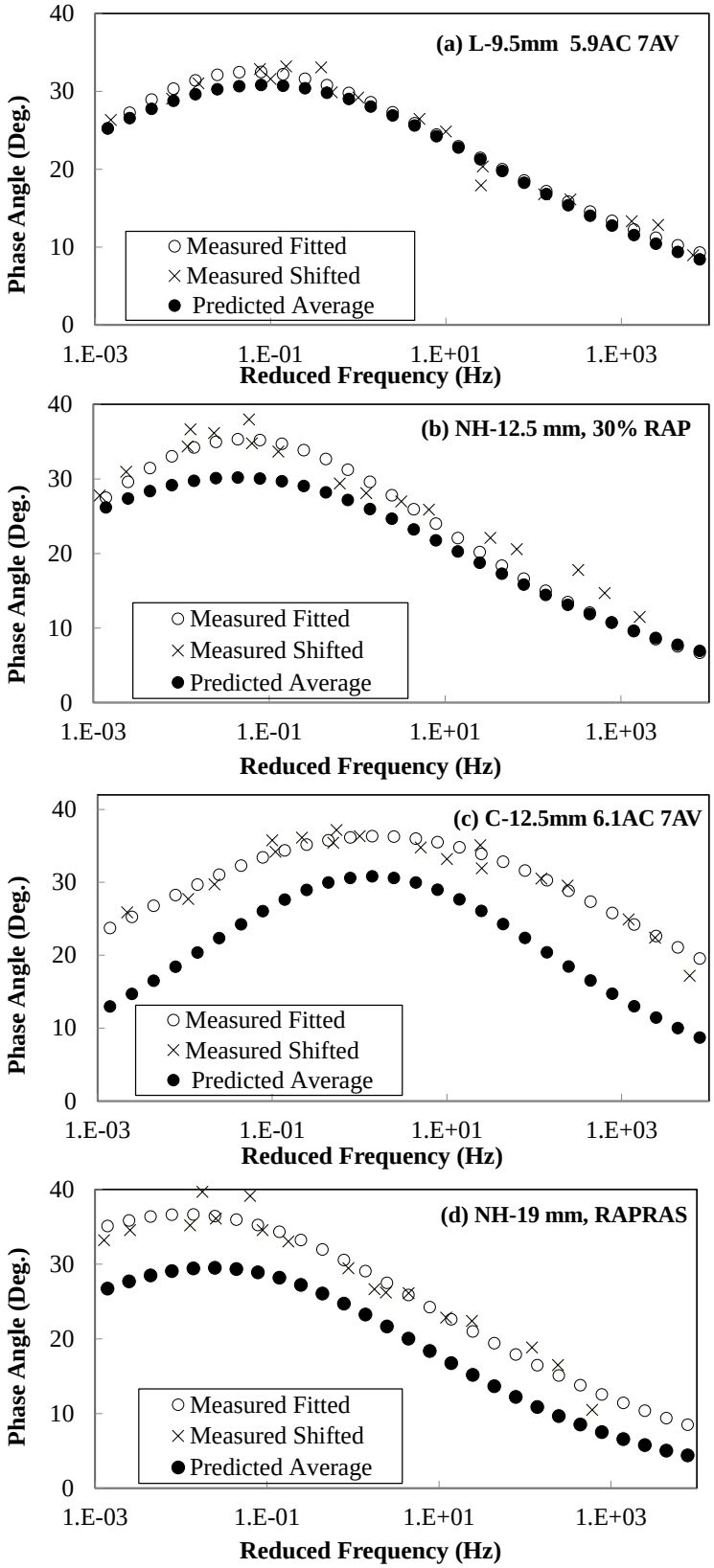

Figure 3. 5 Measured and predicted phase angle master curves (a) L-9.5mm 5.9AC 7AV (b)NH-12.5mm, 30% RAP (c) C-12.5mm 6.1AC 7AV (d) NH-19mm, RAPRAS

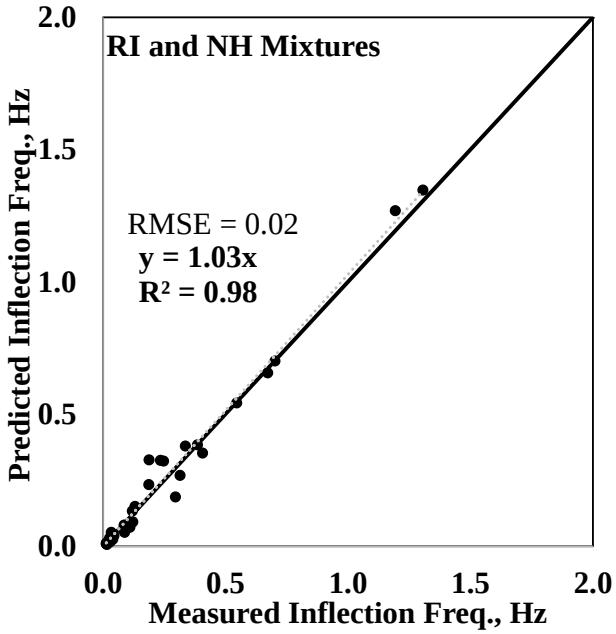

Figure 3. 6 Line of equality plot for measured and predicted inflection point frequency

The statistical analysis for Rhode Island and New Hampshire mixtures is presented in Table 3.2, and the relationship is shown graphically in Figure 3.6. A strong association between measured and predicted values is observed for the L-9.5mm and C-9.5mm mixture whereas the C-12.5mm and New Hampshire mixtures appear to have the least agreement between measured and predicted values. Overall the prediction appears to generate lower phase angle values as compared to measured values. This is indicated by the consistent deviation of the points to the lower side of the equality line.

Generally, the predicted and measured phase angles are in good agreement in terms of shape of the master curve and magnitude for Rhode Island L-9.5mm and C-9.5mm mixtures with 7 and 8% deviation from the equality line and 1.34 and 1.62 RMSE respectively. For the eighteen mixture conditions under the two sets of mixtures the average difference between measured and predicted values is less than 2 degrees. However, a larger difference is observed in New Hampshire mixes followed by the Rhode Island C-12.5mm with RMSE 4.24 and 4.96 and 16 and 17% deviation from the equality line respectively. From the observation it appears that the

difference between measured and predicted values are consistently lower for certain sets of mixtures and are higher for other sets of mixtures despite the same lab measurement procedure and prediction method employed. Particularly the composition in terms of aggregate and binder used for the C-12.5mm mix were similar to the C-9.5mm mix and both mixtures used identical production procedure and equipment, environmental chamber and AMPT. Hence the higher difference observed in the C-12.5mm could not be explained with respect to any of these parameters. However, for the C-9.5mm and L-9.5mm mixtures, for which measured and predicated phase angles are in better agreement (both with low average RMSE of 1.34 and 1.62), spring loaded linear variable displacement transducers (LVDTs) were used to measure specimen deformation. Whereas for the C-12.5mm and New Hampshire mixtures where the differences are higher, loose core LVDTs were used.

For all study mixtures, the same AMPT device is used. There were no differences in calibration, machine compliance, algorithm and PID parameters used. The only difference as stated above is the type of LVDT that were used for deformation measurements. A comparative study done by Lacroix (2013) showed that the measurements from spring loaded LVDTs are less variable (within the tolerance given by the manufacturer) as compared to loose core LVDTs in a situation where both are calibrated. The study also suggested that the alignment between LVDT and the specimen causes higher discrepancy in measurement of displacement and phase angle for loose core models as compared to spring loaded ones. Based on the results presented here as well as from observations by others, the type of LVDTs used could be one of the reasons for higher differences between measured and predicted phase angle values observed.

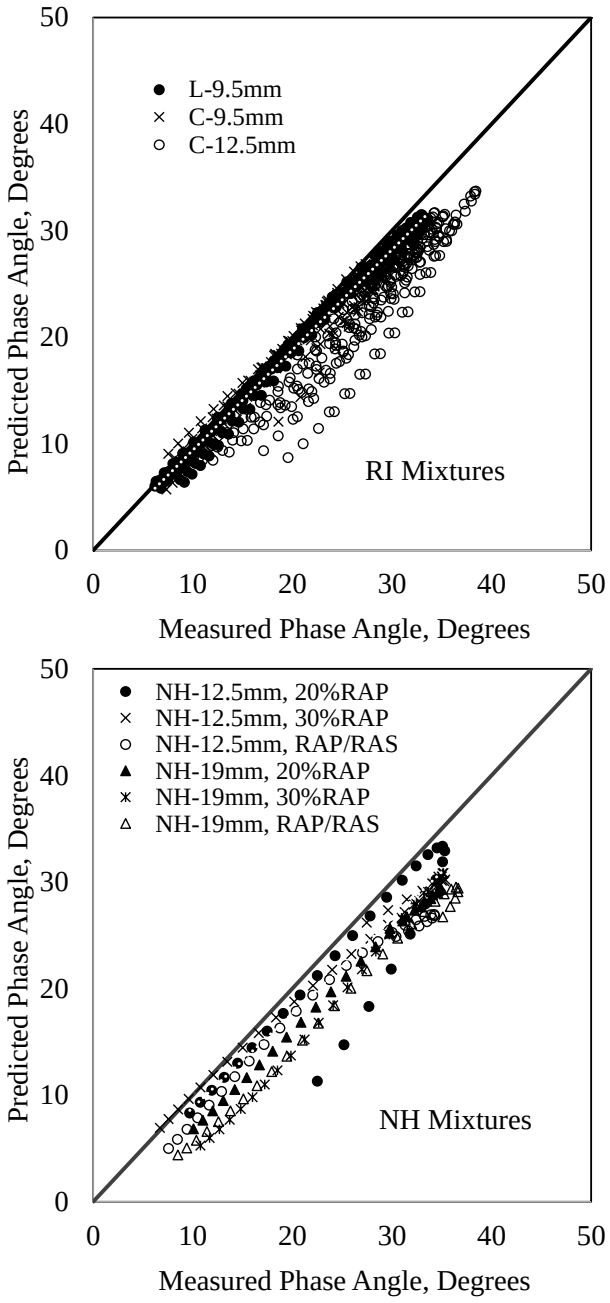

Figure 3. 7 Line of equality plot for measured and predicted phase angle

Table 3.2 Statistical evaluation

RI Mixtures	AC-AV	R^2	Trend line Equation	RMSE
L-9.5mm	5.9-4	1.00	y=0.93x	1.43
	5.9-7	1.00	y=0.96x	0.85
	5.9-9	1.00	y=0.94x	1.15
	6.3-4	1.00	y=0.93x	1.30
	6.3-7	0.99	y=0.94x	1.69
	6.3-9	0.98	y=0.91x	2.28
	6.8-4	1.00	y=0.95x	1.09
	6.8-7	1.00	y=0.94x	1.16
	6.8-9	1.00	y=0.95x	1.14
Average			**94% (6%)**	**1.34**
C-9.5mm	5.9-4	0.99	y=0.94x	1.26
	5.9-7	0.96	y=0.93x	1.31
	5.9-9	0.95	y=0.92x	1.61
	6.3-4	0.97	y=0.93x	1.51
	6.3-7	0.97	y=0.93x	1.46
	6.3-9	0.94	y=0.92x	1.62
	6.8-4	0.95	y=0.93x	1.73
	6.8-7	0.98	y=0.91x	1.95
	6.8-9	0.86	y=0.91x	2.15
Average			**92% (8%)**	**1.62**
C-12.5mm	5.2-3	0.98	y=0.86x	3.57
	5.2-7	0.96	y=0.82x	4.84
	5.2-9	0.89	y=0.87x	2.91
	5.6-5	0.99	y=0.87x	3.41
	5.6-7	0.93	y=0.82x	5.98
	5.6-9	0.97	y=0.81x	4.99
	6.1-4	0.83	y=0.82x	5.59
	6.1-7	0.77	y=0.73x	8.65
	6.1-9	0.95	y=0.84x	4.73
Average			**83% (17%)**	**4.96**
NH Mixtures	**NMAS**	**R^2**	**Trend line Equation**	**RMSE**
NH 12.5mm, 20%RAP	12.5	0.86	y=0.88x	3.05
NH 12.5mm, 30%RAP	12.5	0.99	y=0.89x	2.40
NH 12.5mm, RAP/RAS	12.5	0.99	y=0.82x	4.36
NH 19mm, 20%RAP	19	0.99	y=0.83x	4.45
NH 19mm, 30%RAP	19	0.94	y=0.83x	5.14
NH 19mm, RAP/RAS	19	0.97	y=0.78x	6.03
Average			**84% (16%)**	**4.24**

The prediction of phase angle from dynamic modulus relies upon the assumption of linear visco-elastic behavior in the small strain region and that materials can be considered thermo-

rheologically simple and time temperature supposition is valid. However, it has been known for many years that a true representation of asphalt mixtures over the entire range of temperature and frequency requires the use of visco-elastic-plastic models. The plastic strain that occurs is largely a function of movement within the aggregate skeleton and represents the complex nature of a mixture rather than a bituminous binder. Work conducted on mixture visco-plastic behavior suggests that the plastic deformation occurs at very low stress and most likely can be considered as a stress dependent zero yield plasticity (Darabi et al., 2011; Rowe et al., 2004; Drescher et al., 1993). If the response to load is considered a simple model – zero yield stress dependent linear plastic strain – the strain produced by a sinusoidal stress application will be completely out of phase with the load response in a similar manner to a viscous strain. The stress imposed upon the aggregate skeleton will be higher when the binder is less stiff, associated with lower frequencies or higher temperatures. Thus, the measured phase angle of a mixture (which includes a plastic response) is always theoretically going to be greater than that of a mixture represented only by visco-elastic behavior. Thus, when a viscoelastic consideration is applied to the calculation of phase angle from the complex modulus of a mixture a bias in the data is expected.

It should be noted that the calibration of the phase angle measurement is complex. Phase angle is not a direct measurement but rather a calculation from collected data. The system in use was verified to deliver a zero phase angle with an aluminum specimen fixed in the device. However, at higher frequencies some bias in measurement may exist for reasons not immediately intuitive to the researchers. While magnitudes of these effects are not known –they may exist and are mentioned in this paper for completeness of this discussion. If these effects are insignificant it should be possible to assess the plastic strain effects compared to the various models that exist.

3.3.2 Comparison of Slope Based Prediction Method with Hirsh Model Prediction

A virgin mixture is used to compare phase angle prediction between the slope based method, Hirsch model, and lab measurement. The virgin mixture is used for this comparison because the binder modulus is a direct representation of the material in the mixture; this is not possible with RAP mixtures due to unknown degree of blending between the RAP and virgin binders in the mixture. Phase angle master curves from the slope method, Hirsch model, and lab measurement and the relationship between them are shown graphically in Figure 3.8. The lab measured and predicted phase angle with the slope method are in better agreement in terms of shape and magnitude than Hirsch model which is indicated by the lower RMSE, Figure 3.8(c). The Black space diagram (Figure 3.8(b)) also supports the above observation. While the Hirsch model has been found useful, it tends to follow certain defined shape (as seen in the figure) and does not show the same level of flexibility that is observed with the slope based method.

The mixture data from the LTPP sections is used to produce phase angle master curves using the slope method and Hirsch Model. Although the predictions cannot be verified against lab measurements, the presented plots show some of the possible differences that could be encountered due to use of one method over the other. For the North Carolina mixture, Figure 9(a) the master curves peaks do not match and larger differences are observed in terms of magnitude. Vermont mixture master curves from both methods are relatively similar in terms of shape and peak location but a larger difference is observed in the magnitude of the peak point, Figure 3.9(b). The New Jersey mixture master curves follow distinctly different shapes and the peak points do not match, Figure 3.9 (c). It should be noted here that the Hirsch model predictions here utilized binder |G*| values that were predicted from |E*| values. Ones again due to lack of measured phase angle data it is difficult to comment as to which method provides more accurate predictions and the observations made here are purely comparative in nature.

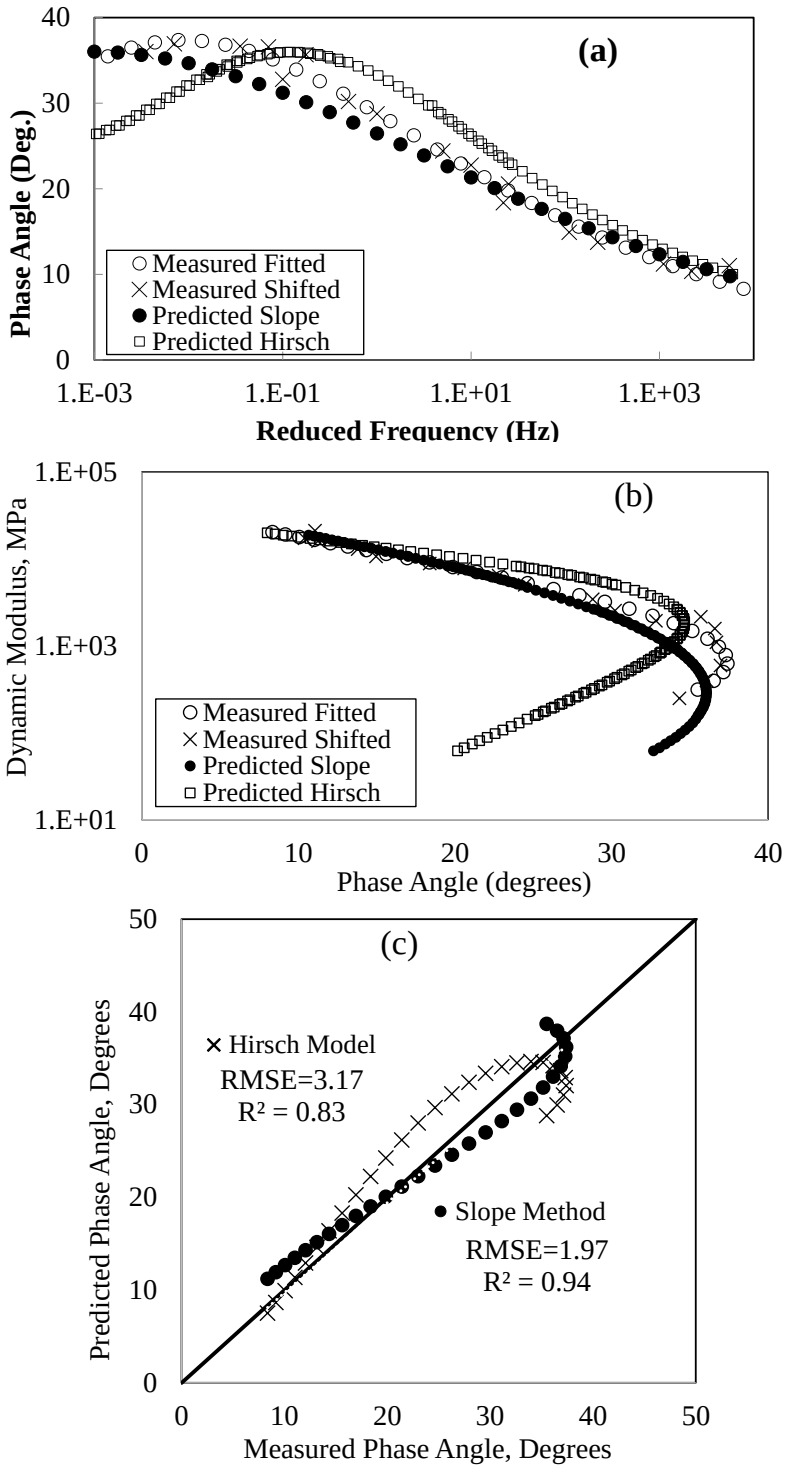

Figure 3. 8 Phase angle master curves (b) Black Space diagram (c) line of equality plot for phase angle predicted using slope and Hirsch model

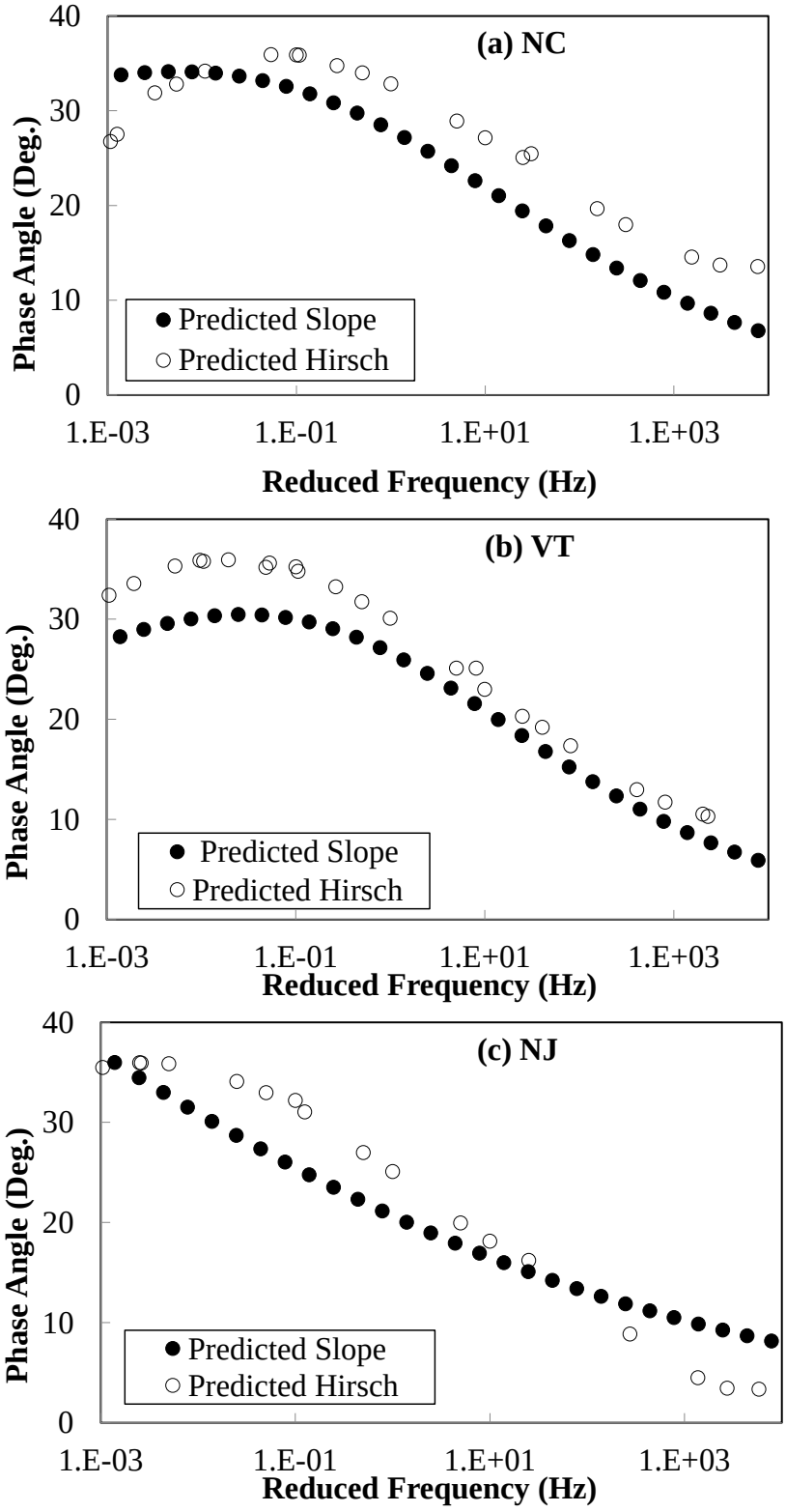

Figure 3. 9 Phase angle predicted using Slope and Hirsch (a) NC (b) VT (c) NJ

3.3.3 Impact on Pavement Performance Evaluation

3.3.3.1 Mixture Black Space Diagram

The mixture Black space diagrams produced using measured and predicted phase angles are shown in Figure 3.10. These plots correspond to the best and worst match between lab measurement and slope prediction among C-9.5mm and L-9.5mm mixtures. Since the |E*| values are the same, the difference due to use of measured versus predicted phase angle is a shift to the right or the left. For the best fit the measured black space points are shifted to the left very slightly. For the poorest fit, there is a larger difference between the points, with the largest difference at 500 rad/s.

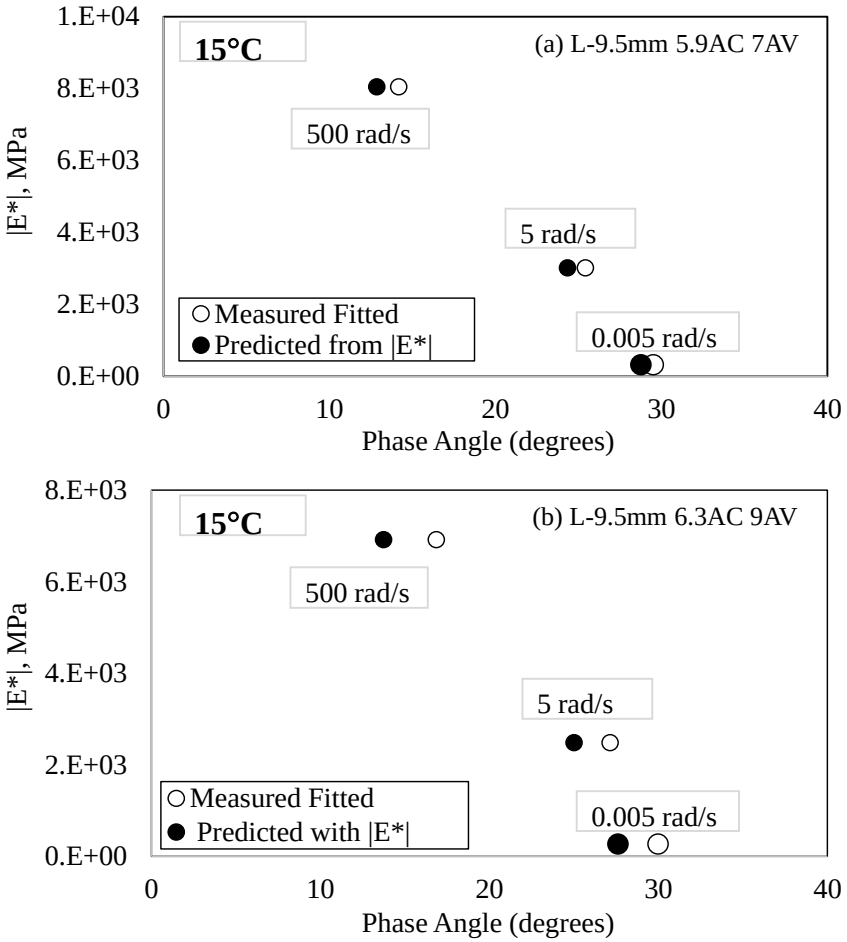

Figure 3. 10 Black Space points determined using predicted and measured phase angle (a) L-9.5mm 5.9AC 7AV (b) L-9.5mm 6.3AC 9AV

3.3.3.2 Pavement Fatigue Life Evaluation, S-VECD and LVECD

The damage characteristic curves (C versus S) and the fatigue failure criterion curves (G^R versus N_f) are generated using measured and predicted phase angle values and are shown in Figures 3.11 and 3.12, respectively. The L-9.5mm 5.9AC 7AV and C-12.5mm 6.1AC 7AV mixture presented here represent the best and worst matches. The damage characteristic and failure criterion curves are almost identical for the best match case. The worst match case shows slightly different damage characteristic curves and a shifted failure criterion curve. The values of the model parameters (a, b, r and s) show how similar the best match curves are and the difference in the worst fit.

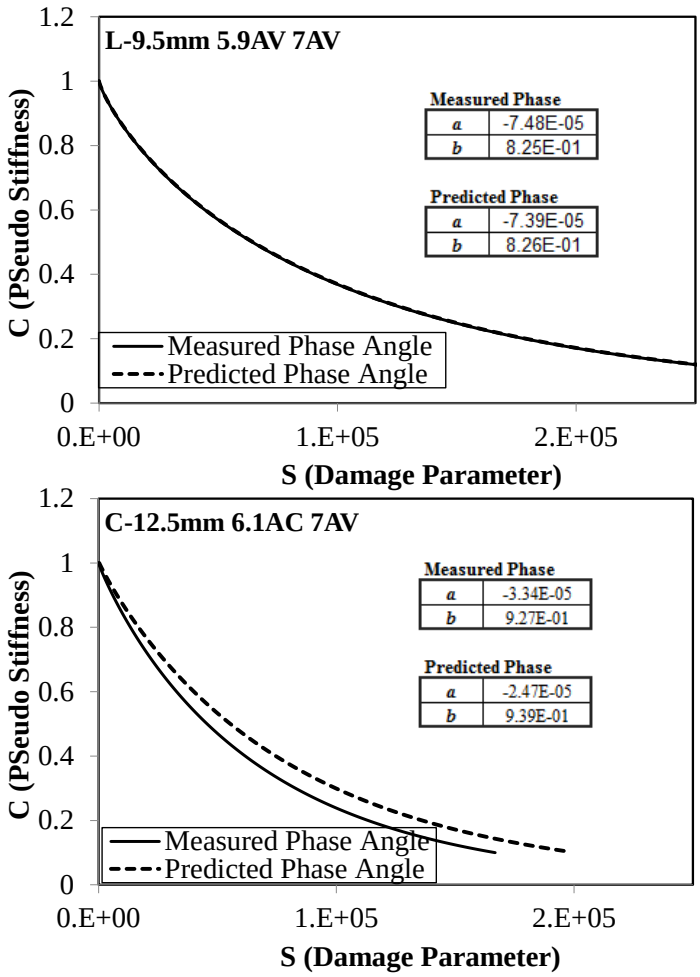

Figure 3. 11 Damage characteristics curves (C versus S) with measured and predicted phase angle

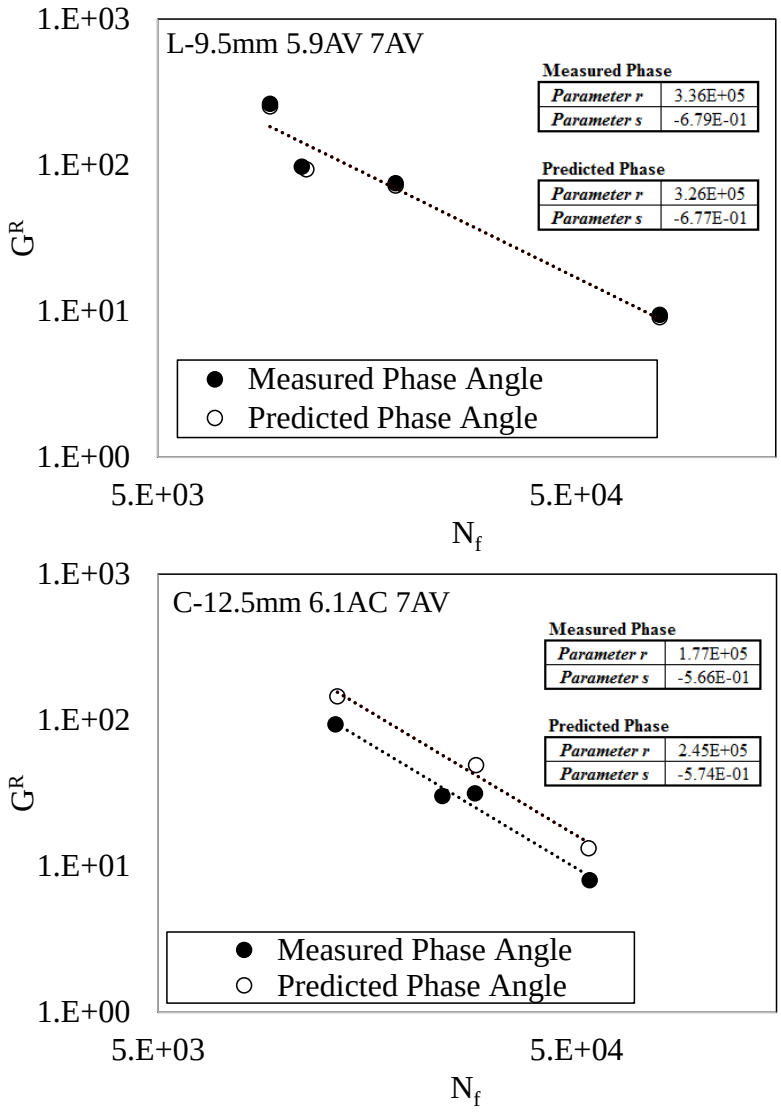

Figure 3. 12 Damage characteristics curves (G^R versus N_f) with measured and predicted phase angle

Figure 3.13 shows the predicted number of failure points in the pavement over 20 years of service for the L-9.5mm 5.9AC 7AV (best match among phase angle values) and C-12.5mm 6.1AC 7AV (worst match among phase angle values) mixtures from the LVECD pavement evaluation. As expected, the pavement simulations for the mixture with the least difference between measured and predicted generated nearly identical curves. The mixture with worst match between measured and predicted phase angles shows a difference of approximately 25 failure points at the end of the analysis period (20 years); this translates to a decrease of approximately 25% in the number of failure points with the predicted values. However, when

this is translated to the percentage of failed points in the overall structure the difference is only 2% (7% using the predicted values, 9% using the measured values). Since the LVECD model is not calibrated with field performance data, it is difficult to translate the differences to actual field cracking and whether this magnitude of difference would change any decisions that would be made with respect to using this mixture or design.

Generally, mixtures where the spring loaded LVDT is used exhibited less variation among measured and predicted values and hence, with missing phase angle data, the phase angle obtained from the slope-based method can be used for linear viscoelastic characterization of mixes in the S-VECD and L-VECD models to obtain a comparable fatigue performance prediction.

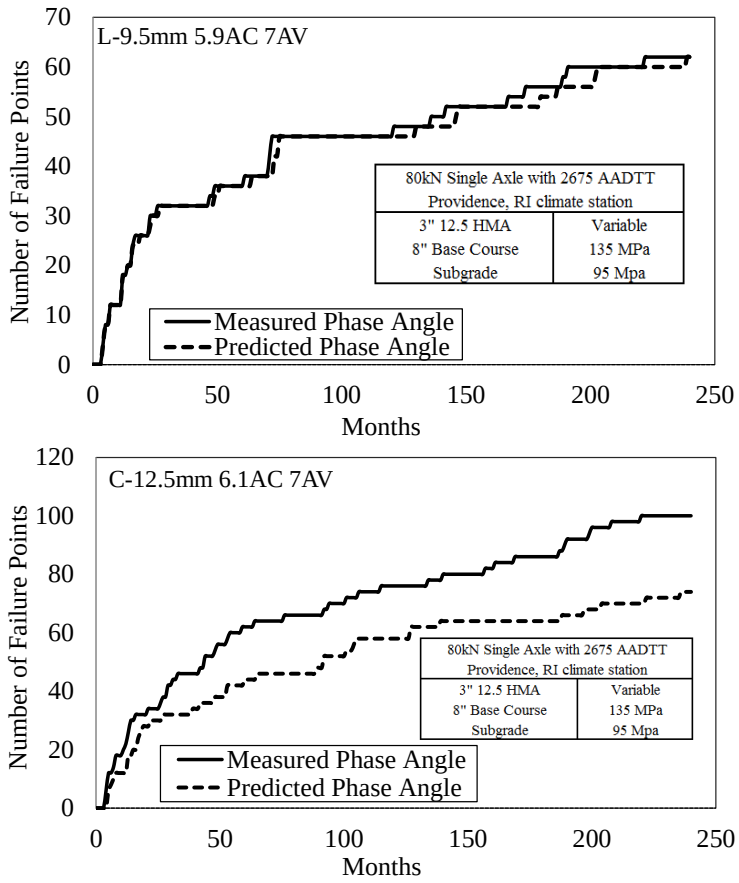

Figure 3. 13 LVECD pavement simulation with predicted and measured phase angle

3.4 Summary and Conclusion

In this study, a fundamental relationship to determine the phase angle from the slope of the log-log of |E*| master curve is evaluated using three sets of independent mixtures. The validity of the method is investigated by comparing predicted values with lab measurements. Further comparison is performed between lab measurements, the slope method, and Hirsch model values. Statistical quantities are calculated to examine the accuracy of the phase angle estimations. Rheological parameters are generated using measured and predicted values and compared. Finally, fatigue characterization using S-VECD approach and pavement evaluation using the LVECD model is conducted using measured and predicted phase angle values to assess the implication of using one over the other in fatigue performance prediction. The following conclusions are drawn based on the observations:

- Overall, the variability in |E*| measurement between replicates was low. Due to this the predicted phase angle values from average |E*|, low and high range |E*| were very close.
- For specimens where the lab measurements were done using spring loaded LVDTs, measured phase angle values match very well with values predicted using the slope method with an average difference of less than two degrees. However, a larger difference (up to an average difference of five degrees) is observed for specimens that used loose core LVDTs for measurement. The highest differences are observed around the peak values where the phase measurements are also more variable due to high test temperatures or low test frequencies. Further study is needed to determine the exact attribution of measurement inaccuracy on the observed differences due to type of LVDT and other factors.
- Generally, the predicted phase angles from the slope method are consistently lower than lab measured values. Two hypotheses were presented as to why this might be observed

for the majority of mixtures. The first is that neglecting the plastic response that might be present at lower frequencies and higher temperatures may cause the measured phase angle to be higher than it actually is. The second reason could be attributed to the complexity in phase angle calibration. The calibration performed at zero phase angle might cause bias during lab measurement of phase angle at different temperatures and frequencies.

- The phase angle master curves constructed from lab measurements and predicted using the slope method follow a comparable shape and exhibit very similar inflection points.
- Though extensive study has not been done for comparing lab measurement, Hirsch model, and slope method, it is observed that measured and slope method values agree very well in terms of master curve shape and magnitude as compared to the Hirsch model. The same interpretation applies for the Black Space diagram generated from the three methods. The comparison between Hirsch and slope methods using LTPP data showed the possible differences that arise due to the use of one method over the other. At different instances the phase angle curves were different in magnitude, shape and peak point location. Generally, it is observed that the Hirsch model lacks flexibility in terms of shape due to the underlying functional form of the model.
- The mixture Black Space points generated using both measured and predicted phase angles from the slope method are comparable.
- For the two set of mixtures corresponding to best match among predicted and measured phase angle values, the damage characteristics curves from S-VECD and number of failure points from LVECD were similar, indicating the phase angle predicted from the slope method can be used when no phase angle data is present for linear viscoelastic characterization of mixtures without affecting the results.

The advancement in pavement performance mechanistic models calls for better accuracy in material characterization. The estimation of phase angle from measured stiffness using the slope method is viable due to availability and growing reliability of stiffness measurements with advancements in equipment as compared to phase angle measurements. With the availability of such a simple and robust method, the phase angle can be computed from |E*| master curves for mixtures where phase angle measurements are missing. This also largely applies to LTPP data. Subsequently, rheological indices which require phase angle can be generated from historic data and can be calibrated with available field performance data. The study also gives insight to some bias that exists during lab measurements.

Since the validation of the prediction of phase from slope of log-log curve is done by comparing with lab measured values, any bias on lab measurement presents the same bias on the validation. Future work is needed to identify the magnitude of bias. Moreover, the binder grades evaluated in this study are limited to PG 58-28 and PG 64-28 binders that are extensively used in the Northeastern part of the United States. Future study is recommended to evaluate the influence of binder grade on the prediction capability of the proposed method. Furthermore, future study should look at the potential effect of permanent strain that could be encountered during complex modulus testing (acceptable up to 1500μs according to AASHTO T 342). Finally, the validity of the method to polymer modified and aged mixtures should be investigated by employing the method described in this study to determine if the modification and aging alters the relationship between dynamic modulus and phase angle.

3.5 Acknowledgments

The authors would like to acknowledge New Hampshire and Rhode Island Department of Transportations for providing the materials for this study. Acknowledgement is also extended to Katie Haslett for her assistance with specimen preparation at University of New Hampshire.

CHAPTER 4: EXPLORING MASTER CURVE PARAMETERS TO DISTINGUISH BETWEEN MIXTURE VARIABLES

4.1 Introduction

It is well known that the common mixture variables such as aging level, rejuvenator use and dosage, content and type of recycled materials (Reclaimed Asphalt Pavement (RAP) or Recycled Asphalt Shingles (RAS)), and binder grade alter the rheological properties of asphalt concrete mixture which are important for design and modeling of asphalt pavements. The ability to understand the changes in rheological properties caused by changes in the mixture variables is beneficial to quantify the effect on mixture field performance. Rheological evaluation of asphalt concrete mixtures is commonly done by measuring the dynamic modulus (|E*|) and phase angle (ϕ) to produce |E*| and ϕ master-curves for a range of temperature and frequency combinations. These two parameters can be determined at the mixture design or production stage directly by performing the complex modulus test (AASHTO T 342, 2015) or indirectly from relaxation modulus and creep compliance tests through interconversion (Baumgaertel et al., 1989; Park and Kim 1999). Moreover, different researchers have developed regression equations that can be used to determine dynamic modulus (Bari et al., 2006; Christensen et al., 2003) as well as phase angle (Rowe, 2009a; Oshone et al., 2017) values mainly from mixture design parameters. A study by Oshone et al. (2017) proposed an approach for obtaining dynamic modulus master-curves from falling weight deflectometer (FWD) measurements taken throughout the pavement life. Due to the increasingly reliable and versatile ways to determine |E*| and ϕ master curves at different stages of the pavement life,

researchers have tried to investigate the ability of master-curve parameters to track the changes in mixture properties due to different mixture variables (Mensching et al., 2017; Rowe et al., 2009b, Kaseer et al., 2017). However, previous studies have not focused on a comprehensive statistical analysis to link the changes in mixture variables to master curves parameters.

In this study, a comprehensive statistical analysis was performed to investigate the ability of master curve parameters to capture changes in mixture properties due to aging level, the addition of RAP/RAS, dosage of rejuvenator, and change in binder grade. Evaluated master-curve parameters are the mixture Glover-Rowe (G-R) parameter which relates |E*| and ϕ in Black space, and master-curve shape parameters (log of the inflection point frequency ($-\beta/\gamma$), log of the distance between the glassy modulus and the inflection point modulus (γ), $-\beta/\gamma$ vs γ and lower and upper asymptotes of the sigmoidal form of the master curve). The effect of the changes in the parameters on performance due to variation in the mixture variables is described qualitatively. It is believed that the master curve parameters identified in this study can be used by mixture specifiers and producers during design, construction and service life of the pavement to determine the effect of the different mixture variables on performance.

4.2 Materials and Methods

For this study 29 mixtures were used. The mixtures include eight mixtures from Texas, five mixtures from Nevada, three mixtures from Indiana and four mixtures from Wisconsin that are being evaluated as part of the NCHRP 9-58 project. The variables in these mixtures include aging levels (short-term oven aging (STOA) and long-term oven aging (LTOA)), rejuvenator dosage, recycled binder ratio ((RBR) which defines the amount of RAP and RAS binder in the mixture as percent of total binder), binder grade (PGHT (high temperature performance grade), PGLT (low temperature performance grade) and PG spread (the difference between high and low temperature performance grade). Nine mixtures from New Hampshire (NH) are also

included. These mixtures represent different percentages of RAP and RAS, binder grade and different aging levels (STOA and LTOA). The LTOA includes 5 days at 85ºC on compacted specimens, and 5 days at 95ºC, 24 hours at 135ºC and 12 days at 95ºC on loose mixture. Table 1 shows the mixture variables considered for the study along with the levels considered. All the mixtures were designed to optimum asphalt content using Superpave approach and test specimens were produced at a consistent air void level.

|E*| and ϕ master curves were produced using isotherms measured at three temperatures and six frequencies. A generalized sigmoidal equation with five parameters (indicated in Equation 4.1) was used to fit the |E*| master curves: ω is loading frequency, δ is the lower asymptote, α is the difference between the values of upper and lower asymptote and λ, β and γ define the shape between the asymptotes and the location of the inflection point.

$$log|E^*| = \delta + \frac{\alpha}{\left(1+\lambda e^{[\beta+\gamma(logw)]}\right)^{1/\lambda}} \quad [4.1]$$

The mixture G-R parameter in Black space and master curve shape parameters investigated in this study are described below and are illustrated in Figures 4.1(a) and (b).

- Mixture G-R parameter (|E*| cosϕ^2/sinϕ) combines the |E*| and ϕ values to describe the stiffness and relaxation properties of an asphalt concrete mixture. For this study the parameter was determined at 15ºC and 5 rad/s to track the changes in mixture properties due to changes in mixture variables.

Table 4.1 Mixtures information

Mixture Variables	Range of Mixture Variables				
	Texas	**Nevada**	**Indiana**	**Wisconsin**	**New Hampshire**
RBR (%)	0-50	0-30	0-42	27-36	20-30
Rejuvenator, %	0-12.5	0-2	0-3	1.2	-
PGHT, ºC	64, 70	64	59	52, 58	52, 58
PGLT, ºC	-22, -28	-28	-28	-28, -34	-28, -34
PG spread, ºC	86, 92	92	86	86	86
Aging level	5 days 85ºC[a]	5 days 85ºC[a]	5 days 85ºC[a]	5 days 85ºC[a]	5 days at 85 ºC[a] 5 days at 95 ºC[b] 24 hours at 135 ºC[b] 12 days at 95ºC[b]

[a] aging on compacted specimens [b]aging on loose mixture

- Log of the inflection point frequency (-β/γ) describes the elastic-viscous transition exhibited as a result of a shift from aggregate structure to binder dominating behavior. It marks the peak of the ϕ master curve or the inflection point in the |E*| master curve.

- Log of the distance between the glassy modulus and the inflection point modulus (γ) describes the width of the relaxation spectra and is computed from the difference between the glassy modulus and infection point modulus. As the |E*| master curve flattens which typically happens with aging, the γ value increases.

- Lower (δ) and upper (δ+α) asymptotes represent the maximum and minimum points of the |E*| master curves and are primarily related to aggregate properties.

- -β/γ vs γ shows the log of the inflection point frequency against the log of the distance between the glassy modulus and the inflection point modulus. This is similar to the plot of crossover frequency versus rheological index for binders. The points are expected to move to bottom right with aging and to the top left corner with the addition of rejuvenators as indicated in Figure 4.1(b) (Rowe, 2014). In this study the effects from the two parameters are combined by calculating ($-\beta/\gamma^2$) to obtain a single term that can be used in the regression

analysis. While the term doesn't have a physical meaning, this is done to capture the combined effect from the shift in both parameters as material properties changes due to change in the mix variables. For example, with aging the -β/γ term shifts to the left (to a more negative value) whereas the γ term shifts to the right (to a lower negative value). To account this opposite effect the reciprocal of the γ term is multiplied by the -β/γ term resulting in the $-\beta/\gamma^2$ parameter considered in the study for regression analysis.

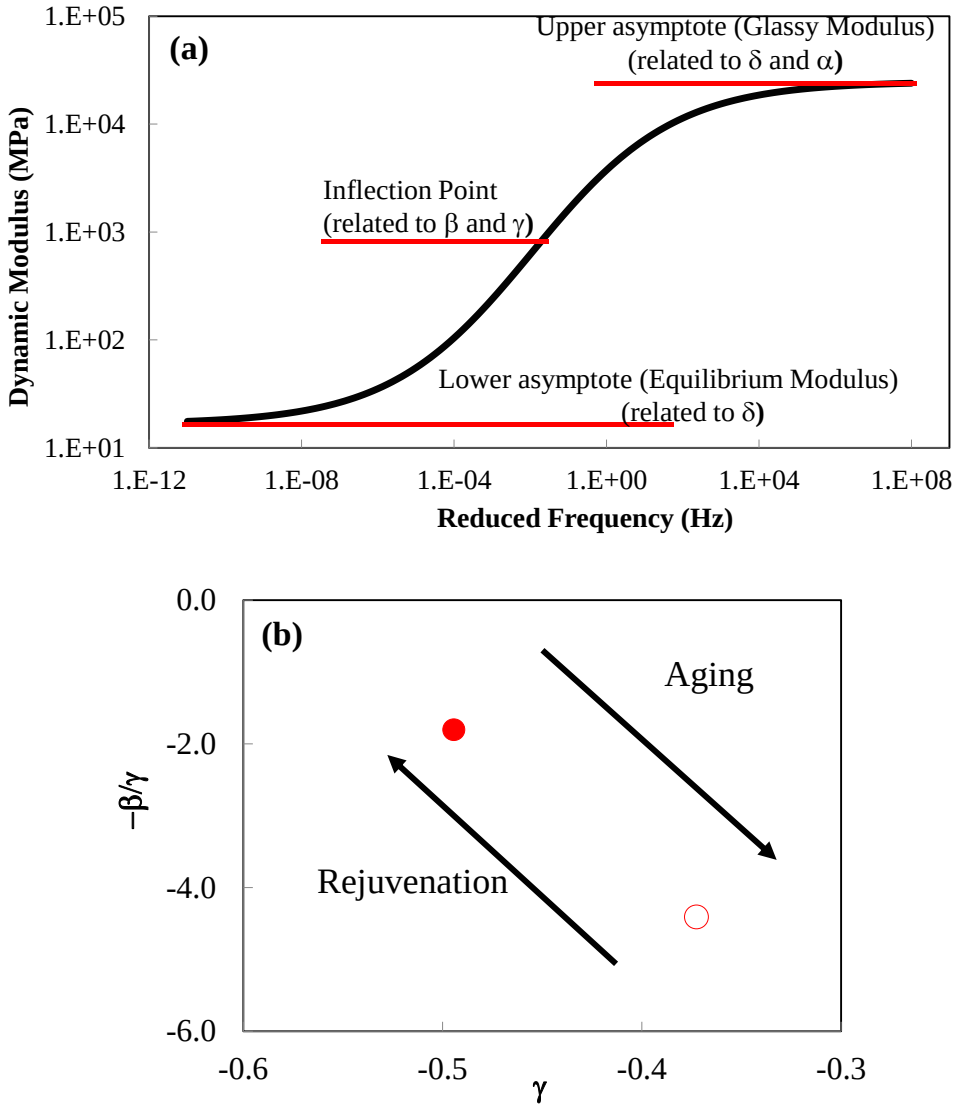

Figure 4. 1 (a) |E*| Master curve shape parameters (b) -β/γ vs γ plot showing impacts of aging and rejuvenation

A stepwise regression analysis performs an iterative screening to determine the presence of a mathematical relationship between two variables such that a linear function of one can predict the other at a given confidence level. In this study a stepwise regression analysis was utilized to identify the significance of the different mixture variables on the master curve parameters. The analysis made inferences about the larger population to recognize the ability of master curve parameters to capture the changes in mixture properties caused by changes in mixture variables. This was accomplished by using the p-values from the analysis as an indicator for the existence of a relationship. For this study, the common practice of utilizing p-value < 0.05 is adopted and the null hypothesis is rejected for a p-value <0.05 indicating the mixture variables has contributed significantly to the changes observed in the master curve parameter.

4.3 Results and Discussion

The stepwise regression analysis performed on study mixtures was able to provide a platform to distinguish between master curve parameters that can track the changes in mixture properties due to aging level, RBR, rejuvenator dosage and binder grade. The p-values obtained from the analysis are presented in Table 4.2. A p-value < 0.05 was used as a threshold to identify the existence of a relationship between the mixture variables and the master curve parameters. In other words, a p-value of <0.05 (indicated in bold) shows the ability of the master curve parameter to capture the change in mixture property caused by the corresponding mixture variable.

Table 4.2 p-values from stepwise regression analysis

Mixture Variables	G-R Parameter	$-\beta/\gamma^2$	$-\beta/\gamma$	γ	δ	$\delta+\alpha$
Aging	**<0.001**	**<0.001**	**<0.001**	**<0.001**	**<0.001**	**<0.001**
RBR	**0.05**	0.57	0.20	0.55	0.91	0.18
RA	0.90	0.90	0.89	0.32	0.70	0.30
PGHT	0.16	0.37	0.29	**0.05**	0.35	0.20
PGLT	**0.02**	0.49	**0.05**	0.11	**0.04**	0.25
ΔPG	0.67	0.80	0.59	0.71	0.35	0.95

Mixture G-R parameter - The regression analysis indicated the ability of the mixture G-R parameter to capture the changes in mixture properties caused by aging, RBR and PGLT of the binder (p-value for aging <0.001, RBR=0.05 and PGLT=0.02). The changes due to aging are shown in Black space diagram (Figures 4.2(a) and (b)), which similarly combines the effects of |E*| and ϕ in one plot. The plot shows that with aging the points shift towards the top left implying a change to a stiffer and less viscous material. For NH mixtures the shift increases as the aging level changes from 5 days at 85ºC to 5 days at 95ºC followed by 12 days at 95ºC and 24hr at 135ºC, Figure 4.2 (b). This increment in increasing stiffness and decreasing relaxation capacity is expected to increase the propensity of the mixture to cracking. In addition to the aging effect, the mixture G-R parameter appears to capture the effects of RBR and low temperature grade which also play a significant role in the cracking property of asphalt mixtures. The cumulative effect of these three parameters can be tracked and entered into a pavement performance prediction model to quantify the effect on field performance.

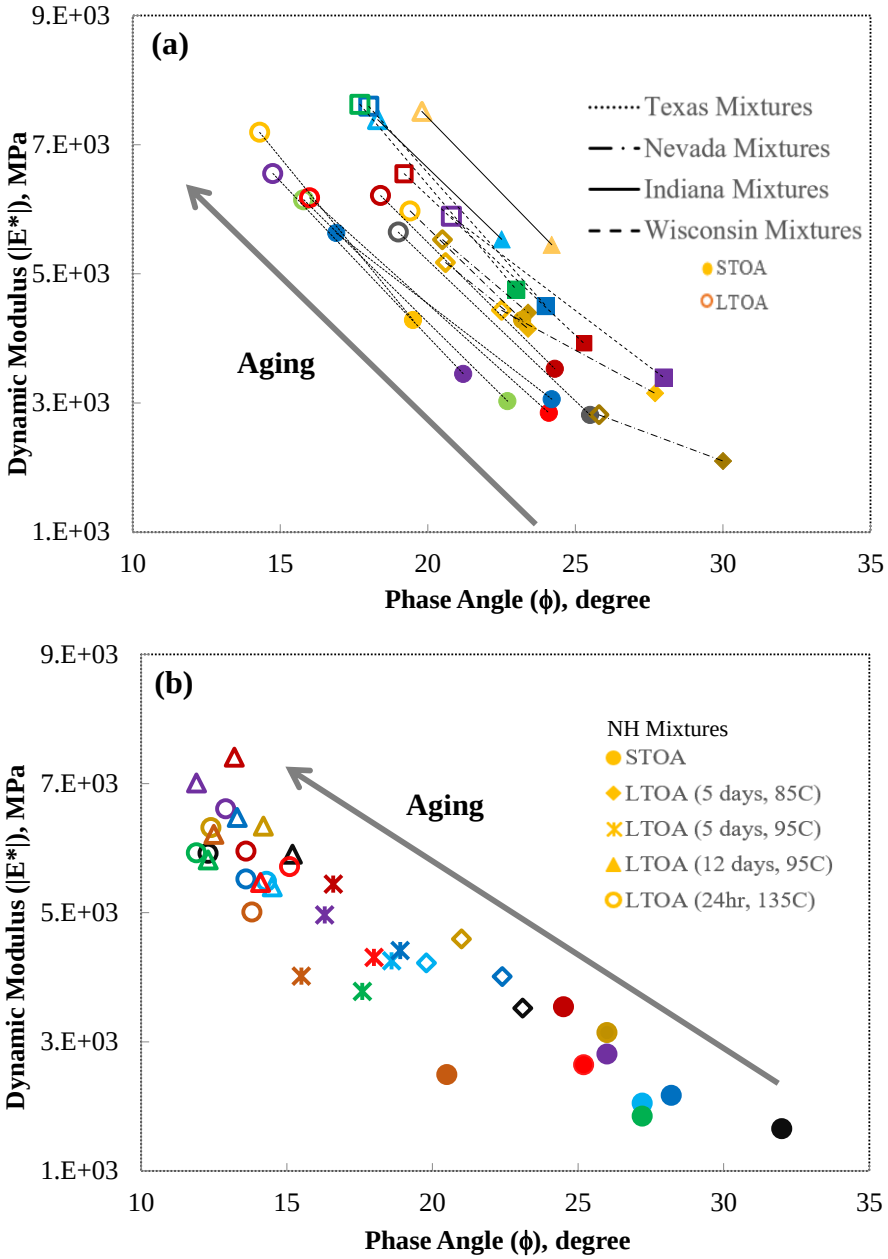

Figure 4. 2 Shift in Black Space points (15ºC and 5 rad/s) due to aging (a) NCHRP mixtures (b) NH mixtures

$-\beta/\gamma$ vs γ parameter – The regression analysis indicated that the changes in the $-\beta/\gamma^2$ term are primarily impacted by aging (p-value <0.001). These changes in the $-\beta/\gamma$ vs γ points due to aging are shown in Figures 4.3 (a) and (b). The plots show that the $-\beta/\gamma$ vs γ points tend to shift towards the bottom right with aging with the exception of one mixture where the point shifted vertically indicating no change in γ with aging. For NH mixtures the shift increases as the aging

level changes from 5 days at 85ºC to 5 days at 95ºC followed by 12 days at 95ºC and 24hr at 135ºC which is a similar observation from the Black space plot in Figure 4.2 (b). This shift occurs due to the movement of the inflection point to the left in the |E*| master-curve as a result of the change in dominance of the binder at a lower loading frequency due to age induced decrease in viscosity. Moreover, with aging a larger width of the relaxation spectra is exhibited. A combination of the lower relaxation capacity and increased relaxation width results in a mixture that is more susceptible to thermal cracking. The researchers recommend the use of the $-\beta/\gamma$ vs γ plot when tracking changes in mixture properties only due to aging.

$-\beta/\gamma$ parameter - The $-\beta/\gamma$ parameter when considered separately appears to be influenced by both aging and PGLT of the binder. This indicates that a shift in inflection point frequency is mainly a result of a change in these two parameters and can be used to track the changes in material properties due changes in these two mixture variables.

γ parameter - The statistical analysis shows the ability of the γ parameter to capture the changes due to aging and PGHT of the binder. With aging, the dynamic modulus curve becomes flatter which increases the width of the relaxation spectra resulting in a greater propensity to thermal cracking.

Lower and upper asymptote - Both lower and upper asymptote appear to be affected by aging whereas only lower asymptote is impacted by PGLT.

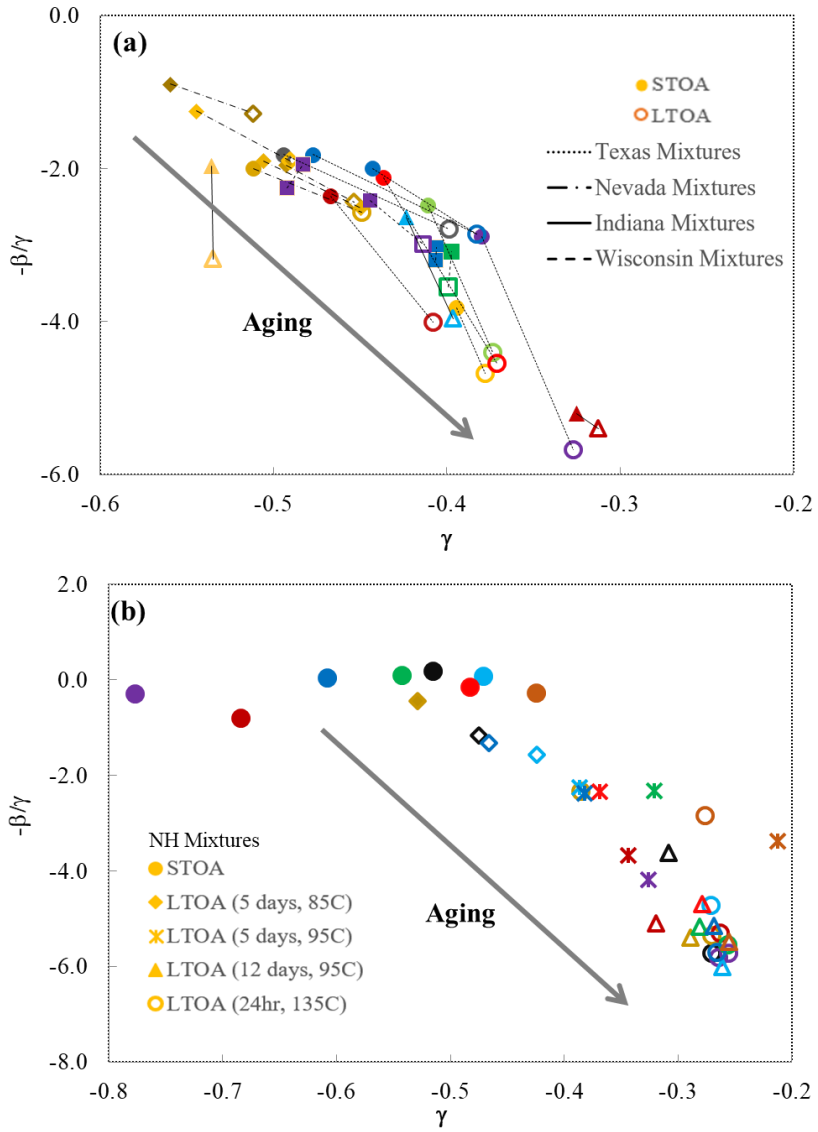

Figure 4. 3 Shift in -β/γ vs γ points due to aging (a) NCHRP Mixtures (b) NH Mixtures

It should be noted that all master-curve parameters were able to capture the effect of aging whereas on the contrary the effects of rejuvenator were not captured by any of the parameters. The authors believe that the use of low dosages and different types of rejuvenators for the mixtures obtained from Texas, Nevada, Indiana and Wisconsin could have impacted the mixture parameters differently resulting in the statistically insignificant effect of the rejuvenator on the rheological properties of the mixture.

It is believed that the changes observed in the master-curve parameters can be attributed to changes in mixture field performance. Therefore, these changes can be entered into pavement performance prediction models to quantify the effect of aging level, addition of rejuvenator, recycled material binder content and binder grade on field performance of asphalt concrete mixtures.

4.4 Summary and Conclusion

In this study master curve parameters such as the G-R parameter, log of the inflection point frequency (-β/γ), log of the distance between the glassy modulus and the inflection point modulus (γ), -β/γ vs γ and lower and upper asymptote of the sigmoidal form of master curve were investigated to identify their ability to distinguish between mixture variables by performing a comprehensive statistical analysis. The evaluated mixture variables included aging level, rejuvenator dosage, RBR, and binder grade. A stepwise regression analysis conducted on the mixtures indicated that the mixture G-R parameter can capture the changes in mixture properties due to aging, RBR, and PGLT whereas the $-\beta/\gamma^2$ term was able to capture the effect of aging only. A shift of Black space points to the top left has been observed with aging whereas the opposite trend was observed in the -β/γ vs γ plot which is associated more with cracking susceptibility in both cases.

Depending on the mixture specifier's or producer's interest in evaluating the effect of one or more of the mixture variables, the parameters identified in this study can be used to track the changes in rheological properties due to changes in specific mixture variables.

It is believed that the changes observed in the master curve parameters can be attributed to changes in mixture field performance. Therefore, in future work these changes will be used to illustrate the changes in mixture field performance due to the presence of RAP/RAS, addition of rejuvenator, binder grade and aging level. This will be done by quantifying the changes in

master curve parameters and inputting the values into pavement performance prediction models.

CHAPTER 5: ASSESSMENT OF VARIOUS APPROACHES TO DETERMINING BINDER BENDING BEAM RHEOMETER LOW TEMPERATURE SPECIFICATION PARAMETERS FROM DYNAMIC SHEAR RHEOMETER TEST

5.1 Introduction

In an effort to develop a performance based specification for asphalt binders, the Strategic Highway Research program (SHRP) developed a new system of binder grading (Superpave system) based on rheological properties measured using Dynamic Shear Rheometer (DSR) and Bending Beam Rheometer (BBR) (Hardin 1995). During its first development, DSR was devised to measure binder rheological properties at intermediate and high temperatures. Due to issues associated with DSR instrument compliance to measure binder properties below 5°C, the second instrument, Bending Beam Rheometer (BBR) (AASHTO T 313, 2008), was developed to measure the low temperature rheological properties of asphalt binders.

The DSR test was originally introduced as a standard method to characterize the rheological properties of asphalt binders at intermediate and high temperatures using 8 and 25 mm parallel plates, AASHTO T 315 (2000). From the test, the shear modulus (|G*|) and phase angle (ϕ) of asphalt binders at a range of temperatures is determined. Then, limiting parameters developed based on |G*| and ϕ are used to grade asphalt binders based on their projected performance with respect to fatigue and rutting. Recently, researchers have made an effort to investigate the applicability of 4 mm parallel plates in the DSR for low temperature asphalt binder rheological characterization (Derewecki, 2013). Following this effort, the Western Research Institute (WRI) has successfully developed a 4 mm DSR approach and made it possible to reliably

measure binder properties at low temperatures as low as -40ºC by applying instrument compliance corrections on the DSR measurements (Sui et al. 2010 and 2011). Further details on the method is available in the draft AASHTO standard "Standard Method of Test for Determining the Low Temperature Rheological Properties of Asphalt Binder Using a Dynamic Shear Rheometer (DSR)" (AASHTO, 2012)

The BBR test is introduced to assess the low temperature properties of asphalt binder taking into account both the stiffness and relaxation properties from a creep test. The test output is used to determine the low temperature stiffness (S) and relaxation properties (m-value) to give an indication of the asphalt binder's capabilities to limit thermal stress generation and stress relaxation to provide good resistance to thermal cracking. The S and m-value are determined from the magnitude and the slope of the creep stiffness curve at 60 seconds loading time at test temperature of 10°C above the low temperature Performance Grade (PGLT + 10°C). The specification limits maximum stiffness of 300 MPa and minimum m-value of 0.300. To perform a full characterization at low temperature, the BBR method requires approximately 40 to 65 g of material. Obtaining this amount of material from asphalt mixture samples through extraction and recovery or emulsion residues from evaporative recovery is often difficult and time consuming.

Due to the substantially smaller amount of binder (approximately 0.15g) required for testing, increased reliability of DSR low temperature measurement and the possibility of using one equipment for full characterization of asphalt binders, researchers have investigated different approaches to determine low temperature parameters (S and m-value) from DSR testing. A study by Sui et. al (2011) showed S and m-value from BBR creep stiffness curve (S(t)) at 60s and 10ºC above the PG low temperature grade correspond to the magnitude and slope of the shear relaxation modulus curve (G(t)) interconverted from DSR measurement at 2 hours and PG low temperature grade. Later the temperature and time to determine the S and m-values

from DSR was modified to 60 s and PGLT + 10ºC (Farrar et al. 2015). A study by Rowe (2014b) developed an equation that can be applied to determine the BBR S and m-value from DSR shear modulus and phase angle or vice versa. The higher correlation observed between the parameters for the study binders showed the strength of the developed equation to estimate BBR S and m-value from DSR |G*| and ϕ . A study by Lu et al., 2017 indicated a certain statistical correlation between DSR dynamic modulus and BBR creep stiffness as well as between phase angle and m-value. Moreover, the study indicated a strong correlation between stiffness limiting temperatures determined from BBR and DSR whereas the correlation was weak for m-value limiting temperature. It should be noted that the methods proposed by Sui et al. (2011), Rowe (2014b) and Lu et al. (2015) implemented different methods to convert DSR complex modulus data to shear relaxation modulus or creep stiffness and subsequently to equivalent BBR S and m-value. Therefore, the method employed for interconversion plays a significant role and could significantly affect the S and m-value estimation from DSR.

A number of interconversion methods (exact and approximate) are available to estimate relaxation modulus and creep stiffness from complex modulus data. However, the applicability of the methods for any linear viscoelastic has to be investigated and determined per material type. With this aim Tarefder et al. (2016) validated the applicability of different interconversion methods for asphalt mixtures by showing a good agreement between laboratory measured data and interconverted relaxation and creep stiffness data. For the present study, the selection of an appropriate interconversion method is crucial in determining S and m-value from DSR data. Therefore, the study employed different interconversion methods and investigated their applicability and relative performance to convert DSR complex shear modulus to shear relaxation modulus and creep stiffness using lab measured asphalt binder data. The effectiveness of the methods is assessed by using graphical comparison as well as by comparing

the S and m-value determined from interconverted relaxation modulus and creep stiffness with measured BBR values.

The objective of this study is to assess applicability of determining low temperature BBR specification parameters, S and m-value, from DSR testing for twenty-two neat and extracted and recovered binders from mixtures with a wide set of variables. The variables in the mixtures includes (lab versus plant), aggregate size and gradation, binder PG grade and source, and recycled materials' type and content. Statistical analysis is employed between S and m-value estimated from DSR and measured S and m-value to examine the reliability and differences between the different approaches. Finally, a simple equation is developed to enable estimation of BBR specification parameters from a single point measurement of dynamic shear modulus and phase angle corresponding to BBR test temperature and single angular frequency.

5.2 Material and Testing

For this study, four virgin binders and 18 extracted and recovered binders were used. The variables in the mixture samples include production type (lab/plant), aggregate size (12.5mm/19mm), binder PG grade and source (PG 58-28/PG 52-34), recycled material type and content (RAP/RAS). The wide set of extracted and recovered binders used in this study is expected to give insight to the potential effect of these variables on the applicability and effectiveness of the evaluated methods. Information for the extracted and recovered binders (designated as 1-18) and virgin binders (designated as 19-22) is summarized in Table 5.1.

Extraction of binder was done using a centrifuge extractor and toluene solvent following the AASHTO T 164 procedure. Binder recovery was done in accordance with ASTM D7906-14 using a rotary evaporator. The extracted and recovered binder was then subjected to 20 hr PAV

aging; it was assumed that short term aging (normally done using RTFO) was completed through the plant production or short-term oven aging on the mixture in the laboratory.

The 4mm DSR testing was performed for binder characterization following the test procedure developed by Western Research Institute (Sui. et al., 2010) on all binders. The test was conducted at temperature ranges of -36 to 50°C and a frequency sweep at each test temperature from 100 radians/s to 0.2 radians/s using five test points per log decade for a total of 15 test values per test temperature. BBR testing was performed on extracted and recovered binders following the test procedure in AASHTO T313 to characterize low temperature binder properties. The test was conducted on all extracted and recovered binders at two temperatures: -12°C and -18°C for all except #15, 17 and 18 where the test is run at -6°C instead of -18°C. Low temperature cracking parameters, creep stiffness (S) and the rate of change of creep stiffness (m-value), corresponding to the test temperature and 60s loading time were obtained from the test. BBR testing on virgin binders is not performed.

Table 5.1 Binder and test information for study mixtures

#	Mixture Designation	Source of Mix	PG Grade	NMAS	% Total binder replacement	DSR	BBR test temperature
1	PG 58-28, 12.5, 18.9% RAP	Lab	58-28	12.5	18.9	✓	-18°C, -12°C
2	PG 58-28, 12.5, 18.9% RAP	Plant	58-28	12.5	18.9	✓	-18°C, -12°C
3	PG 52-34, 12.5, 18.9% RAP	Lab	52-34	12.5	18.9	✓	-18°C, -12°C
4	PG 52-34, 12.5, 18.9% RAP	Plant	52-34	12.5	18.9	✓	-18°C, -12°C
5	PG 58-28, 12.5, 28.3% RAP	Lab	58-28	12.5	28.3	✓	-18°C, -12°C
6	PG 58-28, 12.5, 28.3% RAP	Plant	58-28	12.5	28.3	✓	-18°C, -12°C
7	PG 52-34, 12.5, 28.3% RAP	Lab	52-34	12.5	28.3	✓	-18°C, -12°C
8	PG 52-34, 12.5, 28.3% RAP	Plant	52-34	12.5	28.3	✓	-18°C, -12°C
9	PG 58-28, 12.5, 18.5% RAP/RAS	Plant	58-28	12.5	18.5	✓	-18°C, -12°C
10	PG 52-34, 12.5, 18.5% RAP/RAS	Plant	52-34	12.5	18.5	✓	-18°C, -12°C
11	PG 58-28, 19, 31.9% RAP	Lab	58-28	19	31.9	✓	-18°C, -12°C
12	PG 58-28, 19, 31.9% RAP	Plant	58-28	19	31.9	✓	-18°C, -12°C
13	PG 52-34, 19, 31.9% RAP	Lab	52-34	19	31.9	✓	-18°C, -12°C
14	PG 52-34, 19, 31.9% RAP	Plant	52-34	19	31.9	✓	-18°C, -12°C
15	PG 58-28, 19, 20.8% RAP/RAS	Lab	58-28	19	20.8	✓	-12°C, -6°C
16	PG 58-28, 19, 20.8% RAP/RAS	Plant	58-28	19	20.8	✓	-18°C, -12°C
17	PG 52-34, 19, 20.8% RAP	Lab	52-34	19	20.8	✓	-12°C, -6°C
18	PG 52-34, 19, 20.8% RAP/RAS	Lab	52-34	19	20.8	✓	-12°C, -6°C
19	Virgin PG 58-28 source 1	Virgin	58-28	NA	NA	✓	NA
20	Virgin PG 58-28 source 2	Virgin	58-28	NA	NA	✓	NA
21	Virgin PG 52-34 source 3	Virgin	52-34	NA	NA	✓	NA
22	Virgin PG 52-34 source 4	Virgin	52-34	NA	NA	✓	NA

5.3 Research Approach

5.3.1 Shear Complex Modulus Master Curve Construction

For tests performed in the linear viscoelastic range, the time-temperature superposition principle can be applied to shift test isotherms to a reference temperature at a reduced frequency to construct a master curve. In this study, the RHEA^{TM} software (Rowe et al., 2001) is used to construct shear modulus, shear storage modulus, shear loss modulus and phase angle master curves by shifting DSR measured data points measured at different temperatures using the time temperature superposition principle. The shifting in RHEA^{TM} software is done following the work done by Gordon et al. (1994). The shifted data is then fitted to the Christensen, Anderson and Marasteanu (CAM) model, Marasteanu et al. (1999), Equations 5.1 to 5.3.

$$G^*(\omega) = G_g\left[1 + (\frac{\omega_c}{\omega})^{\beta}\right]^{-1/\beta} \quad [5.1]$$

$$\phi(\omega) = \frac{90}{\left[1 + (\frac{\omega}{\omega_c})^{\beta}\right]} \quad [5.2]$$

$$\beta = ln\left(\frac{G_g}{2}\right)/ln\left(G^*(\omega_c)\right) \quad [5.3]$$

where;

G(w)* = Complex shear modulus

Gg = Glassy modulus

w_c = cross over frequency

w_r = reduced frequency

β = fitting parameter

ϕ(ω) = phase angle

Figure 5.1 shows the shear complex modulus master curves constructed using data points obtained from DSR testing for the study binders. The plot is presented to show the good quality of the measured data shifted to reference temperature of -18°C. Accordingly, the shear modulus data for all binders was deemed acceptable for use in further analysis that includes estimation of relaxation modulus, creep stiffness and BBR S and m-value estimation. The plot also shows the stiffness difference between virgin and extracted and recovered binders. The four virgin binders have lower stiffness as compared to binders extracted and recovered from lab and plant produced material, as expected.

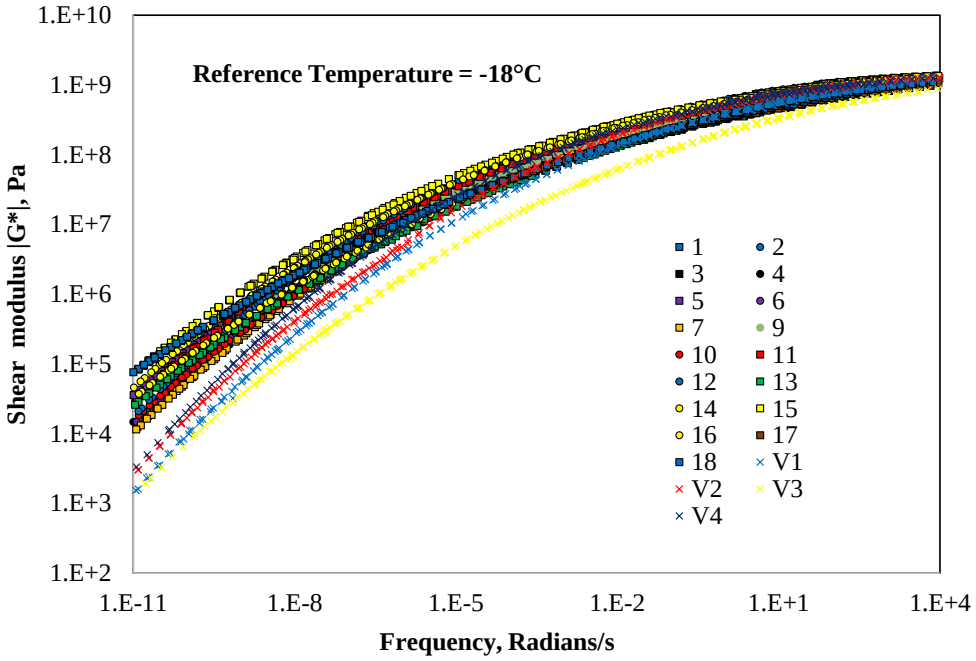

Figure 5. 1 Shear complex modulus master curves for study binders

5.3.2 Interconversion of Dynamic Data to Relaxation Modulus and Creep Stiffness

The methods investigated in this study to determine S and m-value from DSR data use the shear relaxation modulus or creep stiffness master curves that are interconverted from DSR data.

Therefore, it is important to understand the accuracy and differences among the different interconversion methods. This study employs the Christensen approximate interconversion equation which hereinafter will be referred as the Christensen method and the exact interconversion using a fitted generalized Maxwell model (referred to as Maxwell model) to determine the relaxation modulus and creep stiffness curves from the DSR complex modulus data and subsequently use them to determine S and m-value from DSR.

5.3.2.1 Christensen Approximation Method

Christensen (1982) proposed an approximate interconversion method expressed in Equation 5.4 to determine the relaxation modulus from complex modulus test data. The equation relates the relaxation modulus at time t to the shear storage modulus at a frequency ω, where $\omega = 2/\pi$. For this study, the shear storage modulus master curve is constructed at -18°C and -12°C using RHEA. Equation 5.4 is used to determine the shear relaxation modulus from the respective storage modulus curves.

$$G(t) \approx G'(\omega);\ \text{where},\ \omega = 2/\pi t \qquad [5.4]$$

5.3.2.2 Exact Interconversion using Fitted Generalized Maxwell Model

In the generalized Maxwell Model, complex shear modulus components (G' and G") and shear relaxation modulus (G(t)) are expressed by a discrete set of exponential decays, Equations 5.5 to 5.7. The generalized Maxwell model is fitted to complex modulus data to determine the parameters λ_i and g_i for *n* number of relaxation modes (or Maxwell units) (Equations 5.5 and 5.6) and the parameter values are then used in Equation 5.7 to determine the shear relaxation modulus for a required time range.

$$G'(\omega) = \sum^{n} g_i\ (\omega\lambda_i)^2/(1 + (\omega\lambda_i)^2) \qquad [5.5]$$

$$G''(\omega) = \sum^{n} g_i \ \omega\lambda_i/(1 + (\omega\lambda_i)^2) \quad [5.6]$$

$$G(t) = \sum^{n} g_i \ \exp(-t/\lambda_i) \quad [5.7]$$

where the *n* relaxation modes are defined by their relaxation strength g_i and their relaxation times λ_i.

For conducting an exact interconversion to shear creep compliance (J(t)) and to determine the creep stiffness S(t) from the relaxation spectrum, G(t), the following steps are employed:

1. Determine the Laplace transform of the relaxation modulus, Equation 5.8

$$G(S) = \sum_{i=1}^{N} \frac{g_i}{s + 1/\lambda_i} \quad [5.8]$$

2. The Laplace transform of relaxation modulus and the creep compliance are related as, Equation 5.9

$$G(s)\, J(s) = \frac{1}{s^2} \quad [5.9]$$

3. Substituting Equation 5.8 to Equation 5.9 and transforming to time domain using the inverse Laplace transform of J(s) gives Equation 5.10.

$$J(t) = J_g + \frac{t}{\eta} + \sum_{i=1}^{N-1} j_i \ \left[1 - \exp(-\frac{t}{\lambda_i})\right] \quad [5.10]$$

4. The creep stiffness S(t) and J(t) are related as expressed in Equation 5.11

$$S(t) = \frac{1}{J(t)} \quad [5.11]$$

5.3.3 Estimating BBR S and m-value from 4mm DSR Data

5.3.3.1 Method Developed by Sui et al., 2011

The successful application of instrument compliance correction to asphalt binders DSR testing by Sui et al. (2010) enabled researchers to measure low temperature rheological properties of asphalt binders reliably. Following this, Sui et. al. (2011) developed a method to determine BBR S and m-value from DSR test data. The method correlates the slope and magnitude of the shear relaxation modulus master curve, G(t), at 2700 s and binder PG low temperature grade to the S and m-value determined from BBR S(t) data at PGLT+ 10ºC and 60 s. Farrar et al. (2015) later modified the temperature and loading time combination to binder PGLT +10 ºC and 60s (similar to BBR temperature and loading time to determine S and m-value), Figure 5.2. This method is adopted in this study to determine S and m-value from shear relaxation modulus master curve interconverted from DSR data. The same temperature and loading time combinations as the BBR testing is used to allow direct comparison between S and m-value estimated from DSR to S and m-value determined from BBR testing.

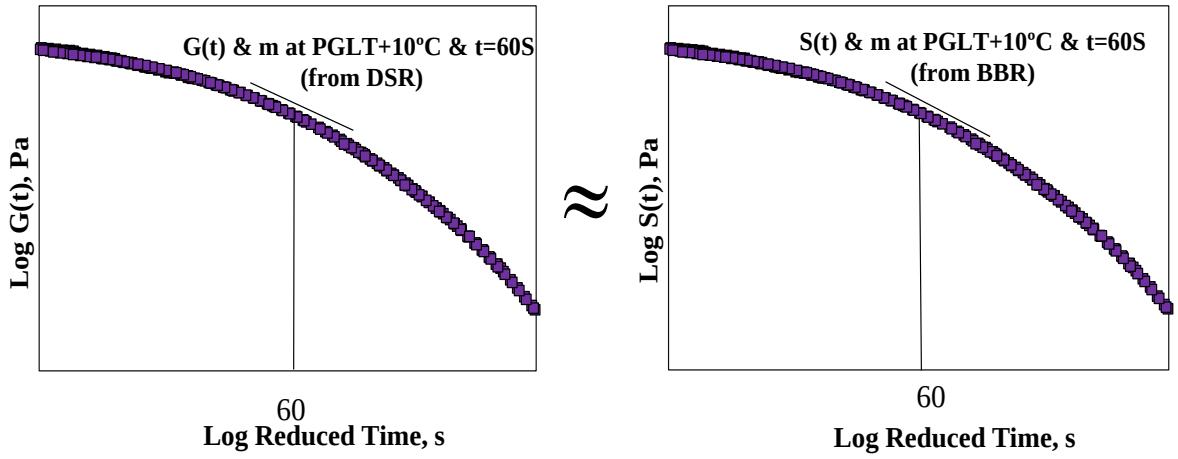

Figure 5. 2 Correlation of G(t) at PGLT+10ºC and 60S from DSR and S(t) and m at PGLT+10ºC and 60s from BBR

The low temperature grades of the binders used for this study are -28 ºC and -34 ºC. However, BBR testing was performed at -18 ºC and -12 ºC on the majority of the study binders and

subsequently the S and m-values corresponding to only these two temperatures and 60s loading time are available. This means if the above method is implemented and estimation of S and m-value from BBR is done at PGLT +10 ºC, comparison can only be made for the PG 58-28 binders which have a corresponding BBR measurements at -18 ºC. For this reason, the G(t) curves are constructed and subsequently used to determine the S and m-value from DSR testing at a constant temperature of -18 and -12 ºC. This allows for comparison of the S and m-values estimated from DSR data to the corresponding S and m-values determined from BBR test for all extracted and recovered binders.

5.3.3.2 Equation Developed by Rowe 2014

Rowe (2014b) investigated the possibility of a relationship between DSR parameters |G*| and ϕ, and the low temperature specification parameters S and m-value. The study was conducted on data obtained from six SHRP core asphalts. A strong correlation between the dynamic parameters |G*| and ϕ and BBR S and m-value was observed and Equations 5.12 and 5.13 were developed as a tool to estimate BBR S and m-value from DSR |G*| and δ or vice versa.

$$|G^*| = 0.3759\, S(t)^{0.9992} \quad (5.12)$$

$$\phi = -28.239\,(m)^2 + 96.858\,(m) \quad (5.13)$$

5.3.4 Development of Equation to Estimate BBR S and m-value from |G| and ϕ from DSR*

A study by Oshone et al. (2017) showed that the phase angle can be obtained from the slope of the modulus master curve, similar to the m-value which is estimated from the slope of the creep stiffness curve. Therefore, it is reasonable to assume a correlation exists between low temperature phase angle and m-value as well as creep modulus and dynamic modulus. A closer study of the

relationship between the parameters was performed using values calculated at the same temperature (-18°C) and equivalent loading time/angular frequency. The S and m-value correspond to a loading time of 60s whereas |G*| and ϕ correspond to an angular loading frequency of 0.0167 radians/s. These values were also used to develop a mathematical relationship between the parameters. This is done using a statistical software, JMP®, and by identifying the significance of the parameters on each other. The simple equation developed as part this study is believed to provide a platform for quick and reliable computation of S and m-value from a single measurement of shear modulus and phase angle at the stated temperature and frequency.

5.4 Results and Discussion

5.4.1 Comparison of Interconversion Methods

Figures 5.3 and 5.4 compare the shear relaxation modulus G(t) curves obtained using the Christensen approximate interconversion and the exact interconversion using generalized Maxwell method as well as the creep stiffness S(t) curves interconverted using the generalized Maxwell model from the DSR data. Due to the large number of samples and similarity in shear relaxation modulus and creep stiffness values for the majority of the samples, the plots comparing the relaxation modulus interconverted using the Christensen method and Maxwell model are presented separately (Figures 5.3a and 5.3b) from the plots comparing the relaxation modulus interconverted using Christensen method to creep stiffness interconverted using the Maxwell model (Figures 5.4a and 5.4b). Separate figures are also presented for binders extracted and recovered from plant mixtures and lab mixtures.

Figure 5.3 compares the shear relaxation curves interconverted using the Christensen and generalized Maxwell model for binders extracted from lab produced materials (Figure 5.4a) and

plant produced material (Figure 5.4b). Figure 5.4 compares the shear relaxation curves interconverted using the Christensen and the creep stiffness curve interconverted using the generalized Maxwell method for binders extracted from lab produced material (Figure 5.4a) and plant produced material (Figure 5.4b). The plot comparing the shear relaxation and creep stiffness curves estimated using Maxwell model is not presented here due to the similarity of the curves. From visual inspection, the shear relaxation modulus estimated using the Christensen method appear similar in shape and comparable in magnitude to the shear relaxation and creep stiffness curves estimated using generalized Maxwell model in both Figures 5.3 and 5.4. The approximate location and slope for the S and m-value estimation is also indicated in the figures to understand the differences and similarities at those specific locations. Again, with a visual inspection the magnitude and the slopes appear very close. Further quantification of the similarities and differences in terms of DSR S and m-value estimate is made in the subsequent section to better understand the impact of using either the G(t) or S(t) curves from the different interconversion methods on the S and m-value estimation.

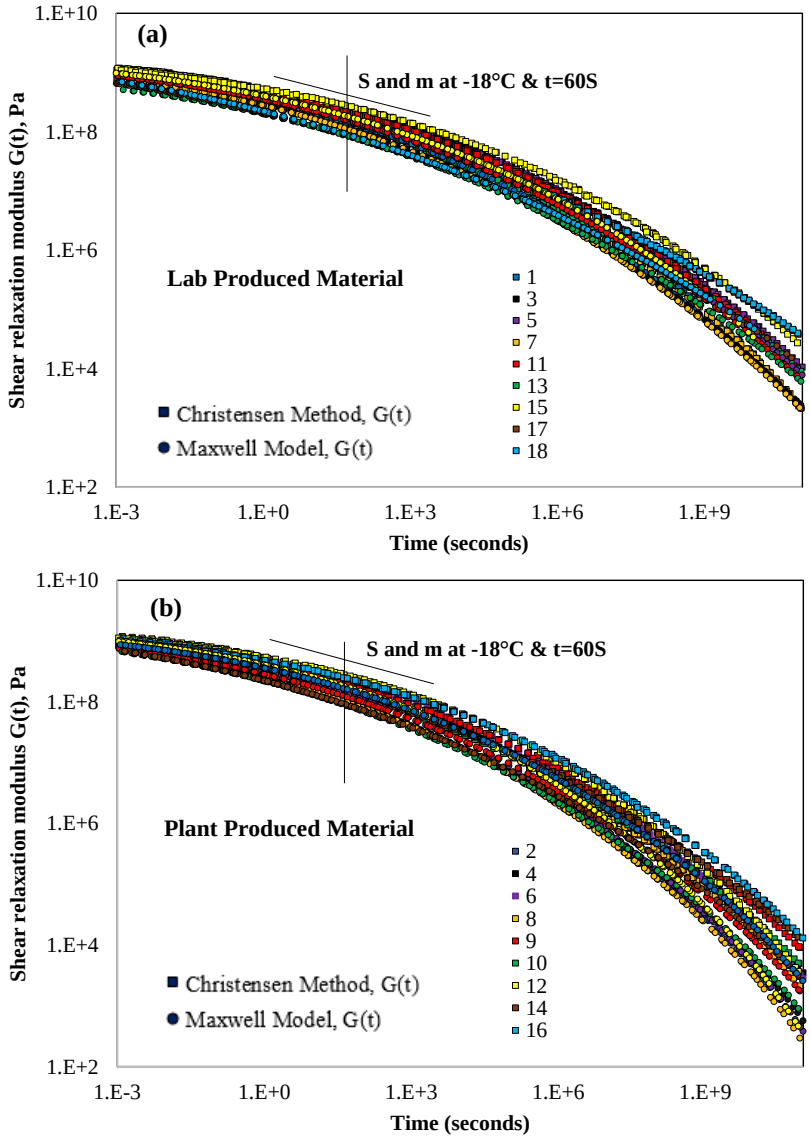

Figure 5. 3 Comparison of relaxation modulus curves interconverted from DSR data using the Christensen method and generalized Maxwell model for (a) lab produced (b) plant produced materials at reference temperature of -18°C

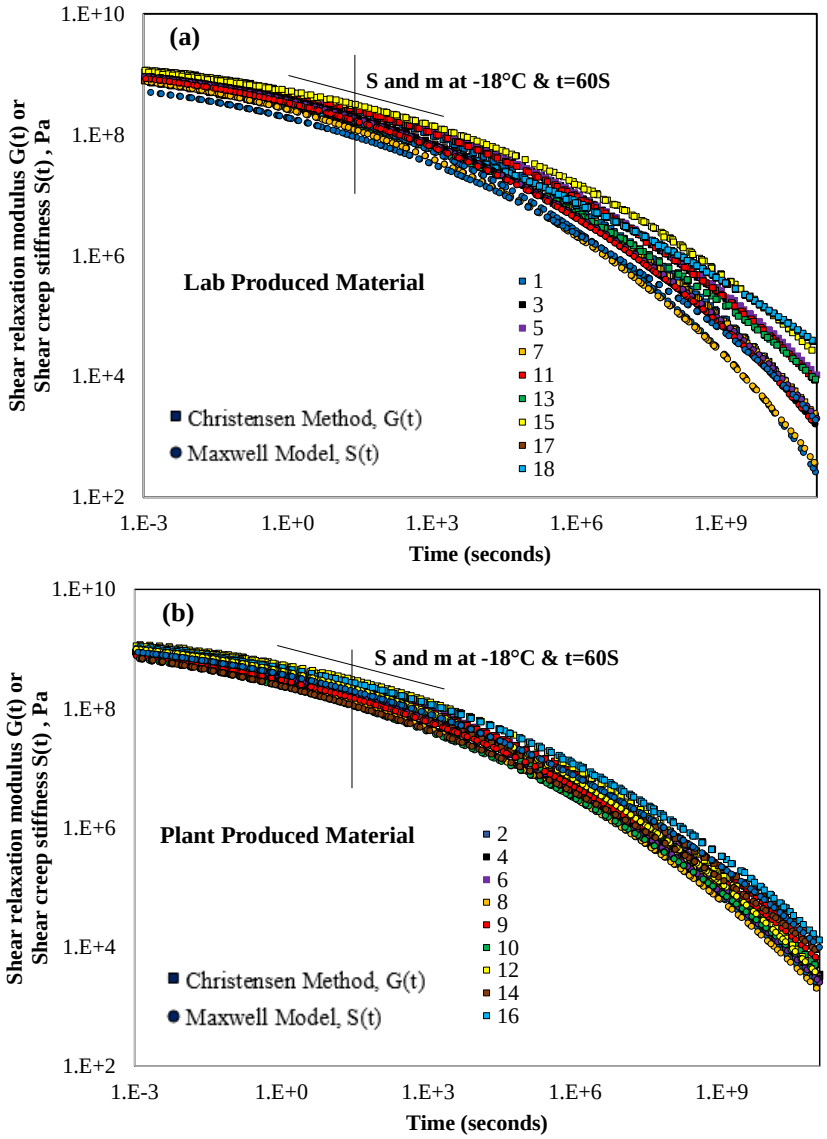

Figure 5. 4 Comparison of relaxation modulus curves interconverted using Christensen method and creep stiffness curves interconverted using Maxwell model for binders extracted and recovered from (a) lab produced (b) plant produced materials at reference temperature of -18°C

5.4.2 Comparison of S and m-values from BBR Measurements and Estimations from DSR Data

5.4.2.1 Method Developed by Sui et al., 2011

The method proposed by Sui was used to determine the S and m-value from the relaxation curve at 60s loading time and -18°C and -12°C for binders extracted and recovered from different

mixture samples. Then these values were compared to the respective S and m-value measured using BBR at -18°C and -12°C. The plots presented in this section show the comparisons between S and m-value determined from BBR (will hereinafter be referred as measured S and m-value) and S and m-value estimated from DSR (will hereinafter referred as estimated S and m-value) corresponding to 60s loading time and -18°C. Then the overall correlations and trends observed for comparison done at both -18°C and -12°C temperatures are summarized in Table 5.2 and is discussed in subsequent section. In this section, comparison of creep stiffness is presented first followed by m-value comparison.

5.4.2.1.1 Creep Stiffness (S) Comparison

Figure 5.5 shows comparison between estimated S and measured S for extracted and recovered binders. The estimated S values in the different plots are obtained by employing different interconversion methods and are indicated on the plots (Figures 5.5a, b, c and d). BBR tests were not conducted on virgin binders and therefore, the data in figures 5.5a-5.5c are only for extracted and recovered binders. Figure 5.5d shows the comparison of estimated S values using the generalized Maxwell interconversion and the Christensen method for virgin binders.

In general, the results indicate that a good estimate of BBR S value can obtained from DSR data by implementing this method. A strong linear correlation between measured and estimated S values is observed when both Christensen and Maxwell interconversion methods are employed ($R^2 = 0.95$ for Christensen G(t) and Maxwell S(t) and $R^2 = 0.94$ for Maxwell G(t)), Figures 5.5a, 5.5b and 5.5c. However, a larger difference between measured and estimated S in terms of magnitude is observed when the Maxwell model is employed for interconversion to either G(t) and S(t) (approximately 35% difference) as compared to when the Christensen method is employed (approximately 1% difference). The root mean square error (RMSE) provides a measure of the

magnitude difference between measured and estimated S values. When the interconversion using Maxwell model is used both G(t) and S(t) show greater RMSE (RMSE = 67MPa) as compared to interconversion done using the Christensen method (RMSE=18 MPa). Since there is no BBR measurement for the four virgin binders, comparison is only done between estimated S values by employing the two different interconversion methods (Maxwell and Christensen). The result indicated a good correlation for estimation done using both interconversion methods ($R^2 = 1.00$), Figure 5.5d. As with other results, there is an approximate 38% difference in magnitude. A potential cause for a somewhat constant 35 - 38% difference between measured S and estimated S from DSR using exact interconversion could be attributed to differences in mode of loading (flexural vs. shear), different testing domain (time vs. frequency), difference in specimen size (thin circular sample vs. asphalt beam), difference in isothermal conditioning (ethanol vs. air) and potential difference in physical hardening.

As mentioned in the previous section, BBR measured creep stiffness represents flexural stiffness whereas DSR measurement is in shear mode; differences in values of these modes are expected and a known Poisson's ratio value can be used to calculate one from the other. A study by Tschoegl et al. (2002) and Graziani et al. (2017) showed that viscoelastic materials exhibit a time dependent Poisson's ratio and follow an increasing trend. However, Lakes and Wineman (2006) showed this might not be the case, meaning the increase with time might not be exhibited. While the works by different researchers have shown that Poisson's ratio for asphalt materials are time and temperature dependent, a constant linear relationship between BBR measured S and DSR estimated S for the binders evaluated herein indicate that the variation of Poisson's ratio is minimal between the materials. This could be partly attributed to use of the same temperature for evaluation of shear and flexural modulus. While the use of constant Poisson's ratio simplifies effort required to

translate shear to flexural, it might introduce error. Therefore, care should be taken when using a poison ratio inferred based on experimental data determined for a specific temperature to other data set. Studies by Lakes and Wineman (2006); Lu et al. (1997), Wang and Lakes (2005) have showed that the Poisson's ratio for polymers ranges between 0.25 and 0.33.

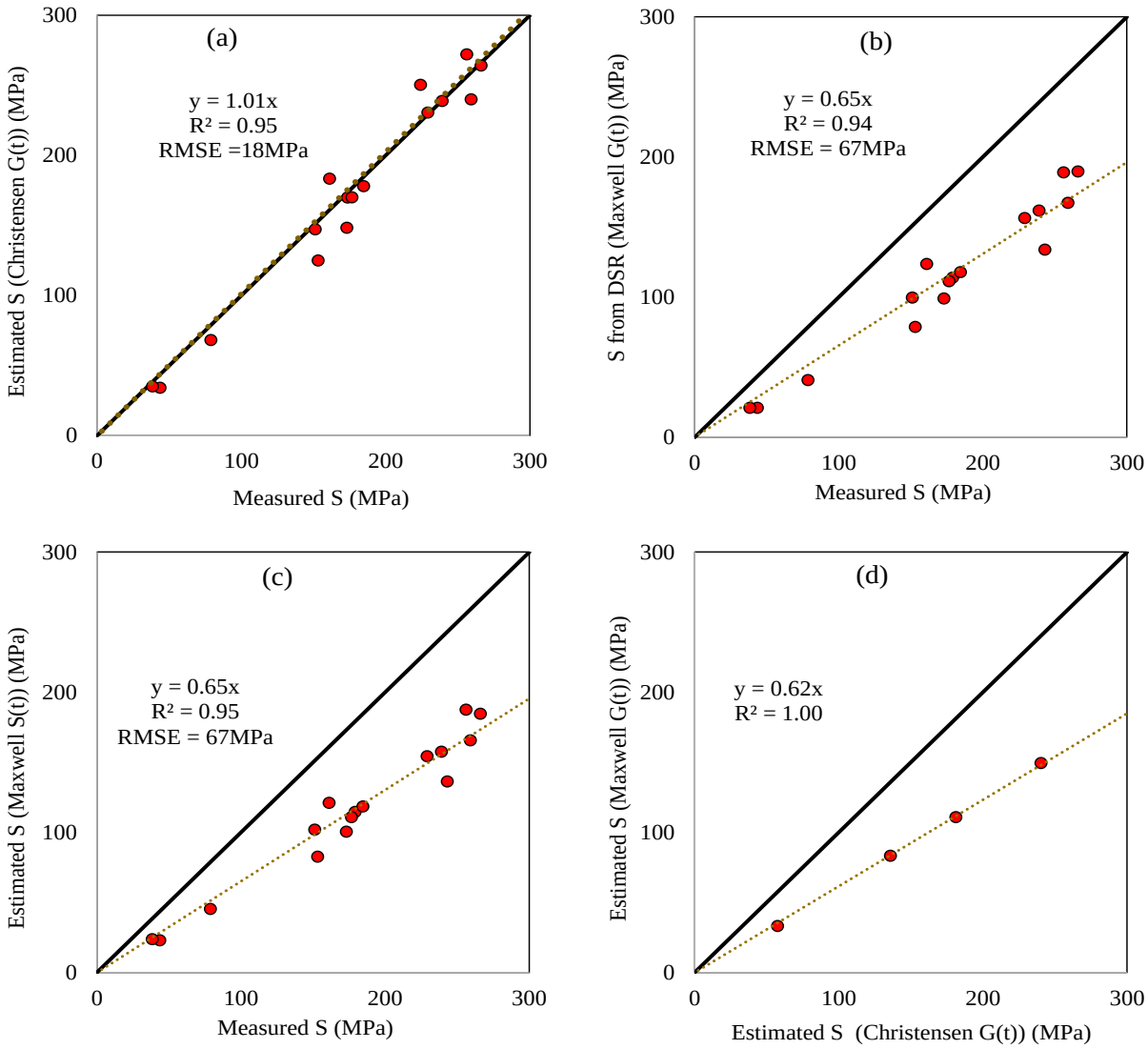

Figure 5. 5 Comparison of measured S to estimated S obtained using the (a) Christensen G(t) (b) Maxwell G(t) and (c) Maxwell S(t) interconversion methods for extracted and recovered binders (d) comparison of estimated S from Christensen G(t) and Maxwell G(t) for virgin binders

Table 5.2 summarizes the comparison done between measured and estimated S value at -18°C and -12°C. The estimated S values are obtained by employing different interconversion methods as indicated in parenthesis. The linear relationships (trendline equations) were found similar for comparison done at -18°C and -12°C. There are also differences in the RMSE (lower RMSE for comparison done at -12°C) but this is expected due to the lower magnitude of S value at -12°C as compared to -18°C. In general, the results indicate that both G(t) and S(t) using both Christensen approximation and exact interconversion (using generalized Maxwell model) are linearly related to BBR measured S values. Christensen approximation provides values very close to lab measurements, whereas exact interconversion leads to a 30-38% linear deviation. The deviation appears to be material and temperature dependent.

Table 5.2 Comparison of measured and estimated S value at -18°C and -12°C

Creep stiffness (S) comparison between				
x	y	R	RMSE, MPa	Trendline Equation
Measured, -18°C	Estimated (Christensen *G(t)*) -18°C	0.97	18	y=1.01x
Measured, -18°C	Estimated (Maxwell *G(t)*), -18°C	0.97	67	y=0.65x
Measured, -18°C	Estimated (Maxwell *S(t)*), -18°C	0.97	67	y=0.65x
Measured, -12°C	Estimated (Christensen *G(t)*), -12°C	0.88	13	y=0.95x
Measured, -12°C	Estimated (Maxwell *G(t)*), -12°C	0.87	43	y=0.60x
Measured, -12°C	Estimated (Maxwell *S(t)*), -12°C	0.89	36	y=0.66x

5.4.2.1.2 Rate of Change of Creep Stiffness (m-Value) Comparison

The m-value determined from the slope of the relaxation modulus and creep stiffness curves interconverted from DSR measurement are compared to the corresponding measurements obtained from BBR in Figure 5.6. The plots compare the measured and estimated m-values corresponding to 60s loading time and -18°C temperature. The correlation and comparison for measurements done at -12°C is summarized in Table 6.3.

The results (Figure 5.6) show a fair linear correlation between measured and estimated m-value when both Christensen and Maxwell interconversion methods are employed (R^2 = 0.74 for Christensen G(t), R^2 = 0.73 for Maxwell G(t), R^2 = 0.75 for Maxwell S(t), Figures 6a, 6b and 6c). The magnitudes of measured and estimated was also found similar with an average difference less than 5% as it relates to all interconversion methods indicating the minimal impact of interconversion method employed on m-value estimation. The same is also witnessed when comparing the RMSE (RMSE = 0.025 for Christensen G(t), RMSE = 0.019 for Maxwell G(t), RMSE = 0. 017 for Maxwell S(t)), which are all low values and less than 10% of the typical specification limit, i.e. 0.300. Comparison between estimated m-values by applying the Maxwell model interconversion and Christenson equation resulted in a strong linear correlation (R^2=0.94) for virgin binders, Figure 5.6d.

In general, there is a lower correlation observed between measured and estimated m-values as compared to measured and estimated S values, this could be attributed due to m-value being a derivative of the stiffness curve. The creep stiffness and relaxation modulus curves form DSR data are determined through fitting of a model and use of fitted equations to conduct interconversions. Thus, any mismatch in fitting process will cause added errors in m-value determination due to use of derivative to calculate slope, as opposed to absolute magnitude as in case of stiffness.

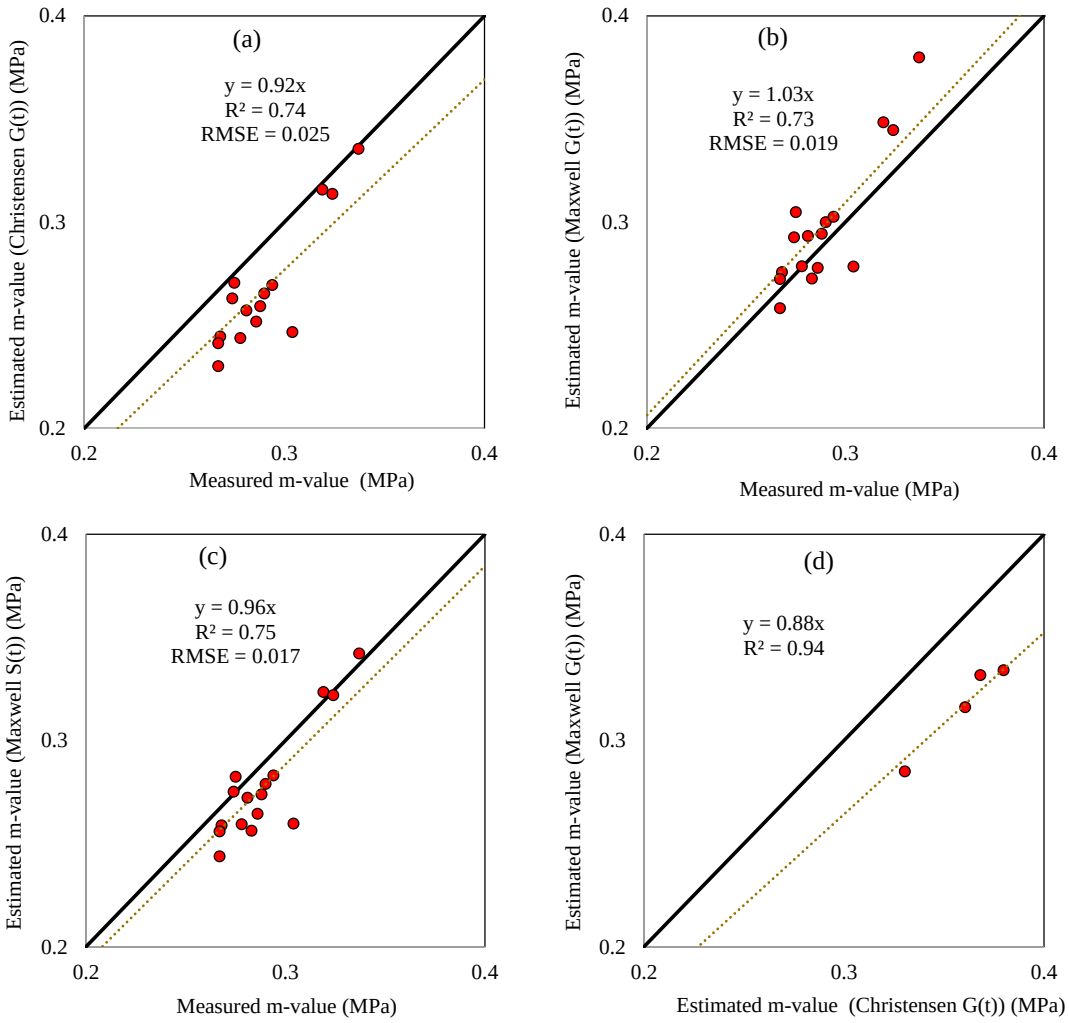

Figure 5. 6 Comparison of measured m-value to estimated m-value obtained using the (a) Christensen G(t) (b) Maxwell G(t) and (c) Maxwell S(t) interconversion methods for extracted and recovered binders (d) comparison of estimated S from Christensen G(t) and Maxwell G(t) for virgin binders

Table 5.3 summarizes the comparison done between measured and estimated m-value at -12°C and -18°C. The estimated m-value are determined using different interconversion methods as indicated in the table. Similar to S, the goodness of linear relationships between measured and estimated m-values degrade at -12°C as opposed to -18°C. In terms of RMSE, the level of difference between measured and estimated values is comparable between the two temperatures,

the estimated m-value using shear relaxation modulus has greatest RMSE at approximately 14% of the specification limit.

Table 5.3 Comparison of measured and estimated m- value at -18°C and -12°C

m-value comparison between				
x	y	R	RMSE, MPa	Trendline Equation
Measured, -18°C	Estimated (Christensen *G(t)*) -18°C	0.88	0.025	y=0.92x
Measured, -18°C	Estimated (Maxwell *G(t)*), -18°C	0.85	0.019	y=1.03x
Measured, -18°C	Estimated (Maxwell *S(t)*), -18°C	0.87	0.017	y=0.96x
Measured, -12°C	Estimated (Christensen *G(t)*), -12°C	0.74	0.014	y=0.98x
Measured, -12°C	Estimated (Maxwell *G(t)*), -12°C	0.75	0.041	y=0.95x
Measured, -12°C	Estimated (Maxwell *S(t)*), -12°C	0.69	0.01	y=1.0x

Residual plots are presented in Figures 5.7(a) and 5.7(b). Residual plots are helpful to identify the existence of a nonlinear relationship between measured and predicted values as well as bias with change in measurement values. The residuals are calculated by deducting predicted values from measured values. In Figure 5.7(a) the residuals are calculated with respect to predicted values obtained from G(t) interconverted using the Christensen method. Here the residual plot indicates the absence of a symmetrical distribution: measured values are always higher than predicted values. In Figure 4(b) the residuals are calculated with respect to predicted values

obtained from G(t) interconverted using the Maxwell model. Here the points are fairly symmetrically distributed and are mostly clustered toward the middle of the plot implying the lower bias exhibited with changes in m-value.

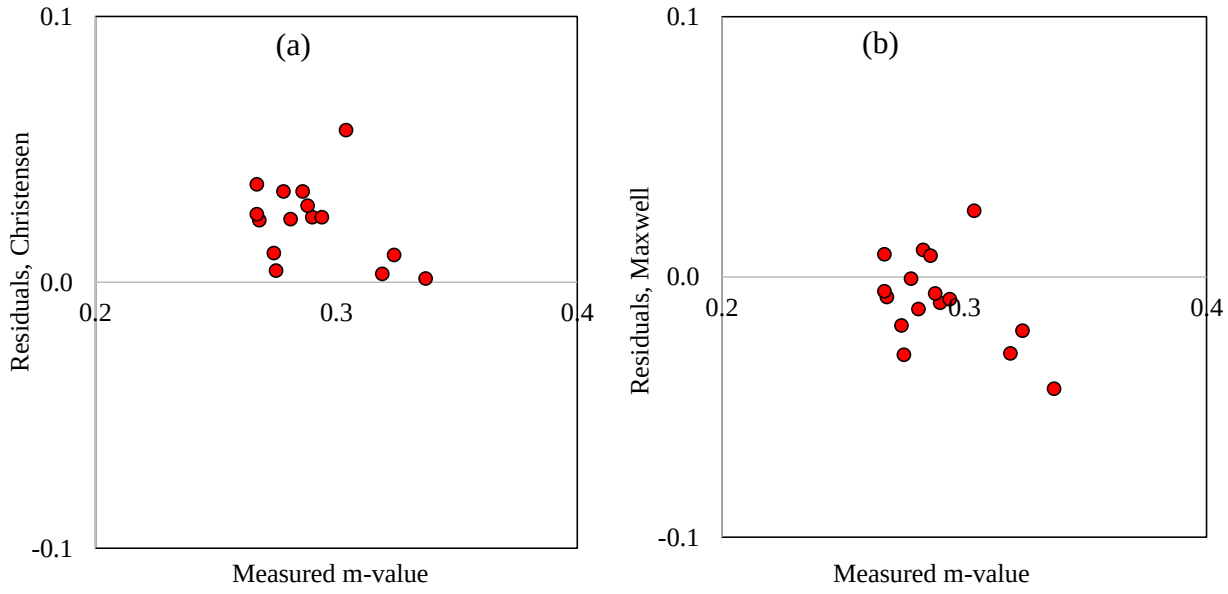

Figure 5. 7 Residual plots with respect to (a) Christensen (b) Maxwell interconversion

5.4.2.1.3 Performance Trends of Mixtures Based on Measured and Estimated S

The comparative analysis performed between measured and estimated S by employing different interconversion methods has shown the presence of differences in magnitude between measured and estimated values. Here the comparison between the relative rankings of mixtures based on measured and estimated is presented. This is done to assess the impact of using estimated S values from DSR measurements to compare between binders as opposed to BBR measured values. Values from the Christensen interconversion were selected for comparison because the method was found promising as compared to the others based on the results presented earlier in this paper.

Figure 5.8a presents the comparison for lab produced materials whereas Figure 5.8b is for plant produced materials. Apart from two mixtures each for plant production and lab mixing, the mixes rank in same order of decreasing S values. Thus, 14 out of 18 mixtures would be ranked in same manner for thermal cracking performance (for S values) when using DSR measurement with Christensen approximation method.

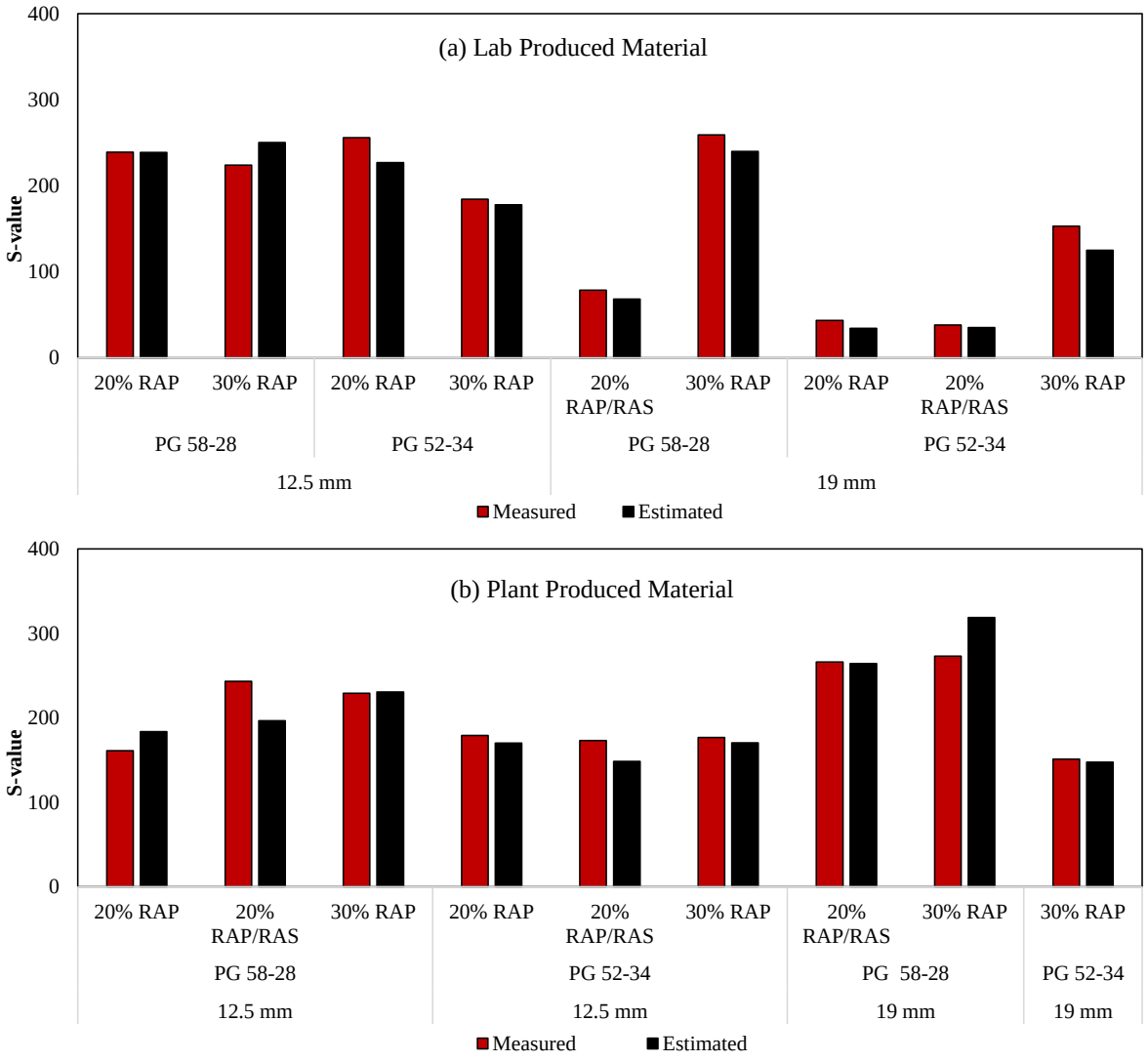

Figure 5. 8 Measured and estimated S for binders extracted and recovered from (a) lab produced materials (b) plant produced materials

5.4.2.1.3 Performance Trends of Mixtures Based on Measured and Estimated m-value

Similar to what has been done for S in the previous section, Figures 5.9a and 5.9b are presented to evaluate the similarities and differences in the performance trend as it relates to measured and estimated m-value for binders. In general, the performance trends are comparable for most mixtures with two exceptions (PG 52- 34, 12.5 mm, 30% RAP from lab produced materials and PG 58-28, 19 mm, 20% RAP RAS from plant produced materials). Thus, from perspective of m-values, 16 out of 18 mixtures would be ranked in same way when using DSR measurement based on Christensen approximation for calculation of m-value as opposed to direct BBR measurement.

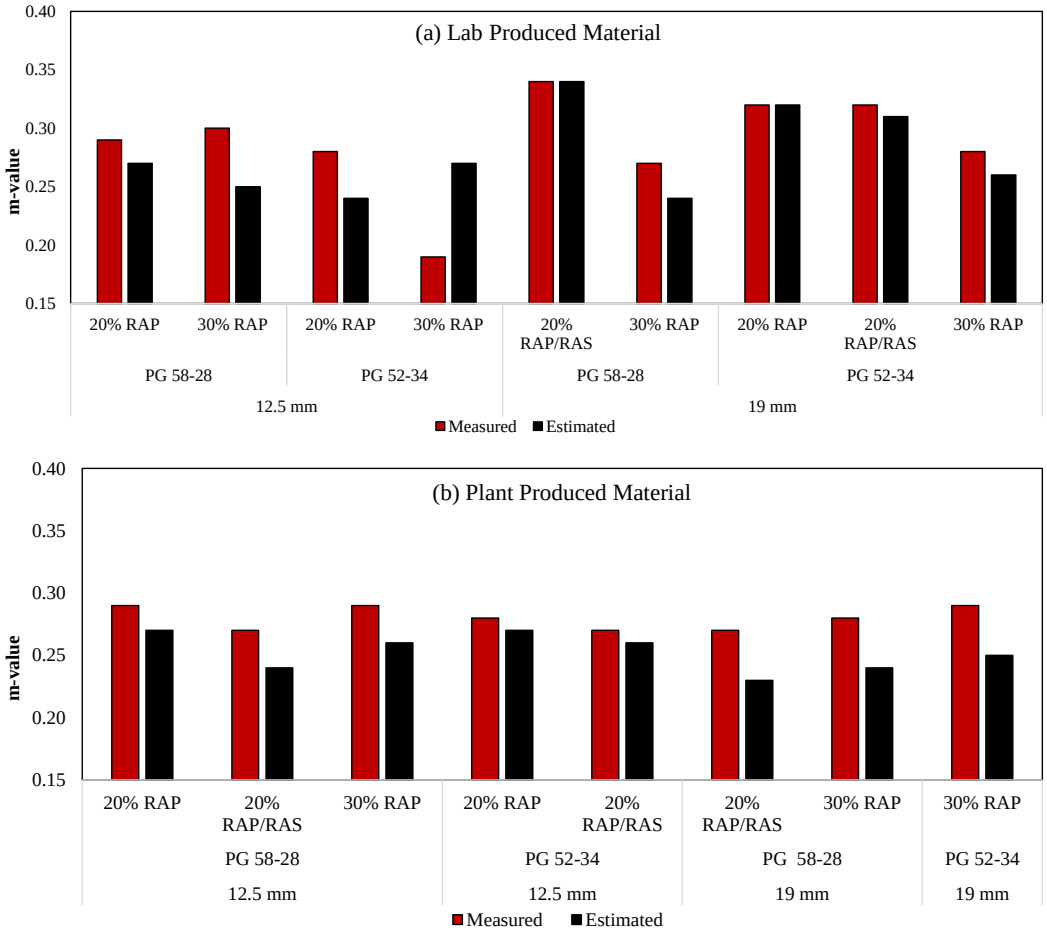

Figure 5. 9 Measured and estimated m-value for binders extracted and recovered from (a) lab produced materials (b) plant produced materials

5.4.2.2 Equation Developed by Rowe 2014

The equation developed by Rowe (2014b) is used here to estimate BBR S and m-values from |G*| and phase angle measurements determined at -18°C and 0.0167 radians/s loading frequency from DSR data. Then the estimated values are compared to measured S and m-values corresponding to same temperature (-18°C) and 60s loading time. This is done to evaluate the robustness of the equation proposed by Rowe (2014) to estimate BBR S and m-value from DSR |G*| and ϕ and vice versa. The result indicated that S estimated by applying the relationship developed by Rowe exhibit a strong linear correlation to measured S values (R^2 = 0.93), Figure 5.10a. However, the linear equation and RMSE indicate significantly larger difference in the magnitude between measured and estimated values (RMSE is more than 50% of typical specification limit of 300 MPa). A fair linear correlation is observed between measured and estimated m-value (R^2=0.75), Figure 5.10b. As compared to S value, the estimated m values show substantially lower RMSE using the predictive equation. It should be noted that the Rowe predictive equation is entirely based on linear regression and developed using five binders. With added datasets, the equation can be improved to get better predictability.

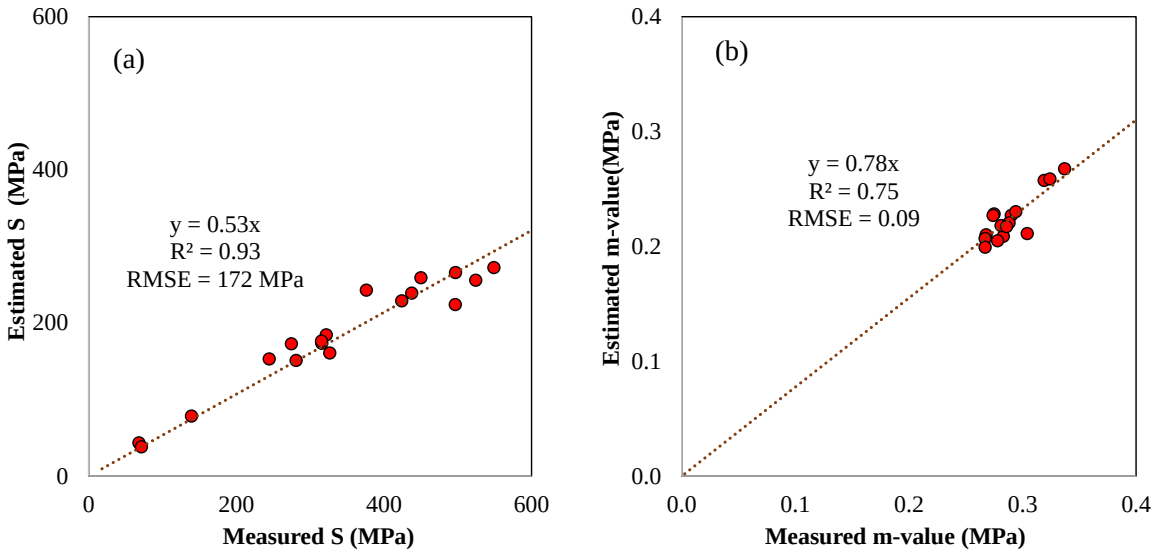

Figure 5. 10 Comparison of estimated and measured (a) S and (b) m-value

5.4.3 Development of Estimation Equations to Determine S and m-value from |G| and ϕ measured in DSR*

The estimation of S and m values discussed in the previous sections of this paper relies on having access to temperature and frequency sweep complex shear modulus results from DSR. Majority of previous research on the topic also relies on conducting temperature and frequency sweeps to estimate S and m values. This section of the paper assesses viability of estimating S and m values using single measurement of dynamic shear modulus and phase angle in DSR at one frequency and PGLT+10ºC test temperature.

Figures 5.11a and 5.11b evaluate the relationship between BBR creep stiffness and DSR shear modulus values for the study binders. |G*| from DSR is compared to measured S in Figure 5.11a, whereas it is compared to estimated S (using Christensen approximation method) in Figure 5.11b. For this comparison, S value corresponding to 60s loading time and -18°C temperature and |G*| measurement at the same temperature and 0.0167 radians/s angular frequency are used. The

comparison of |G*| to both measured and estimated S showed a very strong linear correlation (R^2=0.95 and 0.99). The slightly better correlation of |G*| to S estimated from DSR is hypothesized to be due to the estimation of both parameters from the same DSR data. These observed strong correlations between shear modulus and S value indicates the potential of |G*| as alternative to measure low temperature cracking resistance of binders.

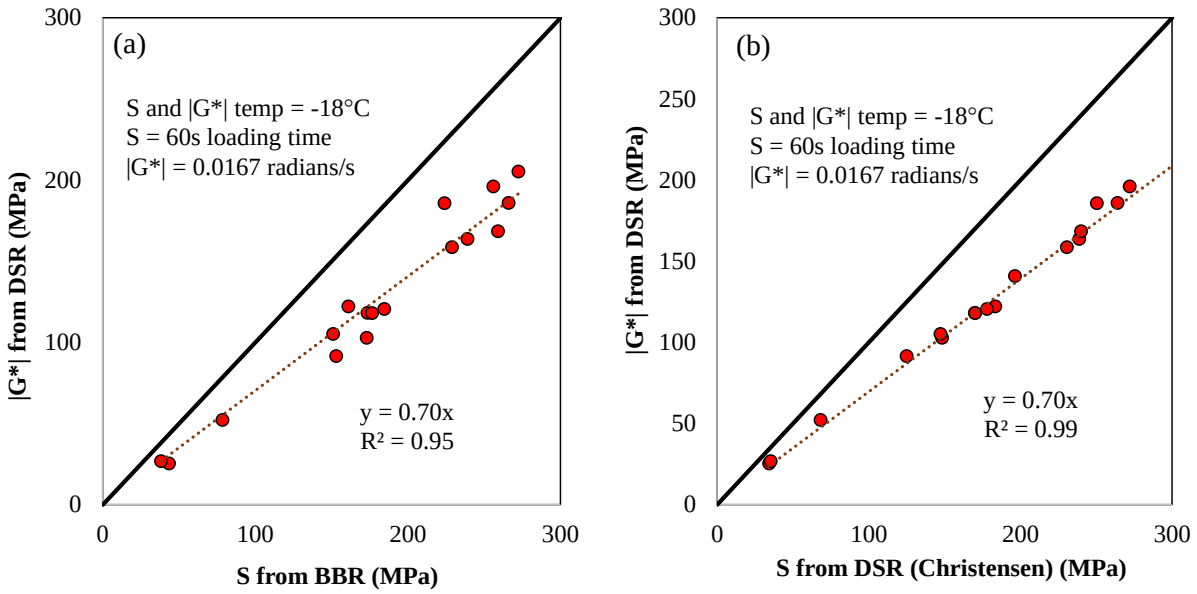

Figure 5. 11 Correlation between shear modulus by DSR and stiffness by BBR.

Figures 5.12a and 5.12b show the correlation between m-value and phase angle. The phase angle is compared to measured m-value in Figure 5.12a, whereas it is compared to estimated m-value (using the Christensen approximation method) in Figure 5.12b. The m-values correspond to 60s loading time and -18°C temperature and the phase angle measurements correspond to the same temperature and 0.0167 radians/s angular frequency. The relationship between phase angle and estimated m-value (R^2=0.93) also appears to be strongly linear as compared to fairly linear for phase angle and measured m-value (R^2=0.74). This could be attributed to the fact that the phase angle and m-value from DSR are obtained from the same test data whereas the measurement from

BBR are from a different test. In general, it is observed that the correlation between S and |G*| is stronger than ϕ and m-value. A higher variability is anticipated in phase angle and m-value measurement as compared to stiffness measurements and this could potentially contribute to the observed lower correlation between ϕ and m-value.

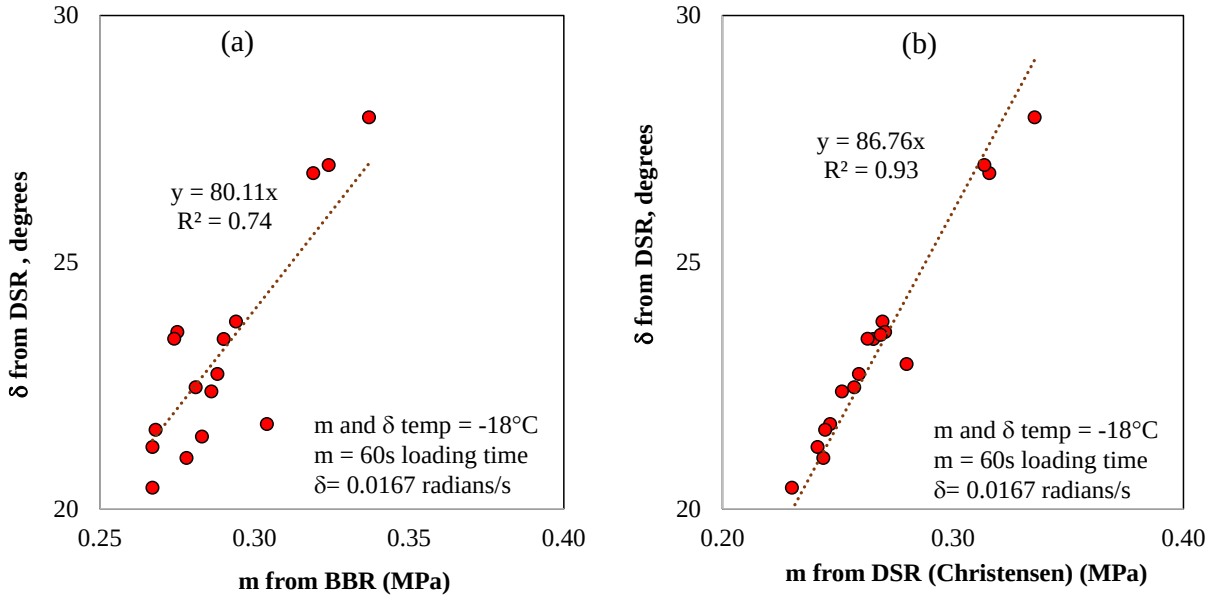

Figure 5. 12 Correlation between phase angle by DSR and m-value by BBR.

Considering the strong correlation observed between |G*| and S as well as ϕ and m-value, the researchers believed developing a simple equation that can be used to translate one parameter to other would have great practical use. This would be particularly important when it is required to obtain a quick estimate of BBR specification parameters from one point measurement of |G*| and ϕ. In this study, BBR data measured at 60s and -18°C and the corresponding DSR measurements at -18°C and 0.0167 radians/s angular frequency are used to conduct linear regression and predictive equation development. Standard least square method is employed. For S, the significance of |G*| and ϕ is evaluated and the result indicated only |G*| has a significant effect on S value. Therefore, the equation to estimate S from DSR data is developed only based on |G*|,

Equation 5.14. As it relates to m-value, only phase angle was found to have a significant effect. Therefore, the equation to estimate m-value from DSR data was developed based only on phase angle, Equation 5.15.

$$S(t) = 1.28\,|G^*(\omega)| + 19.2 \quad [5.14]$$

$$\text{m-value} = 0.008\,\phi + 0.1 \quad [5.15]$$

Figures 5.13a and 5.13b shows the comparison between measured S and m-values and estimated S and m-values predicted using Equations 5.14 and 5.15. The result shows a very close agreement in terms of correlation and magnitude (R^2 =0.97 for S and R^2 = 0.86 for m-value for Y = X correlation; RMSE = 13MPa for S and RMSE = 0.0083 for m-value) between the predicted and measured S and m values. It should be noted that the correlation coefficient observed here is higher whereas the RMSE is lower as compared to all other methods investigated in this study.

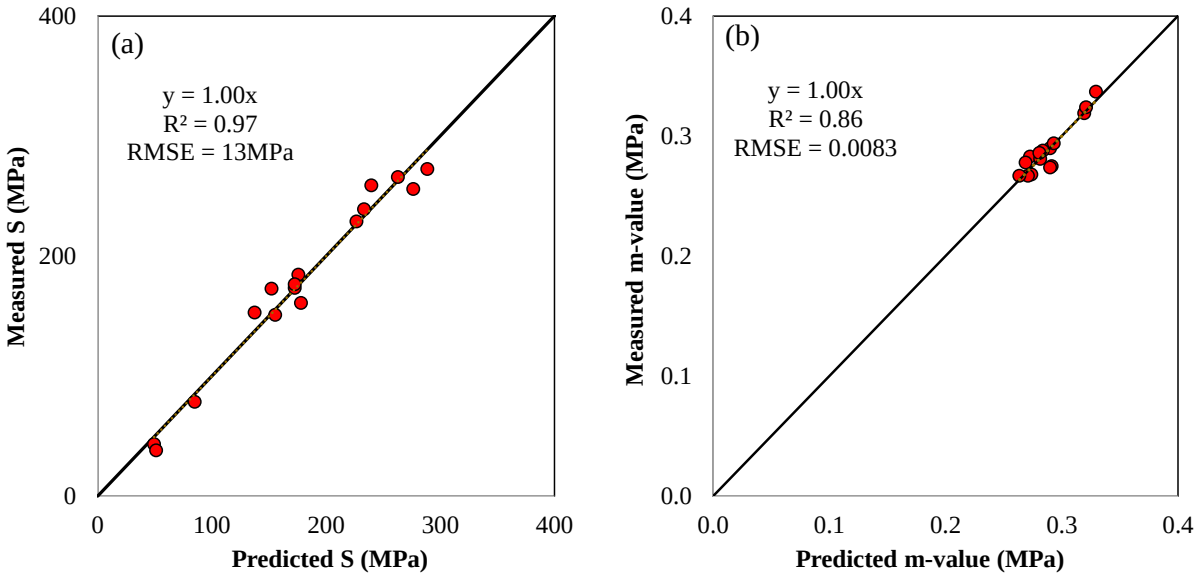

Figure 5. 13 Predicted and measured (a) S and (b) m-values

5.5 Summary and Conclusion

In this study, the applicability of determining low temperature BBR specification parameters, S and m-value, from DSR testing for twenty two virgin and, extracted and recovered binders from mixtures with a wide set of variables is investigated. Different methods proposed by previous research were employed and the robustness of the methods is explored by comparing estimated values from DSR with measured S and m-values from BBR testing. The approaches use different interconversion methods to obtain relaxation modulus or creep compliance from DSR complex shear modulus measurements. Then, the shear relaxation modulus or creep stiffness and slope at the same loading time and temperature as BBR testing are translated to S and m-value. The impact of use of different interconversion method on the S and m-value estimation is assessed. The relationship between BBR creep stiffness and DSR shear modulus as well as BBR m-value and DSR phase angle is evaluated. Finally, a simple equation is developed to enable estimation of BBR specification parameters from a single point measurement of shear modulus and phase angle.

The following conclusions are drawn based on the observations from the study:

- The slope and magnitude of the shear relaxation modulus master curve, G(t), at 60 s and binder PGLT+10 correlates well to the S and m-value determined from BBR. Shear creep stiffness, S(t) at PGLT+ 10^{o}C and 60s can be also be employed successfully to estimate S and m values that linearly correlate with BBR measured S and m values.
- Both, exact interconversion using fitted generalized Maxwell model and Christensen approximation equation estimate S values that are linearly correlated to BBR measured S values. However, the Christensen approximation method results in a better agreement in terms of magnitude (differences up to 1% and RMSE = 18 MPa in this study) as

compared to Maxwell interconversion using either of G(t) or S(t) (differences up to 35% and RMSE =67MPa).

- The estimated m-value from DSR data using both Christensen approximation and exact interconversion with fitted generalized Maxwell model has a fair linear correlation to the BBR measured m-value. The deviation in magnitude between BBR measured and DSR estimated m values (for both G(t) and S(t)) is minimal and comparable for both interconversion (Christensen or Maxwell) methods.
- S and m-values estimated using equation developed by Rowe correlated well with measured S and m-values. However, a noticeable difference in magnitude was observed for both, magnitude differences were quite high for S (RMSE of 172 MPa) as compared to m-value.
- A strong correlation was observed between DSR |G*| and BBR S value as well as DSR ϕ and BBR m-value. This led to the development of a simple equation that can translate a single measurement of |G*| and ϕ to specification S and m-value. These equations are sought to have a great practical use as it eliminates the need to go through the interconversion process and can be used when a quick translation of DSR parameters into BBR or vice versa is required.

The work presented here shows promising results regarding the reliable estimation of BBR specification parameters from DSR test data. The outcome from the study is particularly valuable when it is required to characterize low temperature properties of extracted and recovered binders from field cores pavements. This new possible alternative allows to characterize and to track the evolution of low temperature binder properties with aging and traffic which otherwise would not have been possible as part of quality assurance or pavement management system. Moreover, the

ability of using one piece of equipment for full characterization of asphalt binder will have enormous practical use for owner agencies as well as contractors by drastically reducing time and effort otherwise required.

In this study, binders extracted and recovered from a wide range of mixtures have been used to evaluate the possibility of obtaining BBR specification parameters from DSR test. Even if the mixtures used encompass a wide range of variables, they represent only binders and mixtures from the Northern part of United States. Therefore, extending the study to other set of binders and mixture from a different region could give insight to the possibility of whole country adopting this method. Moreover, the cause for the large magnitude difference between measured and estimated S due to exact interconversion with fitted generalized Maxwell model should be further studied. Furthermore, effects of mix variables, binder types and aging levels on the reliability of estimated S and m values should also be determined.

5.6 Acknowledgments

The authors would like to acknowledge New Hampshire Department of Transportations for providing the materials for this study and for conducting BBR tests on the extracted and recovered binders. Acknowledgement is also extended to Gerry Reinke for carrying out DSR testing on the study binders.

CHAPTER 6: EFFECT OF MIX DESIGN VARIABLES ON THERMAL CRACKING PERFORMANCE PARAMETERS OF ASPHALT MIXTURES

6.1 Introduction

Thermal cracking is the most prevalent distress in asphalt pavements in climates with cooler temperatures and high cooling rates. Tensile stresses induced due to significant changes in temperature is the main cause for thermal cracking. As the temperature drops, the pavement wants to contract but is restrained by friction from underlying layers and lack of contraction joints, subsequently causing tensile thermal stress to build up. When this stress exceeds the tensile strength, microcracks are initiated and these can coalesce into macro-cracks leading to formation of a thermal crack that typically forms in transverse direction on the pavement surface. Asphalt mixture's fracture and viscoelastic properties play significant role in controlling the ability of the mixture in limiting thermal stresses and in maintaining material integrity as stresses approach material stress capacity. These cracks allow water to infiltrate into the pavement structure; this subsequently compromises its performance and structural integrity.

Several efforts have been made to develop performance based binder and mixture specifications to lower the propensity of thermal cracking distress. As part of this endeavor, a number of researchers have developed mixture based thermal cracking performance evaluation tools (Dave et al., 2011a, Anderson et al., 2001, Dave et al., 2011b, Olard et al., 2004). This study focuses on two recently developed lab measured mechanistic thermal cracking evaluation parameters. The

first method uses the fracture energy determined from Disc Compact Tension (DCT) testing to limit thermal cracking by ensuring a minimum fracture toughness of the material and the second method combines the stiffness and relaxation properties of asphalt mixtures in Black space to limit thermal stresses.

Recent studies have shown the correlation between different fracture parameters and thermal cracking resistance of asphalt mixtures. One such parameter is the fracture energy of asphalt mixtures that could be determined from DCT or other geometries, such as semi-circular bend (SCB) test (Marasteanu et al., 2002; Wagoner et al., 2005a; Wagoner et al., 2005b). Some agencies have implemented DCT testing as a requirement and established different limits for fracture energy in their specifications to ensure the thermal cracking resistance of asphalt mixtures at design and production stage. For example, MnDOT limits minimum 450 J/m^2 for traffic levels 1, 2 and 3 or 500 J/m^2 for traffic levels 4 and 5 during mix design phase, and 400 J/m^2 for traffic levels 1, 2 and 3 or 450 J/m^2 for traffic levels 4 and 5 for quality assurance (QA).

Black space is defined as the cross-plot of dynamic modulus (|E*| or |G*|) and phase angle (ϕ) of material at a given temperature or frequency. Recently the Glover Rowe (G-R) parameter (Anderson et al., 2011) was identified as a tool to describe the thermal cracking resistance of asphalt binders in a Black space. The parameter is determined from the |G*| and ϕ of binders at 15^{o}C and a frequency of 0.005 rad/s. A value of 180 kPa and 450 kPa were set as limits to indicate onset of cracking and significant cracking, respectively. Since the binder evaluation in Black space neglects the mix properties, Mensching et al. (2017) expanded the study to mixtures and developed a single parameter (mix G-R) in Black Space as an indicator for thermal cracking performance of asphalt mixtures. Their work utilized thermal cracking performance from thermal stress restrained specimen test (TSRST).

A study by Gaw (1981) identified climate, subgrade type, mix design properties, pavement age and traffic as main factors that influence thermal cracking resistance of asphalt pavements. Kallas (1982) showed that aggregate type affects fracture strength. A study employed by Haas et al. (1987) using multiple regression models concluded minimum pavement temperature, coefficient of thermal contraction and pavement layer thickness have the highest correlation to fracture energy. Abu Abdo et al. (2014) investigated the effect of mix variables on fracture toughness and concluded a decrease in asphalt content is associated with lower fracture toughness values. A study by Braham et al. (2007) performed a statistical analysis and concluded the significance of binder content, aggregate type and temperature on fracture energy of mixtures. As part of an effort to develop a statistical model to predict fracture energy from the DCT test, Marasteanu et al. (2007) identified PG high temperature (PGHT), PG low temperature (PGLT) and aggregate type as significant variables to fit the model. A study by Li et al. (2008) showed the dependency of fracture energy on temperature, type of aggregate and binder modifier. In general, the literature review done as part of this study indicated a lack of consensus in the conclusions drawn from different studies and limited information on the effect of mix design variables (all previous studies were limited to less than 15 asphalt mixtures) on thermal properties as it relates to fracture energy and Black space location (mix G-R value).

Mix specifiers and producers strive to design and produce mixtures that meet established threshold values for fracture energy and mix G-R value by adjusting their mix design variables. Current adjustments are mainly employed on mix design variables that are included in the specification and controlled through current quality control and acceptance procedures. Due to lack of reliable guidance, the adjustment of mix design variables is usually a trial and error process. Therefore, this study was designed to obtain a better understanding on the topic to provide guidance to mix

specifiers and producers on changes they should consider making on the composition of asphalt mixture to achieve specification requirements as it relates to fracture energy and mix G-R value.

The objective of the study is to identify mix design variables that potentially affect the thermal cracking performance properties of asphalt mixtures. Databases developed by Minnesota Department of Transportation (MnDOT) with data from 90 mixtures and University of New Hampshire (UNH) containing data for 81 mixtures were used to determine the statistical significance and correlation between common mix design variables, including recycled asphalt amount, mix volumetric properties and binder grade, to the fracture energy and mix G-R values.

6.2 Thermal Cracking Performance Evaluation Parameters

6.2.1 Fracture Energy from DCT Test

DCT test was developed at the University of Illinois to measure the fracture energy of asphalt mixtures (Wagoner et al., 2005). The test is performed on notched 150mm diameter specimens by applying a constant crack mouth opening displacement (CMOD) at a rate of 1mm/min. The fracture energy is determined from the test by normalizing the area under the load displacement curve by the fractured face area. In general, a higher fracture energy value is desirable and is expected to indicate a better thermal cracking resistance in the field. A 400J/m^2 threshold is commonly employed to ensure the thermal cracking resistance of asphalt mixtures.

The frequency distribution plot presented in Figure 6.1 depicts ranges of fracture energy values used in the study. This shows the wide range of fracture energy measurements used in the analysis and subsequently the increased confidence in the validity of the study conclusions.

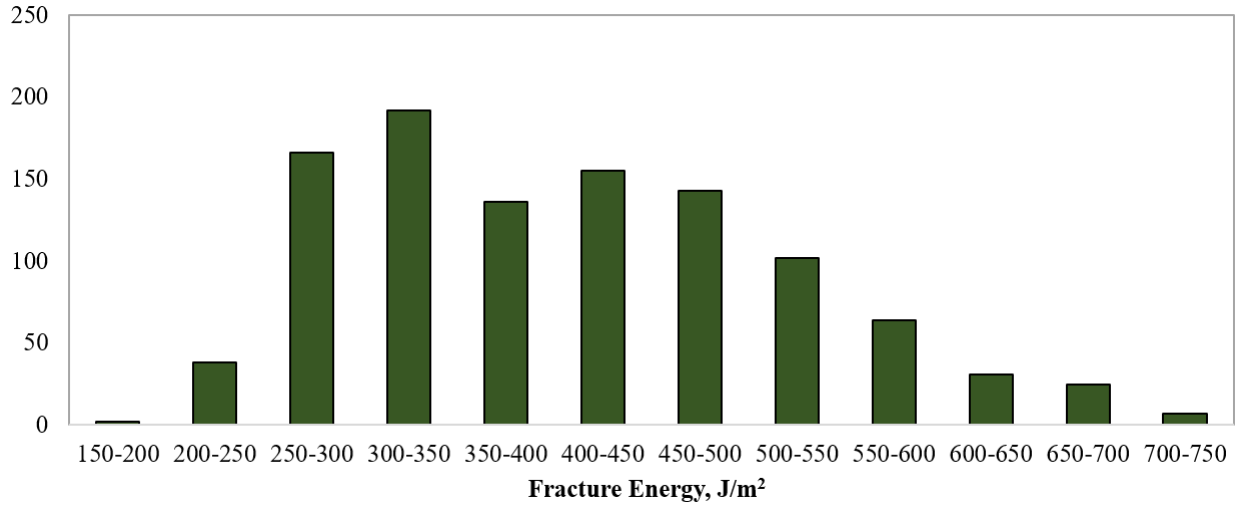

Figure 6. 1 Frequency distribution plot for fracture energy

6.2.2 Mix G-R Parameter

Mixture Black space diagrams assess the stiffness and relaxation capability of mixtures from a plot of |E*| versus ϕ. Mixtures that plot further to the right have more viscous behavior, while the lower phase angle values indicate more elastic behavior. The combination of lower phase angle (less relaxation capability) and higher dynamic modulus (more stiffness) may indicate that the mixture is more susceptible to cracking. A recent study by Mensching et al. (*2017*) evaluated the correlation between mix G-R values in Black space (calculated using Equation 1) to thermal cracking performance. Later a preliminary threshold of 3.684E04 MPa is proposed for mix G-R values corresponding to temperature and frequency combination of PGLT+10°C and 0.01666rad/s. A lower G-R value is desirable as it indicates better thermal cracking resistance.

$$\frac{|E^*|(cos\emptyset)^2}{sin\emptyset} \qquad [6.1]$$

Figure 7.2 shows the Black space plot for the 81 mixes considered in this study at four temperature and frequency combinations. The plot shows that more separation between mixes is observed at

15ºC and 5rad/s, and PGLT+10 and 0.01666rad/s. Thus, these two frequency and temperature combinations were used for further analysis. It should be noted that at 15ºC, mixture evaluation is done at a constant temperature whereas normalization is done with respect to the low temperature grade of the mixtures for evaluation done at PGLT+10 ºC. The mix G-R values were computed at these frequency and temperature combinations and their relationship with various mix design variables is studied.

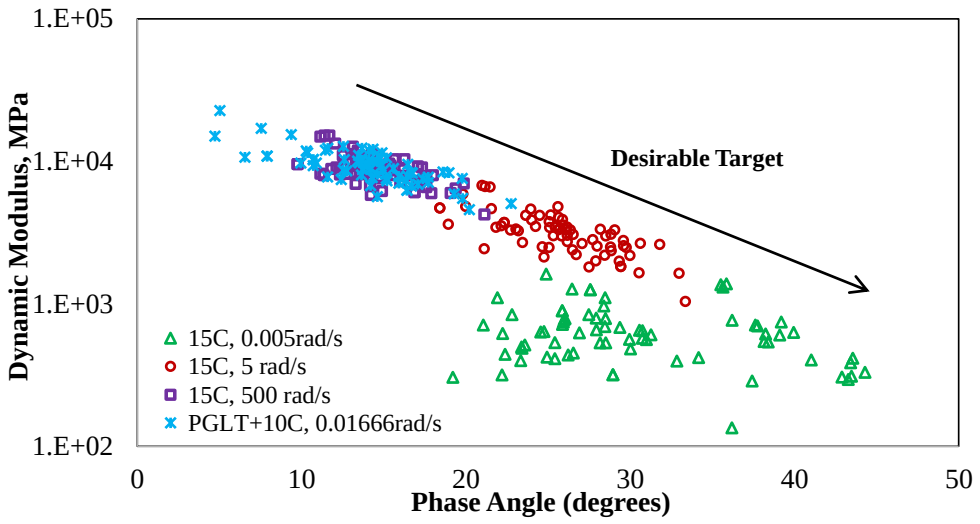

Figure 6. 2 Black Space Diagram for Study Mixtures

6.3 Research Approach and Materials

6.3.1 Materials

To determine the effect of mix design variables on fracture energy, a database developed by MnDOT's Office of Materials and Road Research (OM&RR) containing various information for 90 mixtures and their corresponding fracture energy measurement determined from approximately 1170 DCT tests is utilized. The data includes virgin asphalt content, total binder content, effective binder content, air void content, recycled asphalt pavement amount, asphalt film thickness, PG

low temperature grade, PG high temperature grade and PG spread. The DCT data is from testing conducted on production material that correspond to the data collected at construction stage. DCT test specimen production and testing is carried out following the test procedure of ASTM D7313-13/MnDOT Modified specification. Number of replicates tested for a specific mix range from 12 to 16. DCT test information available in the database includes number of replicates, test temperature, replicate's fracture energy, replicate peak load, average fracture energy and average peak load.

To understand the relationship between different mix design variables and mix G-R value, a database developed at UNH is utilized. The database contains diverse volumetric and test information (dynamic modulus and phase angle) for 81 mixtures representing material from New England region in the United States. Test specimen production is done following AASHTO PP 60 (2011) and complex modulus testing is performed according to AASHTO T 342 (2015) on three replicates to determine the dynamic modulus and phase angle master curves of the mixtures and subsequently the mix G-R values.

Table 6.1 is presented to show the breadth of information available as well as the mix design variables considered for the study.

Table 6.1 Overview of mix design variables used for the study

Performance Criteria	Mix design variable	Acronym	Range of mix variable
Fracture Energy	Virgin asphalt content	$P_{b, V}$	3-5%
	Total binder content	P_b	4-6%
	Effective binder content	P_{be}	4.0-5.5%
	Air voids	AV	3-5%
	Recycled asphalt pavement content	% RAP	10 to 30%
	Voids in the mineral aggregate	VMA	13-16
	Asphalt film thickness	AFT	7-10
	PG low temperature	PGLT	-22 to -34
	PG high temperature	PGHT	52 to 64
	PG spread (PGHT-PGLT)	ΔPG	86 to 98
	Nominal maximum aggregate size	NMAS	9.5, 12.5mm
Mix G-R Parameter	Virgin asphalt content	$P_{b, V}$	4-7%
	Total binder content	P_b	4.5-7%
	Effective binder content	P_{be}	4.0-6.5%
	Air voids	AV	3-10%
	Recycled asphalt pavement content	% RAP	0 to 40%
	Voids in the mineral aggregate	VMA	13-18
	Asphalt film thickness	AFT	5.5-9
	PG low temperature	PGLT	-22 to -34
	PG high temperature	PGHT	52 to 64
	PG spread (PGHT-PGLT)	ΔPG	86 to 92
	Nominal maximum aggregate size	NMAS	9.5-19mm

6.4 Data Analysis Methodology

This section describes the data collection approach and statistical analysis performed to determine the effect of different mix variables on the thermal cracking performance parameters. The mix description in the database is used to identify the different mixtures and map mix variable and test

information to a specific mix. For each mixture, the average values of the parameters were calculated and used for analysis. The statistical analysis is done in three phases described below using JMP® statistical software package.

6.4.1 Explore and Remove Outliers

Exploring and removing outliers is an important part of statistical analysis particularly due to anticipated errors during data measurement and collection. The step is vital as inclusion of outliers in a statistical analysis could cause bias in the conclusions drawn from the analysis. In this study, JMP® is used to locate the outliers by employing the Mahalanobis distance approach. A recent study by Nemati and Dave (2017) used similar approach for removing outliers in complex modulus datasets. The outliers were consequently removed from the input file. It should be noted that the fracture energy measurements obtained from MnDOT database contained only three outliers whereas four outliers were present on G-R value calculated based on data from UNH. The presence of the small number outliers confirms the lower variability encountered during DCT and complex modulus testing.

6.4.2 Determine Significance of Mix Design Variables

Step wise regression analysis was used to evaluate the significance of different mix design variables on thermal cracking properties of asphalt mixture. The analysis makes inference about a larger population to recognize mix design variables with a statistically significant effect on fracture energy and mix G-R value. This is accomplished by performing stepwise regression analysis and assessing p-values. The p-value provides information on the probability of the existence of relationship between different mix design variables and thermal cracking properties as it relates to fracture energy and mix G-R value. The conclusions drawn from this analysis will inform mix

specifiers and producers about the most important mix design variables related to thermal cracking properties.

Throughout the analysis, the null hypothesis assumes that there is no statistically significant relationship between the variables and the thermal cracking evaluation parameter. For this study, the common practice of utilizing p-value < 0.05 is adopted and the null hypothesis is rejected for a p-value <0.05 indicating the parameter has contributed significantly to the thermal cracking performance of a mixture. In other words, the relatively low p-value indicates the presence of a mathematical relationship between the mix parameter and fracture property such that a linear function of this parameter can predict the fracture property of the mixture within a 95% confidence level of the parameter data.

6.4.3 Determine Pearson Correlation Coefficient

In this study, the Pearson correlation is used to understand how the thermal cracking properties of mixtures, specifically fracture energy and mix G-R value, are affected by changes in mix design variables. The Pearson correlation factor is the most widely known type of correlation and is used to measure the degree of relationship between linearly related variables and the direction of the relationship based on the data provided. Based on the strength of the relationship, the value of the correlation coefficient varies between +1 and -1. A correlation of +1 indicates a linear positive relationship whereas -1 indicates a linear negative (inverse) relationship between the variables. As the correlation factor moves towards zero from both directions, the relationship becomes weaker. The analysis is done in JMP® by pairing the results of a mix variable to the corresponding fracture energy/mix G-R values. Based on the correlation factor obtained, the relationship is defined as weak/strong and the direction of the impact is identified.

6.5 Results and Discussion

6.5.1 Statistical Significance between Mix Variables and Thermal Cracking Performance Parameters

The p-values from stepwise regression analysis corresponding to different mix variables and fracture energy are presented in Table 6.2. The p-values indicate whether a statistically significant relationship between mix design variables and fracture energy exists (designated as "Yes") or not (designated as "No"). Overall, the p-values corresponding to mix design variables were low indicating a statistically significant relationship between the mix design variables and fracture energy. The exception to this are recycled asphalt content (p=0.093) and nominal maximum aggregate size (p=0.830) which have a higher p-value than the significance threshold. Therefore, it is concluded that mix specifiers and producers can consider changing PG low and high temperature grades, PG spread, voids in the mineral aggregate, asphalt film thickness, air void, virgin asphalt content, effective binder content and total binder content to adjust mixes to achieve set threshold values effectively.

Table 6.3 displays the p-values between the different mix design variables and mix G-R values corresponding to the two cases selected for this analysis (15°C and PGLT+10°C). Virgin asphalt content, total binder content, nominal maximum aggregate size demonstrated a significant effect on mix G-R value at both temperatures. In addition, PG low temperature and voids in the mineral aggregate were significant at 15°C whereas PG spread and effective binder content have a significant relationship to mix G-R at PGLT+10°C. The significant difference observed for the two cases implies dependence of effect of mix variables on the temperature and frequency combination considered as it relates to mix G-R. This shows that mix variables adjustment should be considered differently and should be made based on results obtained for that specific

temperature and frequency combination. Notably, the PGLT is significant at 15°C but not significant at PGLT+10°C. The non-significance observed at PGLT+10°C could be a result of the normalization done with respect to the low temperature contrary to the 15°C which does the evaluation at a constant temperature.

Table 6.2 Statistical significance (p-values) between mix design variables and thermal cracking performance parameters as it relates to fracture energy

Mix design variable	Prob > F	Significance (Yes/No)
PG low temperature	<.0001	**Yes**
PG high temperature	<.0001	**Yes**
PG spread	<.0001	**Yes**
Voids in the mineral aggregate	<.0001	**Yes**
Asphalt film thickness	0.0006	**Yes**
Air voids	0.001	**Yes**
Virgin asphalt content	0.002	**Yes**
Effective binder content	0.0124	**Yes**
Total binder content	0.024	**Yes**
Recycled asphalt pavement content	**0.093**	**No**
NMAS	**0.830**	**No**

Table 6.3 Statistical significance (p-values) between mix design variables and thermal cracking performance parameters as it relates to mix Glover-Rowe parameter

	Prob > F		Significance (Yes/No)	
Mix design variable	15°C, 5rad/s	PGLT+10°C, 0.01666rad/s	15°C, 5rad/s	PGLT+10°C, 0.01666rad/s
PG low temperature	<.0001	**0.738**	Yes	**No**
Virgin asphalt content	0.001	0.017	Yes	Yes
VMA	0.001	**0.133**	Yes	**No**
Total binder content	0.001	0.001	Yes	Yes
NMAS	0.027	0.0002	Yes	Yes
PG spread	**0.052**	0.008	**No**	Yes
Recycled asphalt pavement	**0.152**	**0.568**	**No**	**No**
Effective binder content	**0.205**	0.034	**No**	Yes
PG high temperature	**0.217**	**0.066**	**No**	**No**
Asphalt film thickness	**0.360**	**0.160**	**No**	**No**
Air voids	**0.376**	**0.070**	**No**	**No**

6.5.2 Pearson Correlation Coefficients of Mix Design Variables and Fracture Energy

Figure 6.3 displays the Pearson correlation coefficients between mix design variables and fracture energy of mixtures. The coefficient value represents the mean change in fracture energy for a one-unit increase in the mix design variable. Based on the results, total binder content, effective binder content, asphalt film thickness, PG spread and air void and showed a stronger correlation to fracture energy as compared to the other parameters included in the study. Out of the five parameters, which indicated a strong correlation, four of them are related to binder. This indicates that binder properties have the major effect on thermal cracking properties of asphalt mixtures.

The positive correlation of effective binder content, asphalt film thickness, air void, voids in the mineral aggregate, nominal maximum aggregate size, PG high temperature and PG spread indicates that an increase in these parameters improves the fracture properties of asphalt mixtures.

The stronger positive correlation of effective binder content and asphalt film thickness leads us to the conclusion that the availability of more asphalt to coat aggregate particles in the mix helps with the relaxation capacity that the pavement requires during temperature fluctuation. Moreover, considering the significance of the correlation between effective asphalt content and fracture energy (Table 6.4), the researchers recommend the inclusion of effective binder content in the specification control since it represents actual binder content available to the mixture. The same conclusion drawn with respect to voids in the mineral aggregate indicates that the more space available to form asphalt film benefits thermal cracking resistance. The positive correlation observed between air void and fracture energy infers to an increase in air void thus, improving the ability of asphalt mixture to contract with less thermal stress build up. The range of air void evaluated in this study (3 to 5%) can limit the observed effect and the relationship might differ as the air void increases beyond 5%. It is also essential to give attention to PG spread of mixtures as it relates to thermal cracking which has the strongest correlation to fracture energy as compared to other mix variables. Nominal maximum aggregate size displayed a weak positive correlation. This could due to use of fracture energy only to evaluate wear courses that resulted in only two NMAS levels (9.5 and 12.5mm) to be included in the analysis.

The statistical analysis performed indicated that total virgin binder, total binder content, recycled asphalt content, and PG low temperature grade have a negative impact on fracture energy implying an increase in these variables results in a potential for thermal cracking related problems. While the total binder contents (P_b and $P_{b,\,v}$) have negative effect, the effective binder content (P_{be}) has positive effect on fracture energy. The authors believe that the presence of binder from RAP in the total binder content could be the cause for the observed negative impact of total binder content on fracture energy. The total virgin binder accounts for absorbed asphalt in addition to the effective

asphalt content. In most cases increment in absorbed asphalt content is related to finer aggregate which is hypothesized as the reason for the impact of virgin binder on fracture energy in a negative manner. The effective binder content is the available binder content in the mixture and having positive contribution to thermal cracking performance. Negative effect of RAP amount agrees with other studies showing aged binder from RAP having negative effects on thermal cracking performance. Negative effect of increasing PG low temperature grade is expected, as PGLT lowers (a better low temperature grade) the fracture energy improves.

Correlation probability of mix variables to fracture energy is displayed in Table 6.4. It is expressed in terms of probability level and indicates how unlikely a given correlation coefficient will occur if there is no relation in the population. Therefore, a smaller p-value indicates the likelihood observed correlation by chance to be minimal (to be at less than 5% confidence level) and we can assume that the observed correlation applies to not only the study data but to general population. Overall, observed correlation probability of all mix variables to fracture is very low, demonstrating the very low probability of observing the correlations by chance. The higher reliability obtained for PG spread, total binder content, effective binder content and air void implies that by extending the correlation obtained for these variables to other sets of mixtures one can achieve required threshold values of fracture energy. While the correlation probability values of other variables are higher than the significance threshold, adjusted asphalt film thickness and PG low temperature grade show p-value very close to significance level.

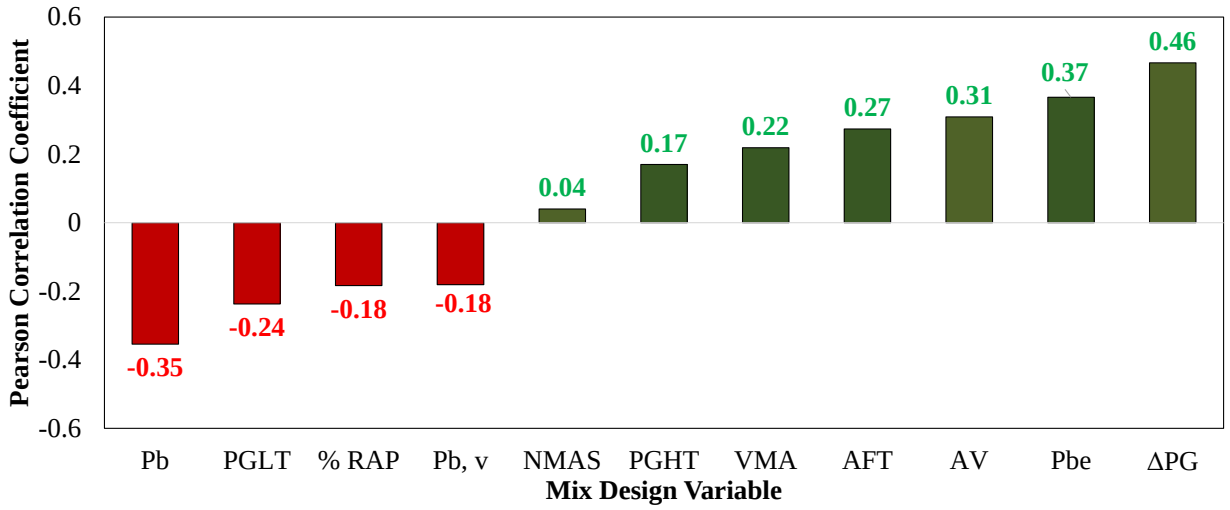

Figure 6.3 Pearson correlation coefficient between mix variables and fracture energy

Table 6.4 Significance of Pearson correlation coefficient between mix design variables and fracture energy

Mix Variables	Acronym	Correlation Probability
PG spread	ΔPG	0.0003
Total Binder Content	P_b	0.017
Effective binder content	P_{be}	0.018
Air void	AV	0.038
Asphalt film thickness	AFT	**0.072**
PG low temperature	PGLT	**0.070**
Voids in the mineral aggregate	VMA	**0.151**
PG high temperature	PGHT	**0.199**
Recycled asphalt pavement content	% RAP	**0.233**
Virgin asphalt content	$P_{b, v}$	**0.239**
Nominal maximum aggregate size	NMAS	**0.790**

6.5.3 Pearson Correlation Coefficient of Mix Design Variables and Mix G-R Value

Figure 6.4 shows the Pearson correlation coefficient between various mix design variables and mix G-R value. The relationship will be discussed based on the results obtained for the two cases (15°C and PGLT+10°C). Total binder content, nominal maximum aggregate size, void in the mineral aggregate and PG low temperature were found to have a stronger correlation to mix G-R as compared to the other mix variables considered in this study.

Recycled asphalt content and nominal maximum aggregate size showed a similar positive correlation to mix G-R parameters in both cases, inferring their potential negative effect on thermal cracking resistance. It is also interesting to see nominal maximum aggregate size having a large influence on thermal cracking performance. This impact can be due to loss of asphalt mixture flexibility with nominal maximum aggregate size increase, typically due to lower asphalt binder content in the mixture.

The negative correlation of total binder content, virgin binder content, effective binder content, air void, voids in mineral aggregate and PG spread in both cases on mix G-R values indicates that increase in these parameters helps with the thermal cracking property. Both an increase in binder content and air void are expected to decrease stiffness and increase phase angle of a mixture, moving mix G-R parameter to more desirable space.

The direction of impact on thermal performance due to PG low temperature and PG high temperature were opposite for 15°C and PGLT+10°C. However, results from the correlation probability show the lower reliability of the correlation values observed for PG low temperature and PG high temperature as it relates to PGLT+10°C. The very low correlation probability observed for PG low temperature for 15°C demonstrates the very low chance of observing

correlations related to these variables by chance. Thus, a conclusion can be drawn that the PG low temperature and mix G-R parameter have a strong positive correlation. This means that as the PG low temperature grade decreases the mix G-R parameter reduces improving the thermal cracking property of asphalt mixtures. For asphalt film thickness, the correlation values corresponding to 15°C and PGLT+10°C were found to be the opposite.

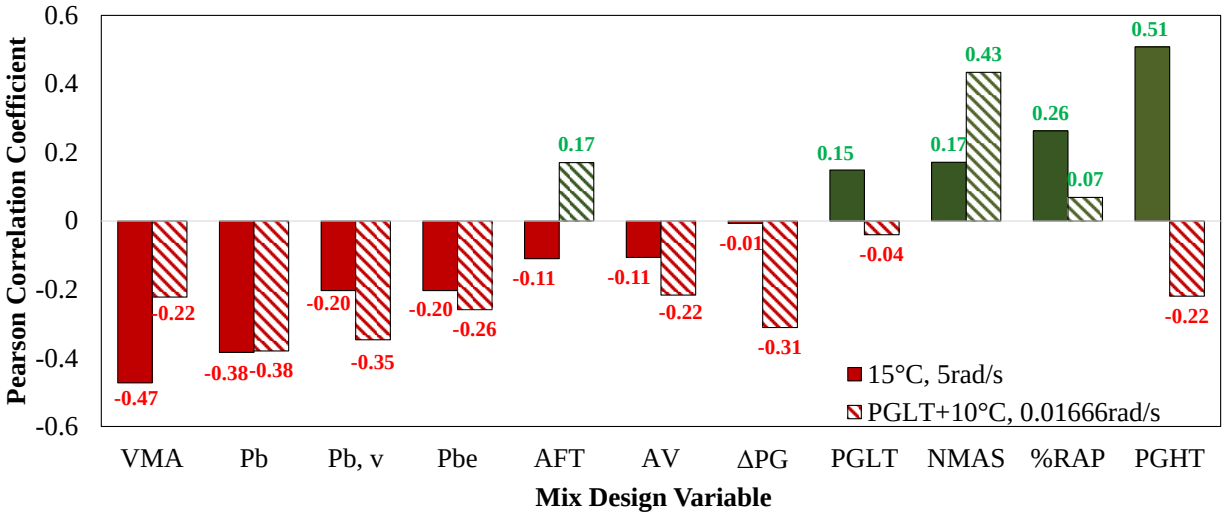

Figure 6. 4 Pearson correlation coefficient between mix variables and mix G-R value

In general, the correlation probability displayed in Table 6.5 shows that the higher reliability of correlation coefficients is obtained at 15°C as opposed to PGLT+10°C. Overall, values related to 15°C were lower than the significance threshold for PG low temperature, virgin asphalt content and voids in mineral aggregate indicating the correlation coefficient obtained from this study applies to a different population as it relates to these variables. However, for PGLT+10°C the values were above the significance threshold with the exception of nominal maximum aggregate size implying higher probability of the observed correlation due to chance.

Table 6.5 Significance of Pearson correlation coefficient between mix design variables and Mix G-R value

	Correlation probability	
Mix design variables	15°C, 5rad/s	PGLT+10°C, 0.01666rad/s
PG low temperature	0.013	**0.855**
Virgin asphalt content	0.019	**0.105**
Voids in the mineral aggregate	0.023	**0.308**
Total binder content	**0.071**	**0.321**
Voids filled with asphalt	**0.105**	**0.299**
Effective binder content	**0.149**	**0.064**
NMAS	**0.225**	0.039
PG spread	**0.288**	**0.148**
Asphalt film thickness	**0.350**	**0.160**
Recycled asphalt pavement	**0.434**	**0.755**
PG high temperature	**0.499**	**0.314**
Air voids	**0.628**	**0.321**

In Table 6.6 accepted basic assumptions regarding the effect of each of the mix variables on thermal cracking performance are compared to the implication from the study with respect to fracture energy and Glover-Rowe parameter. This is particularly important to identify theories that are perceived incorrectly and summarize the findings from the study based on an extensive statistical analysis to understand the effect of mix variables on thermal cracking performance of asphalt mixtures.

Table 6. 6 Comparison of accepted assumptions and study implication

Mix Variable	Accepted assumptions regarding mix variable impact on thermal cracking performance	Study implication based on	
		Fracture Energy	Mix Glover-Rowe parameter @ 15ºC, 5rad/s
PG Spread	Thermal cracking resistance is expected to improve with increase in PG spread. A higher PG spread could be partly attributed to a low PGLT grade which is associated to better performance in thermal cracking	**Met assumption**. PG spread showed a positive correlation to fracture energy. This conclusion is accompanied by a low correlation probability indicating higher confidence in the result	**Neutral towards assumption**. This could be attributed due to the similarity in PG spread of the binders used for the study
PGLT	A lower binder grade is specified to ensure good thermal cracking performance	**Met assumption**. A lower binder grade is associated to better thermal cracking performance	**Met assumption**. The result indicated the positive impact of lower binder grade on thermal cracking performance
PGHT	For binders with the same PG low temperature grade, a binder with a lower PGHT grade is expected to be softer and as a result is anticipated to perform better in the field	**Did not meet assumption**. The result showed that an increase in PG high temperature grade improves thermal cracking performance. It has to be noted that the relationship was found less reliable and further study is needed to verify the conclusion regarding the effect of PG high temperature	**Met assumption**. The result indicated that an increase in PG high temperature grade impacts the thermal cracking resistance in a negative manner. This could be due to a decrease in the softness of binder (less relaxation capacity) with an increase in PG high temperature grade
RAP content	An increase in RAP content is expected to impact the thermal cracking resistance in a negative manner due to aged binder from RAP	**Met assumption.** RAP content showed a negative correlation to fracture energy	**Met assumption.** An increase in RAP content showed a positive correlation to mix G-R indicating a decrease in thermal cracking performance. This is due to the shift of a G-R parameter to undesirable space with an increase in stiffness and decrease in relaxation capacity

Mix Variable	Accepted assumptions regarding mix variables impact on thermal cracking	Study implication with respect to	
		Fracture Energy	**Mix Glover-Rowe, 15°C, 5rad/s**
Total and virgin binder content	In general, an increase in total and virgin binder content is expected to increase the thermal cracking performance by increasing the relaxation capacity of asphalt mixture	**Did not meet assumption**. Both total and virgin binder content showed a negative correlation to fracture energy. For total binder content, this could be due to the aged binder from RAP that is accounted in the total binder content. The binder from RAP could have a counter effect and as a result could result in an overall negative implication on thermal cracking performance. The correlation probability for virgin asphalt content indicated low reliability of the finding. Therefore, further study is needed to validate the result	**Met assumption**. The result indicated that an increase in total and virgin binder content improves thermal cracking performance of asphalt mixtures. This is mainly attributed due to the lower stiffness and higher phase angle with an increase in asphalt content which shifts the G-R parameter to a more desirable region indicating better thermal cracking performance
Effective binder content, asphalt film thickness and voids in the mineral aggregate	The availability of more asphalt to coat aggregate particles in the mix due to increase in effective binder content, asphalt film thickness and voids in the mineral aggregate is expected to help with relaxation property resulting in better thermal cracking performance	**Met assumption**. The result indicated the positive impact of an increase in these variables on thermal cracking performance. The result from the correlation probability showed the more confidence of the conclusion drawn as it relates to effective binder content and asphalt film thickness	**Met assumption**. The result indicated an increase in one of these variables enhances the thermal cracking performance of asphalt mixture

6.6 Summary and Conclusions

This study investigated the effects of different mix design variables on thermal cracking performance properties of asphalt mixtures in terms of Black space location and fracture energy. Primary objective of this work is to provide insight and tools to mix designers and specifiers in terms of effects of mix properties on performance properties. Black space location controls thermal stress build-up due to consideration of asphalt mixture stiffness and relaxation capabilities. Fracture energy provides measure of crack resistance when thermal stresses approach and exceed material strength. Study utilized 90 mixtures from a MnDOT database and 81 mixtures from a UNH database. A stepwise regression analysis which accounts for a broader population is used to determine statistical significance between the different mix variables and thermal cracking performance properties. The Pearson correlation coefficient was determined to quantify and gain insight to the direction and extent of effect that a mix variable would have on performance property. Based on the results of this study, the following conclusions can be drawn:

- The p-values from stepwise regression analysis indicated a significant relationship between fracture energy and PG low temperature grade, PG high temperature grade, PG spread, voids in the mineral aggregate, asphalt film thickness, air void, virgin asphalt content, effective binder content and total binder content. This indicates that manipulation of any of these parameters could have a potential effect on thermal cracking performance. The extent of the impact is variable and assessed through correlation analysis.

- The p-values between mix variables and G-R parameter indicated a significant relationship between virgin asphalt content, total binder content, nominal maximum

aggregate size and mix G-R value at both 15°C and PGLT+10°C. For the other mix variables, significance of the effect is dependent on the temperature and frequency combination used to determine the mix G-R value. Due to the normalization done with respect to the PGLT+10°C, PG low temperature was found insignificant on the mix G-R value at 15ºC temperature.

- The result from Pearson correlation coefficient indicated stronger correlation of binder related mix design variables (total binder content (negative), effective binder content (positive), asphalt film thickness (positive), PG spread (positive)) to fracture energy as compared to the other mix design variables. This verifies the vital role binder plays in thermal cracking performance.

- Effective binder content, asphalt film thickness, air void, VMA, PG high temperature and PG spread showed a positive correlation to fracture energy implying an increase in one or more of these variables is expected to result in improved thermal cracking performance. However, a negative correlation is observed between total virgin binder, total binder content, RAP content, and low temperature grade with fracture energy. The correlation probability corresponding to PG spread, total binder content, effective binder content and air void were found to be lower than the threshold, implying that these variables can be employed confidently to obtain required fracture energy level. The results support consideration for using effective binder content to improve thermal cracking performance as opposed to total binder content.

- PG low temperature, recycled asphalt content and nominal maximum aggregate size displayed a positive correlation to mix G-R value. A negative correlation was found

between total binder content, virgin binder content, effective binder content, air void, voids in the mineral aggregate, and mix G-R parameter implying an increase in these parameters could potentially improve thermal performance of asphalt mixtures. The correlation probability indicated the better reliability of correlation coefficients obtained at 15°C for PG low temperature, virgin asphalt content and voids in the mineral aggregate.

The findings from this study give additional insight as to the influence of different mix variables on fracture energy and mix G-R value. This provides information to mix specifiers and producers in determining how to adjust mix composition effectively and efficiently to meet minimum threshold values and subsequently result in more crack resistant pavements.

It is possible for two variables to have zero linear relationship and a strong curvilinear relationship at the same time, so future research should evaluate the existence of a nonlinear relationship between the mix variables and thermal parameters. Future research efforts are also needed to adapt the findings from the study in actual projects to validate and make any needed adjustments to the conclusions drawn. Finally, work presented here serves as foundation for developing predictive models for thermal cracking performance properties in the future.

CHAPTER 7: INCREASING PRECISION AND ACCURACY IN FRACTURE ENERGY MEASUREMENT BY OPTIMIZING THE NUMBER OF TEST REPLICATES DURING DIRECT COMPACT TENSION TESTING

7.1 Introduction

Current specifications based on the Superior Performing Asphalt Pavement (Superpave) system tries to address the problem associated with low temperature cracking by specifying a low temperature grade of the asphalt binder (Anderson et al., 1994). However, researchers have shown that only binder test is not sufficient to ensure good performance in the field since it doesn't account for mixture properties such as aggregate type and gradation, recycled material type and amount and others (Lee and Hesp, 1994; Morrison et al., 1994). Thus, in recent years advancements have been made to develop fracture tests that give a better understanding on the mechanism of low temperature cracking. These tests include disk-shaped compact tension test (DCT), single edge notched beam (SEB), and semi-circular bending test (SCB) (Li and Marasteanu, 2004; Wagoner, Buttlar, & Paulino, 2005a; Wagoner, Buttlar, and Paulino, 2005b). These tests measure the effort required to form a crack throughout the specimen along initial fractured surface to characterize the response of materials to thermal loading. The test data from these tests is used to calculate key fracture parameters such as fracture energy, stress intensity factor and others to determine the low temperature cracking resistance of asphalt mixtures. Easy specimen fabrication and use of standard fracture test configuration are accounted as two of the

main benefits of implementing the tests to evaluate the low temperature cracking resistance of asphalt mixtures.

In an effort to address the problem associated with low temperature cracking MnDOT has taken the initiative to incorporate DCT test as one of the requirements in their low temperature performance-based specification. This is accomplished by measuring fracture energy of asphalt mixtures and comparing the values to a minimum threshold value at limiting temperature values. Researchers (McCarthy, Callans, and Scott, 2016; Van Deusen et al., 2015) have proposed a minimum threshold value of 400 J/m^2 for short-term aged mixtures to ensure the low temperature performance of asphalt mixtures in the field. The aforementioned MnDOT specification requires DCT testing to be performed during mix design and production phase. Mix design is accepted if meets minimum fracture energy requirement of 450 J/m^2 for traffic levels 1, 2 and 3 or 500 J/m^2 for levels 4 and 5. Similarly, during production phase mix is required to meet fracture energy of 400 J/m^2 for traffic levels 1, 2 and 3 or 450 J/m^2 for levels 4 and 5.

Due to the variability associated with all mechanical tests on heterogeneous materials such as asphalt mixtures, typically a certain number of replicates are tested and the results from the replicates are averaged to increase the confidence in the conclusion drawn from the experiment. While it is known that increasing the number of replicates improves the precision in the result and helps to detect outliners, the increased time and effort required to perform the experiments constrain the number of replicates in most studies. Therefore, when establishing the number of replicates required for a certain test the effort required for carrying out the test should be balanced against the quality of data. This is commonly referred as a practical limit and helps in making a decision regarding the number of replicates required for materials such as asphalt concrete that exhibits high measurement variability during testing.

With this aim, this study undertook an effort to determine the number of replicates required to obtain an accurate and precise fracture energy measurement from DCT testing. The study seeks to establish the number of replicates required during DCT testing to obtain a fracture energy measurement that is representative of the mixture and unbiased in terms of results from small enough sample size. It strives to reduce measurement variability to an acceptable level and enable producers and agencies to be confident when they reject or accept mixes based on measurements from the test. In this study, measurements based on different number of replicates were assessed to observe their impact on the conclusion reached based on experimental result. The outcome from this study will be used to make decision on the number of replicates which will be subsequently incorporated into the MnDOT modified DCT performance specification.

7.2 Materials and Methods

7.2.1 DCT Testing

The Disc-Shaped Compact Tension test was developed at University of Illinois to determine the low temperature fracture properties of asphalt mixtures based on fracture energy measured on laboratory and field produced specimens. Information on the DCT test development can be found in Wagoner et al. (2005c) and Wagoner (2006). For this study, DCT test was carried out on a cylindrically-shaped asphalt concrete specimen following the test procedure on ASTM D7313 -13 /MnDOT Modified specification. The test specimen is conditioned to a recommend standard test temperature of 10°C warmer than the PG low temperature value for a minimum of 2 hours. The test is performed by applying a tensile load on the specimen at a constant CMOD rate of 1mm/min until the post peak load level is reduced to 0.1kN. From the test, the fracture energy of the specimens is determined by computing the area under the load displacement curve normalized by the ligament length times the thickness of the specimen (Figure 7.1). The test configuration and

the output from the test (load-displacement curve) and fracture energy determination are demonstrated in Figure 7.1.

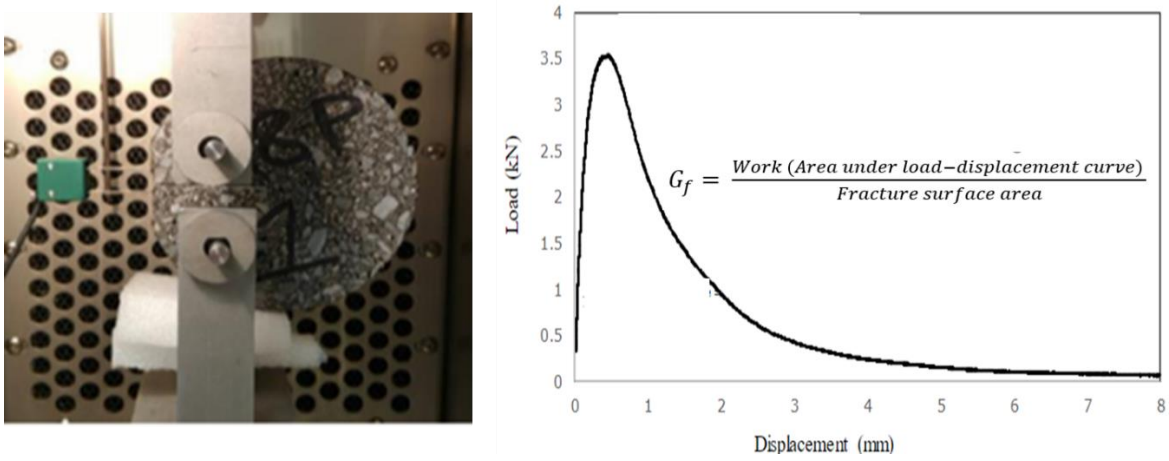

Figure 7. 1 DCT test configuration and fracture energy determination from load-displacement curve

7.3 Study Mixtures Information

According to the research objective of this study, mixes from TH14, TH15, I-90 and MnROAD projects were utilized to determine the number of replicates required to achieve accurate and precise fracture energy measurement from DCT test. Overall, 23 different mixtures were used, five from TH14, seven from TH15, two from I-90 and eight from MnROAD research facility. From the loose mix a total of 16 replicates corresponding to each mix were tested. The mixes were obtained in buckets and four specimens were produced from each bucket and are accounted as specimens obtained from one set. A total of 4 buckets of mixtures were used to produce a total of 16 replicates for each mix. DCT testing was conducted on all 368 (16×23) specimens to determine the fracture energy of the mixes. The following terminologies are used in the discussion as defined below to help readers follow the paper easily.

- The term “Set” is used to refer all specimens produced from mix in a bucket
- “Replicates” generically refers to individual specimens produced from the same mix
- “Specimen” generically refers to any individual specimen produced from any bucket

7.4 Research Methodology

A total of 16 replicates (4 *Sets*) were tested for each mix to determine their respective fracture energy. Each *Set* were combined in different ways to produce 4 (individual set), 8 (combining two sets) and 12 (combining 3 sets) replicate scenarios. This is done to simulate different replicate scenarios and examine how measurement variability changes based on the number of total replicates tested for a mix. The combinations used to produce 4, 8 and 12 replicates for a specific mix are explained below; the procedure is illustrated in Figure 7.2 as well.

1. The first combination represents a scenario where only four replicates are tested for each mix. In this case, none of the *sets* were combined but treated separately resulting in 4 sets of *4 replicate scenario* for a mix which will be referred hereinafter as *4 replicate scenario*.
2. The second combination represents a scenario where eight replicates are tested for a mix. This is achieved by combining 2 sets at a time and producing 6 different combinations for each mix. This will be referred hereinafter as *8 replicate scenario*.
3. The third combination corresponds to a scenario where twelve replicates are tested for a mix. This is achieved by combining 3 sets at a time and producing 4 different combinations for each mix. This will be referred hereinafter as *12 replicate scenario*.

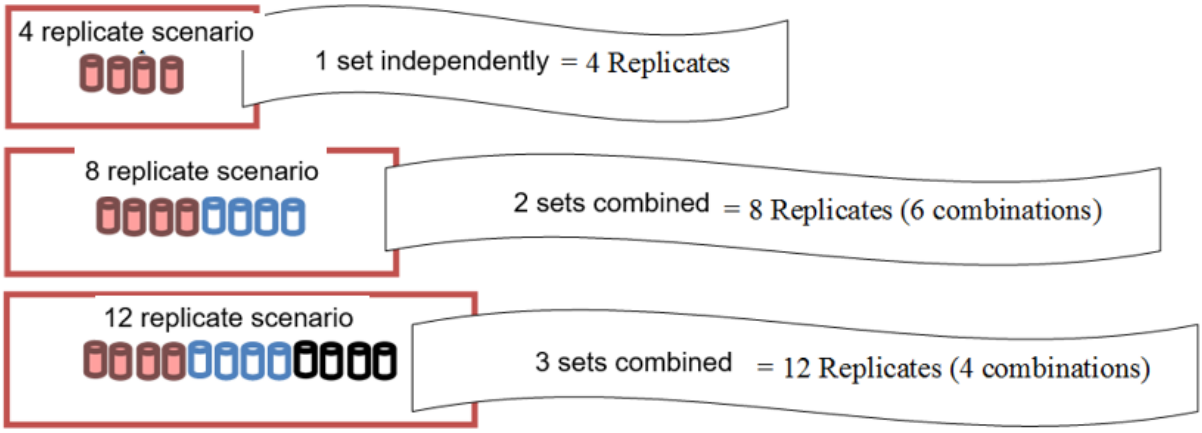

Figure 7. 2 Combinations used to produce 4, 8 and 12 replicate scenarios

7.5 Analysis Methods

Different mathematical and statistical analysis, discussed below in detail, were performed to determine the optimal number of replicates required for DCT testing to achieve accurate and precise fracture energy measurement during DCT testing. Each analysis method was believed to be relevant and informative regarding the accuracy and precision of the different replicate scenarios. Based on the results from the analysis comparisons were made between measurement variability as the number of replicates changes from 4 to 8 and then to 12.

7.5.1 Mathematical Evaluation of Measurement Variability

7.5.1.1 The Percent Difference between the Low and High Fracture Energy

For the different replicate scenarios, the percent difference between the low and high fracture energy measurement was calculated using Equation 7.1. This is done to determine the maximum difference between the low and high fracture energy measurement values corresponding to 4, 8 and 12 replicate scenarios. It should be noted that the different combinations produce different sets

corresponding to 4, 8 and 12 replicates for a specific mix and the sets which exhibited the highest and lowest measurement are used for the calculation. The value for each mix is determined to allow comparison between the maximum difference for different replicate scenarios. The analysis is useful to determine how close the low and high values are relative to the larger value. This gives a better platform for comparison as compared to the absolute difference calculation which might misinform in terms of how much the measurements differ.

$$\%\ \text{Maximum Difference} = \frac{\text{High } G_{f_{Avg}} - \text{ Low } G_{f_{Avg}}}{\text{High } G_{f_{Avg}}} * 100 \qquad [7.1]$$

7.5.1.2 The Percent Difference between the Overall Fracture Energy with Low and High Fracture Energy (Overall to Low Difference or Overall to High Difference)

The percent difference between the overall fracture energy with the low and high fracture energy (overall to low difference or overall to high difference) is computed for 4, 8, and 12 replicate scenarios. In this case the overall fracture energy corresponds to the average fracture energy calculated considering all 16 replicates for a specific mix. This is done to determine how close the low and high measurements from different replicate scenarios are close to the overall fracture energy value which is determined considering all the 16 replicates. The difference from overall to low and high values is calculated using Equations 7.2 and 7.3.

$$\text{Overall to Low Difference} = \frac{\text{Overall } G_{f_{Avg}} - \text{ Low } G_{f_{Avg}}}{\text{Overall } G_{f_{Avg}}} \qquad [7.2]$$

$$\text{Overall to High Difference} = \frac{\text{Overall } G_{f_{Avg}} - \text{ High } G_{f_{Avg}}}{\text{Overall } G_{f_{Avg}}} \qquad [7.3]$$

7.5.2 Statistical Evaluation of Measurement Variability

7.5.2.1 The Coefficient of Variation (COV)

The coefficient of variation measures data variability with respect to the mean and is a useful tool to compare the degree of variation from one data series to another in a way that does not depend on variable measurement unit. It is the ratio of standard deviation to mean: the higher coefficient variation, the greater dispersion in the measurement. For this study the high observed coefficient of variation value for a mix is determined. This is accomplished by comparing the values from all possible combination and choosing the case where the COV value is the highest for each mix. Then the value is compared to the coefficient of variation value determined for overall specimens (considering all 16 replicates) for each mix in terms of percent difference. The percent difference between overall COV and high COV is calculated using Equation 8.4. This is done to compare the difference in COV as the replicate number changes from 4 to 8 and then to 12 for the critical case which is when high COV is observed.

$$\%\ \text{Difference between Overall and High COV} = (\text{Overall COV} - \text{High COV}) * 100 \qquad [7.4]$$

7.5.2.2 Comparison of Mean Differences

Data obtained from a certain number samples can be used to infer matters representative of the population and make conclusion about the population based on the sample. This method is referred as inferential statistics. In this study the population mean that is representative for the mixes is determined from fracture measurements obtained assuming 4, 8 and 12 replicate scenarios. Determining population mean is beneficial as oppose to sample mean because it allows to make a statement not only about the study sample but to the general population. For this study, the population mean for 4,8,12 and 16 replicate scenarios were determined based on the test

measurements for each mix using a statistical software, JMP®. Then the percent difference between mean determined from 4, 8 and 12 replicate scenarios with respect to the 16 replicates mean is determined using Equation 7.5. This is done to see how the population mean corresponding to the 16 replicate scenario deviates as the replicate number is reduced to 12, 8 and then further to 4 replicates.

$$\% \text{ Difference between means } = \frac{\frac{\sum(\text{Mean}_{(16\text{ rep})} - \text{Mean}_{(4,\ 8 \text{ or } 12\text{ rep })})}{\text{Mean}_{(16\text{ rep})}}}{\text{n}} * 100 \qquad [7.5]$$

where:

n = total number of combinations for 4, 8 or 12 replicate scenarios

7.5.2.3 One Sample t-test

A one sample t-test is a statistical tool used to determine whether a sample of observations share a similar mean value or not. Commonly two kinds of hypotheses are implemented, the null hypothesis and the alternative hypothesis. The null hypothesis assumes that no difference exists whereas the alternative hypothesis assumes that some difference exists between the true mean and the comparison value. The purpose of the one sample *t*-test is to determine if the null hypothesis should be rejected, given the sample data.

For this study, a one sample t-test is performed on fracture energy values obtained by combining different sets to represent 4, 8 and 12 replicate scenarios. The one sample t-test is used to test the fracture energy measurement obtained assuming different replicate numbers to the well-established threshold value of 400J/m^2. The population mean from each of 4, 8 and 12 replicates was compared to the hypothesized value of 400J/m^2 to determine the level of confidence for an alternative hypothesis which assumes the population mean is greater than 400J/m^2. For mixtures

with population mean greater than the threshold value, results which indicated 95% ($P<0.05$) confidence are counted. This is done to determine the number of mixes for which the conclusion that the measurement is greater than the threshold value applies to general population with a 95% confidence.

7.5.2.4 Two Sample t-test

Two sample t-test is a statistical tool that is used to determine if two population means are equal. It is applied to compare whether the average difference between two observations is significant or not. Similar to one sample t-test the null and alternative hypotheses are implemented. In this case the null hypothesis assumes that there is no difference between the means from the different scenarios whereas the alternative hypothesis assumes the existence of a difference between the means. In this study two-sample t-test is used to determine if there is a statistical significant difference in mean response between 16 replicates and other sets of replicates considered in this study. This is done to statistically compare the variation in population mean as the number of replicates change from 16 to 4, 8 and 12.

7.6 Results and Discussion

7.6.1 The Percent Difference between the Low and High Fracture Energy

The maximum difference between fracture energy measurements for 4, 8 and 12 replicate scenarios corresponding to the 23 mixtures is indicated in Figure 7.3. The maximum difference ranges from 3 to 25% for 4 replicate scenario, 2 to 14% for 8 replicate scenario and 1 to 9% for 12 replicate scenario. The result indicated that the maximum difference between measurement values reduces as the number of replicates increase from 4 to 12. This in general indicates testing higher number replicates results in reduction of overall difference between observed measurements.

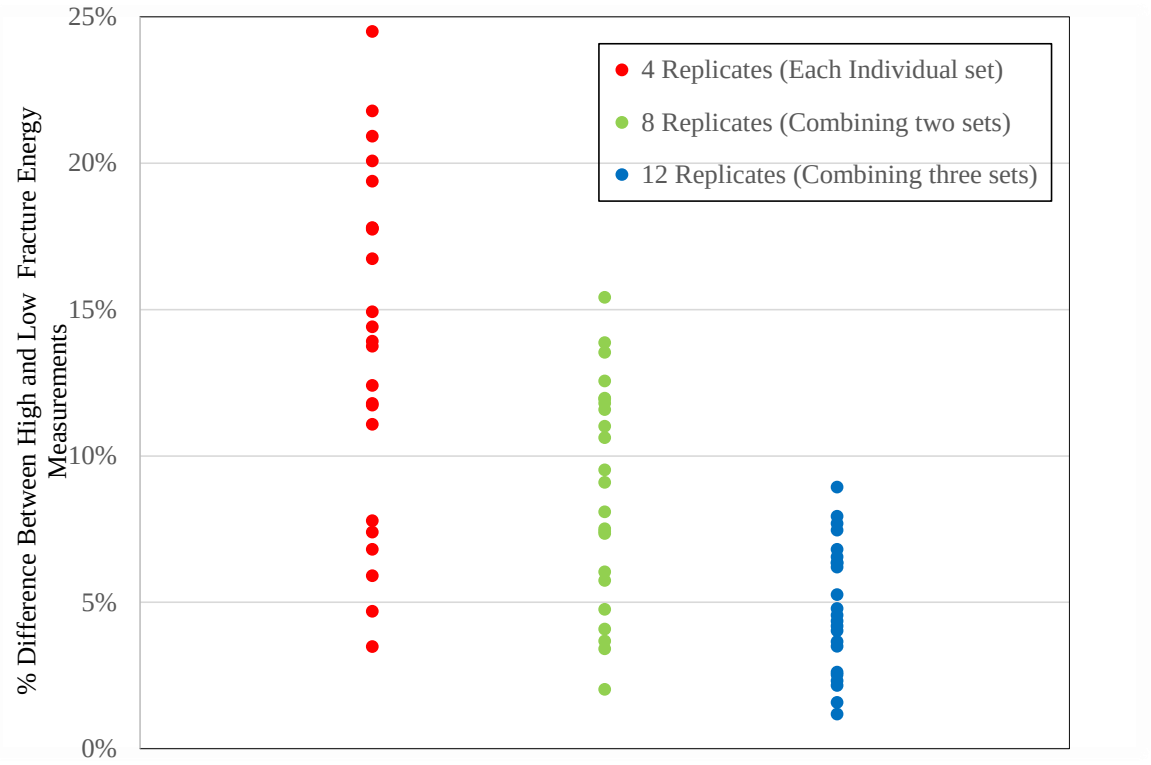

Figure 7. 3 Percent difference between the low and high fracture energy measurements for the 23 mixtures corresponding to 4, 8 and 12 replicate scenarios

7.6.2 The Percent Difference between the Overall Fracture Energy with the Low and High Fracture Energy (Overall to Low Difference or Overall to High Difference)

The percent difference between the overall fracture energy with the high and low fracture energy measurements are displayed in Figure 7.4 for 4, 8 and 12 replicate scenarios. The results indicate that the difference reduces as the number of replicates increases from 4 to 8 and then to 12. The low to overall difference ranges from 2 to 16% for 4 replicate scenario, 1 to 9 % for 8 replicate scenario and 0 to 9% for 12 replicate scenario. Overall to high difference ranges from 2 to 14% for 4 replicate scenario, 1 to 7% for 8 replicate scenario and 0 to 5% for 12 replicate scenario. This indicates that variability with respect to the overall measurement is reduced as the number of replicates is increased.

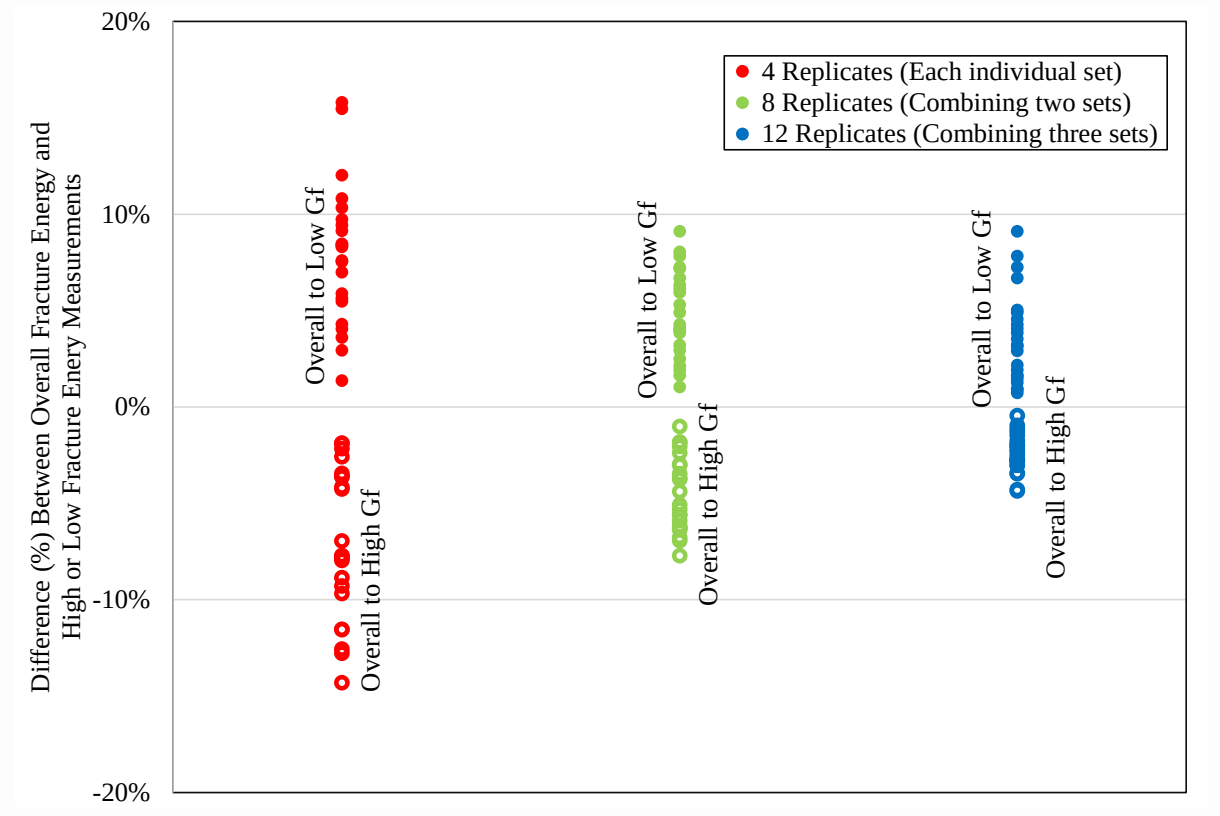

Figure 7. 4 Percent difference between the overall fracture energy with the high and low fracture energy (low to overall difference or overall to high difference) for the 23 mixtures

7.6.3 The Coefficient of Variation

Figure 7.5 displays the difference between overall COV and high COV values corresponding to different replicate scenarios. The result indicates that the difference between overall to high COV is reduced as the number of replicates increases from 4 to 8 and then to 12. The difference between overall COV and high COV reduces to an average of 2% as we get to 12 replicates. This indicates that the COV variation becomes close to the overall COV as the number of replicates increases. The result in general indicates the difference can be minimized by increasing the number of replicates.

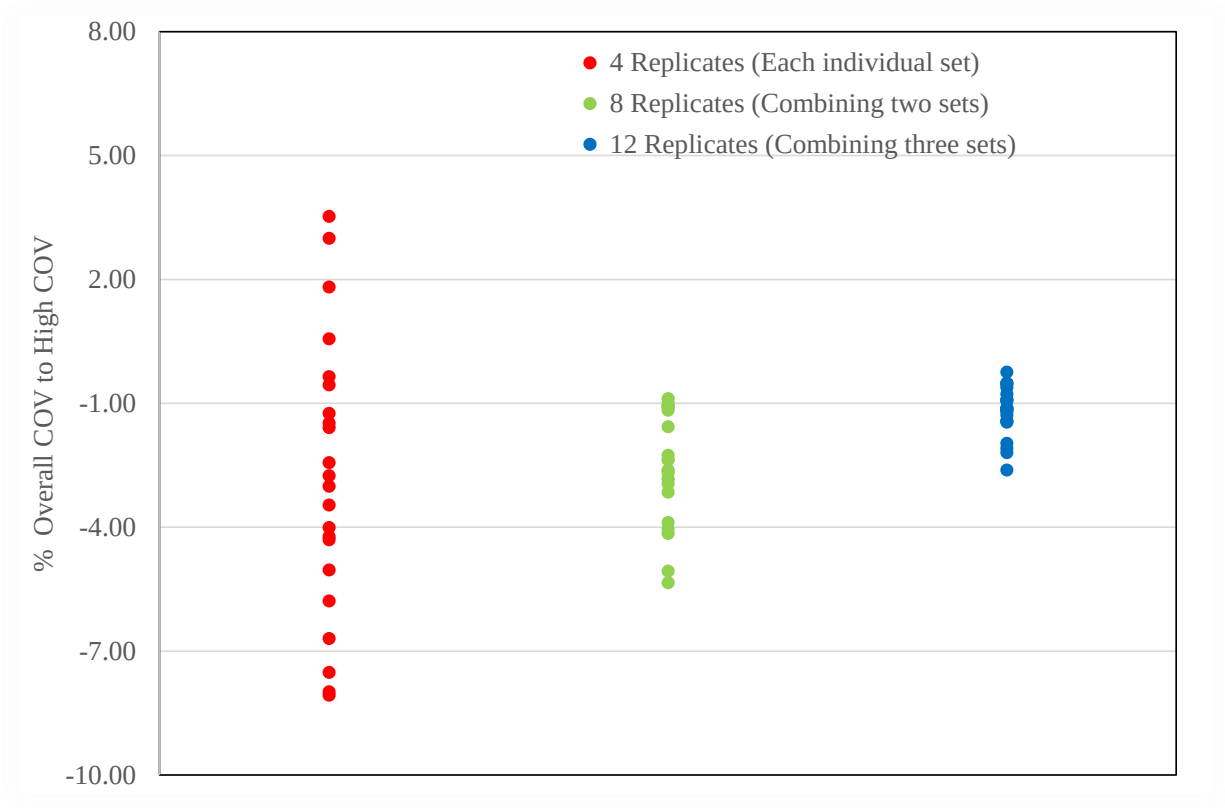

Figure 7. 5 Percent difference between the overall COV to high COV for the 23 mixtures

7.6.4 Comparison of Mean Differences

Figure 7.6 displays the percent difference of each mean determined assuming 4, 8 and 12 replicate scenario with respect to mean determined considering all 16 replicates. The difference ranges from 1 to 9 % for 4 replicate scenario, 1 to 5.5% for two 8 replicate scenario and 0.5 to 3% for 12 replicate scenario. The result indicated that the population mean deviates by 5%, 3% and 1.5% on average from the population mean determined by testing 16 replicates as the number of replicates changes to 4, 8 and 12 replicates respectively. Assuming measurement determined from the 16 replicates scenario gives a better representation of the population, we can conclude that a better precision (only 1.5% deviation) could be achieved if measurement of fracture energy is determined by testing 12 replicates. This deviation grows as the replicate number reduces to 8 and then to 4

indicating the increased possibility of the population means determined from these two cases being non-representative of the overall population.

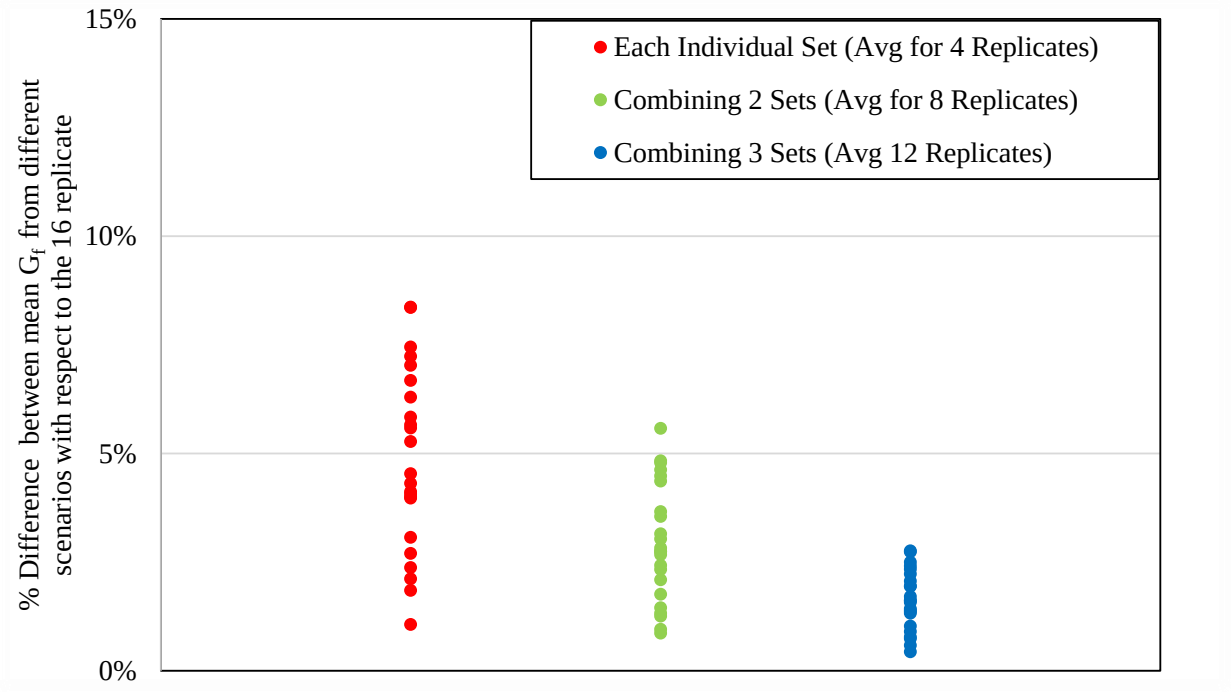

Figure 7. 6 Percent difference between the population mean corresponding to different replicate scenarios and the population mean determined based on16 replicates

7.6.5 One Sample t-test

Figure 7.7 shows the population mean estimated based on the data collected for the 23 study mixes, Figure 7.7 (a) corresponds to 4 replicate scenario, Figure 7.7(b) corresponds to 8 replicate scenario whereas 7.7(c) corresponds to 12 replicate scenario. For mixes which exhibited a mean fracture energy greater than 400J/m^2 (threshold value) a one sample t-test is performed to determine the level of confidence associated to an alternative hypothesis which assumes that the population mean is greater that 400J/m^2 for these mixes. Based on the analysis mixes which indicated more than 95% confidence ($P<0.05$) were identified and displayed in Figure 7.7 along with mixtures which exhibited a level of confidence less than 95% ($P>0.05$). From the figure mixes which indicted 95%

(P<0.05) confidence are counted and the numbers and percentages are summarized in Table 7.1 for each replicate scenario. The result indicated that for a test with 4 replicates, we can confidently tell for an average of 10 mixtures out of 17 (59%) whether they meet the minimum threshold value or not even if their estimated population mean is greater than 400J/m^2. In other words, there is a 41% probability that there can be false positive due to use of 4 replicates. With 8 replicates the confidence grows to 76% (13 out of 17) and with 12 replicates to 88% (on average 15 mixtures from 17). Thus, the probability of error is reduced to 24 and 12% due to use of 8 and 12 replicates respectively. This indicates that as the number of replicates increase to 12 the false positive rate is very low resulting in a reliable conclusion regarding the fracture energy measurement determined from DCT test.

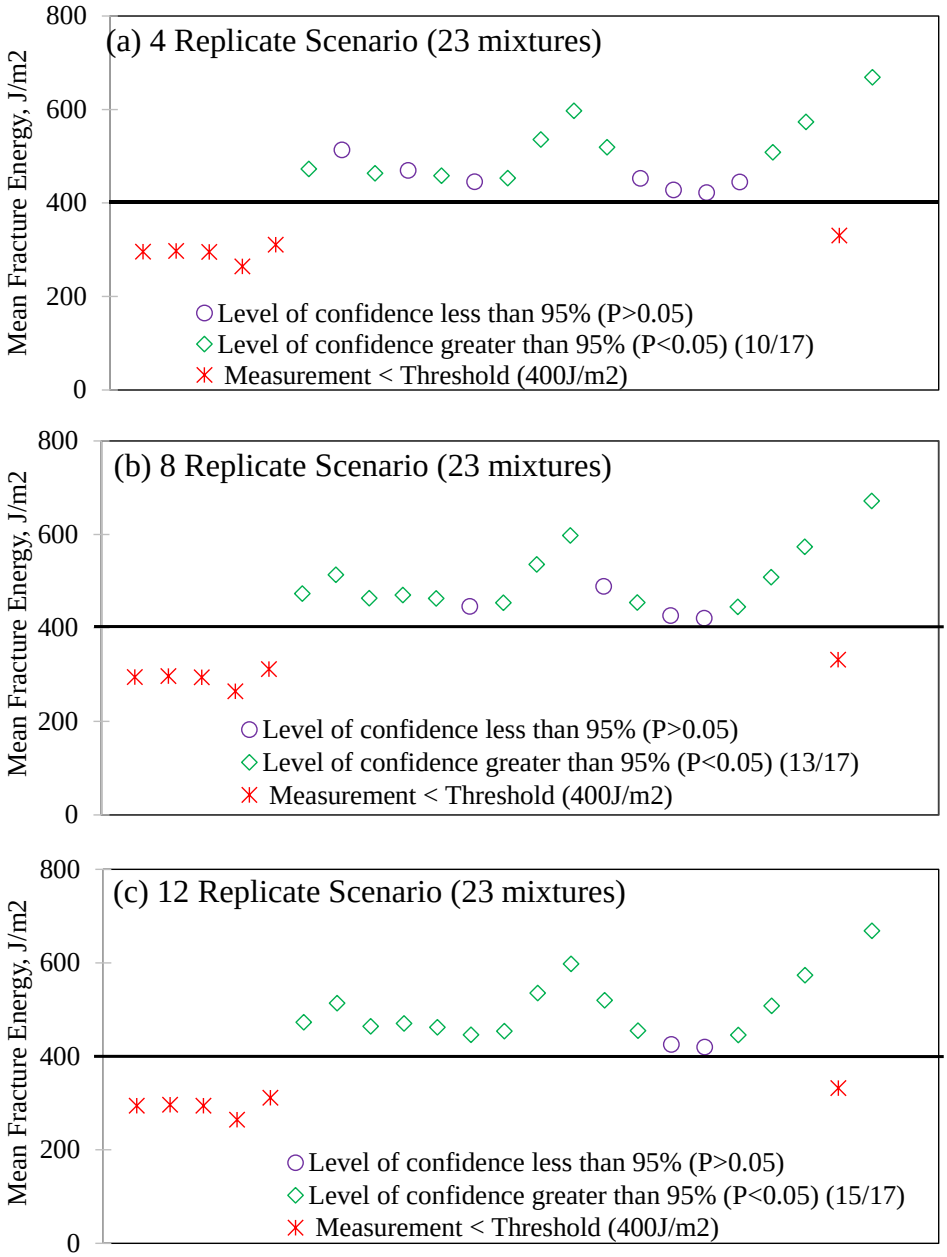

Figure 7. 7 Population mean determined from sample data for the 23 mixtures assuming (a) 4 replicate (b) 8 replicate and (c) 12 replicate scenarios

Table 7.1 One sample t-test summary

Scenarios	No of mixtures ($p<0.05$) or 95 % confident in results of	% of mixtures ($p<0.05$) or confidence in percentage	Probability of error
4 replicates	10/17 specimens	59%	41%
8 replicates	13/17 specimens	76%	24%
12 replicates	15/17 specimens	88%	12%

7.6.6 Two Sample t-test

Two sample t-test is used to determine if there is a statistical significant difference in mean response between 16 replicates and other sets of replicates considered in this study. However, the t-test results indicated that there is no statistically significant difference between the means. The authors hypothesized that since the 4, 8 and 12 replicates were a subset of the 16 replicates the differences were hindered when a two sample t-test is performed. For future analysis, if a separate set of replicates are used, information could be obtained on whether there is a statistically significant difference between 16 replicates and the other replicate scenarios.

7.7 Summary and Conclusions

To establish the number of replicates required for DCT testing to obtain a larger accuracy and precision in fracture energy measurements, different mathematical and statistical analysis were performed assuming a 4, 8 and 12 replicate scenarios. For the study, 23 mixtures were used and DCT testing was performed on 16 replicates corresponding to each mix. The results from the analysis persistently indicated that measurement variability is in general minimized as the number of replicates increases from 4 to 8 and then to 12. The comparison done with respect to the 16

replicate measurement indicate the increased reliability achieved as the number of replicates increased to 12 replicates as well. This was also prevalent in the results obtained from one sample t-test which indicated a higher confidence obtained when a mix is accepted by comparing to the threshold value when 12 replicates are tested. It is especially interesting to see the very low confidence associated to the 4 replicate scenario (59%) as opposed to 88% for 12 replicate scenario.

Based on the finding from this study, it is believed that testing 12 replicates would give a true representation of the fracture resistance of the asphalt mixture. Therefore, for purposes of performance-based specifications using DCT fracture energy 12 replicate specimens are recommended to ensure necessary accuracy and repeatability. This will enable producers and agencies to be confident when they reject or accept mixes based on measurements from the test.

CHAPTER 8: CONCLUDING REMARKS

The motivation for this study initiates from the need to transition from widely employed current empirical methods to performance based evaluation to ensure longevity of pavements. In the last three decades researchers have taken the initiative to develop performance based material selection and pavement design methods for this effect. However, agencies have been hesitant to introduce the methods to their design and pavement evaluation for reasons related to complexity and uncertainty associated to accuracy of the methods. Therefore, this dissertation contributes to the ongoing effort to simplify and increase the confidence in the methods by addressing known gaps related to linear viscoelastic and fracture characterization of asphalt concrete.

The increased accuracy, simplicity and understanding realized from this dissertation regarding linear viscoelastic and fracture properties of asphalt mixtures will culminate in a more effective and efficient mixture and pavement design. Incorporation of the new approaches introduced to determine key material inputs such, phase angle, low temperature S and m-value into the methods results in a more reliable and simple pavement evaluation tools. Moreover, the increased understanding achieved regarding fracture properties of asphalt mixtures helps agencies to make informed decision during mix design and production.

The primary findings from each chapter of the dissertation are summarized in subsequent paragraphs and gaps are identified for future work. Furthermore, discussion is presented regarding authors vision on how researchers, agencies and contractors can incorporate them for the development of performance based mixture design, evaluation and performance based specifications.

In chapter 3 a fundamental relationship to determine the phase angle from the slope of the stiffness curve is evaluated. Comparison done between predicted and measured phase angle values indicated that the inference from the results is dependent on the type of LVDT used: measured phase angle values match very well with predicted values when spring loaded LVDTs are used whereas larger differences were observed for specimens that used loose core LVDTs. It was also apparent that the prediction resulted in a consistently lower value as compared to measured values. The hypothesis of the researchers to the observed difference is the contribution of plastic strain, which may create a difference in phase angles of 1 to 2 degrees. The implication on different pavement performance evaluation methods (Black Space, S-VECD and LVECD) due to use of predicted values as opposed to measured values manifested considerably similar predictions.

Chapter 4 investigates the ability of master curve parameters such as the G-R parameter, log of the inflection point frequency ($-\beta/\gamma$), log of the distance between the glassy modulus and the inflection point modulus (γ), $-\beta/\gamma$ vs γ and lower and upper asymptote of the sigmoidal form of master-curve to identify between mixture variables. The evaluated mixture variables included aging level, rejuvenator dosage, RBR, and binder grade. The result indicated that the mixture G-R parameter can capture the changes in mixture properties due to aging, RBR, and PGLT whereas the $-\beta/\gamma^2$ parameter was able to capture the effect of aging only. A shift of Black space points to the top

left has been observed with aging whereas the opposite trend was observed in the $-\beta/\gamma$ vs γ plot which is associated to more cracking susceptibility in both cases.

In Chapter 5, due to the substantially smaller amount of binder required for testing, increased reliability of DSR low temperature measurement and the possibility of using one piece of equipment for full characterization of asphalt binders, the study investigated the applicability of different approaches to determine low temperature specification parameters (S and m-value) from DSR testing. The results showed that the slope and magnitude of the shear relaxation modulus and shear creep stiffness curve correlates linearly with BBR measured S and m-values. The magnitudes were similar when the Christensen method is employed for interconversion whereas a consistent deviation in magnitude was observed when using the exact interconversion method. Moreover, a strong correlation observed between DSR $|G^*|$ and BBR S value as well as DSR ϕ and BBR m-value led to the development of a simple equation that can translate a single measurement of $|G^*|$ and phase angle to specification S and m-value.

Chapter 6 identified mix design variables that potentially affect the thermal cracking performance of asphalt mixtures. Statistical analysis was employed to determine the significance and correlation between common mix design variables, including recycled asphalt amount, mix volumetric properties and binder grade to fracture energy and mix G-R values. The result indicated stronger correlation of binder related mix design variables (total binder content (negative), effective binder content (positive), asphalt film thickness (positive), PG spread (positive)) to fracture energy as compared to the other mix design variables. This verifies the vital role binder plays in thermal cracking performance. Effective binder content, asphalt film thickness, air void, voids in the mineral aggregate, PG high temperature and PG spread showed a positive correlation to fracture energy implying an increase in one or more of these variables is expected to result in improved

thermal cracking performance. A negative correlation was found between total binder content, virgin binder content, effective binder content, air void, voids in the mineral aggregate, and mix G-R parameter implying an increase in these parameters could potentially improve thermal cracking performance of asphalt mixtures.

An effort is undertaken in chapter 7 to determine the number of replicates required to obtain an accurate and precise fracture energy measurement from DCT testing. The results from the analysis consistently indicated that measurement variability is reduced when 12 replicates are tested. The maximum difference between measurements when 4 replicates are used ranges from 3 to 25% but reduces to 1 to 9% for 12 replicates. For 4 replicates there was 41% margin of error for false positives however, this error margin dropped to 12% when using 12 replicates. Based on the finding from this study, it is believed that testing 12 replicates would give a true representation of the fracture properties of asphalt mixture. Therefore, for purposes of performance-based specifications using DCT fracture energy 12 replicate specimens are recommended to ensure necessary accuracy and repeatability.

The following gaps are identified for future study.

- The potential effect of permanent strain that could be encountered during complex modulus testing (acceptable up to 1500μ according to AASHTO T 342) on the prediction of phase angle from stiffness data should be investigated.
- The cause for the large magnitude difference between measured S from BBR and estimated S from DSR due to exact interconversion with fitted generalized Maxwell model should be further studied.

- It is possible for two variables to have zero linear relationship and a strong curvilinear relationship at the same time, so future research should evaluate the existence of a nonlinear relationship between the mix variables and thermal parameters. Future research efforts are also needed to adapt the findings from the study in actual projects to validate and make any needed adjustments to the conclusions drawn.

The author of this dissertation envisions use of the finding from the dissertation by researchers, agencies, contractors and others as part of performance based pavement design, evaluation and specification as follows:

- The simple and robust phase angle prediction method evaluated in the dissertation presents a reliable method of confirming or supporting lab measured phase angle data and replacing when measured data has issues.
- Depending on the mixture specifier's or producer's interest in evaluating the effect of one or more of the mixture variables, the master curve parameters identified in this study can be used to track the changes in rheological properties due to changes in specific mixture variables.
- The reliably estimated BBR specification parameters from DSR test data can be particularly used for characterization of low temperature properties of extracted and recovered binders from field cores. Moreover, one piece of equipment can be used for full linear viscoelastic characterization of asphalt binder. This will result in enormous practical use for owner agencies as well as contractors by drastically reducing time and effort otherwise required for full characterization of binder.
- The better understanding obtained in this dissertation on how to adjust mix composition effectively and efficiently to meet minimum threshold values can be used as a guidance by

mix specifiers and producers to achieve specification requirements as it relates to fracture energy and mix G-R value.

- Agencies can perform DCT tests on recommended replicates to ensure necessary accuracy and repeatability and increase their confidence when they reject or accept mixes based on measurements from the test.

In closing, refinement and simplification done in this dissertation in relation to material properties commonly used in performance based evaluation encourages both owner agencies and contractors to shift from empirical to performance based pavement evaluation methods and performance based specification. This shift allows owner agencies to set their own performance limits and obtain confidence that the pavement can avoid failure for a given period of time based on accurately predicted performance while contractors, with the knowledge of the key parameters for improving the cracking resistance of pavements, will be driven to adjust their mix accordingly.

CHAPTER 9: REFERENCES

AASHTO, PP 60. Standard practice for preparation of cylindrical performance test specimens using the Superpave gyratory compactor (SGC). American Association of State Highway Transportation Officials, 2011.

AASHTO, T164 “Standard Method of Test for Quantitative Extraction of Asphalt Binder from Hot Mix Asphalt (HMA),” American Association of State Highway and Transportation Officials, 2014.

AASHTO, T313 “Standard Method of Test for Determining the Flexural Creep Stiffness of Asphalt Binder Using the Bending Beam Rheometer (BBR),” American Association of State Highway and Transportation Officials, 2008.

AASHTO, T315 “Standard test method for determining the rheological properties of asphalt binder using a dynamic shear rheometer (DSR)," Provisional Standard Test Methods, 2000.

AASHTO draft standard method of test for determining the low temperature rheological properties of asphalt binder using a dynamic shear rheometer (DSR), 2012.

American Association of State Highway and Transportation Officials, “Standard Method of Test for Determining the Damage Characteristic Curve of Asphalt Concrete from Direct Tension Cyclic Fatigue Tests,” AASHTO T107, 2014.

AASHTO, T 342. Standard Method of Test for Determining Dynamic Modulus of Hot-Mix Asphalt Concrete Mixtures. American Association of State Highway Transportation Officials, 2015.

Abu Abdo, A. M., Eckwright, F., Jung, S. J., Bayomy, F., & Nielsen, R. (2014, February). Semi-circular notched beam testing procedure for hot mixture asphalt. In *Proceedings of the Institution of Civil Engineers-Transport* (Vol. 167, No. 1, pp. 48-58). Thomas Telford Ltd.

Airey, G. D., & Rahimzadeh, B. (2004). Combined bituminous binder and mixture linear rheological properties. *Construction and Building Materials*, *18*(7), 535-548.

Al-Qadi, I., Yang, S. H., Dessouky, S., Masson, J. F., Loulizi, A., & Elseifi, M. (2007). Development of crack sealant bending beam rheometer (CSBBR) testing to characterize hot-poured bituminous crack sealant at low temperature. *Asphalt Paving Technology-Proceedings*, *76*, 85.

Al-Qadi, I. L., Carpenter, S. H., Roberts, G., Ozer, H., Aurangzeb, Q., Elseifi, M., & Trepanier, J. (2009). *Determination of usable residual asphalt binder in RAP*. Illinois Center for Transportation (ICT).

Al-Qadi, I. L., Ozer, H., Lambros, J., El Khatib, A., Singhvi, P., Khan, T. & Doll, B. (2015). *Testing protocols to ensure performance of high asphalt binder replacement mixes using RAP and RAS*. Illinois Center for Transportation/Illinois Department of Transportation.

Andrei, D., Witczak, M. W., & Mirza, M. W. (1999). Development of a revised predictive model for the dynamic (complex) modulus of asphalt mixtures. *Development of the 2002 Guide for the Design of New and Rehabilitated Pavement Structures, NCHRP*.

ASTM D7175. (2006). Standard Test Method for Determining the Rheological Properties of Asphalt Binder Using a Dynamic Shear Rheometer. Annual Books of ASTM Standard Vol. 4.03. West Conshohocken, PA, USA.

ASTM D7313-13. Standard test method for determining fracture energy of asphalt-aggregate mixtures using the disk-shaped compact tension geometry. ASTM International, 2013.

ASTM, D7906 "Standard Practice for Recovery of Asphalt from Solution Using Toluene and the Rotary Evaporator," 2014.

Anderson, D. A., Christensen, D. W., Bahia, H. U., Dongre, R., Sharma, M. G., Antle, C. E., & Button, J. (1994). Binder characterization and evaluation, volume 3: Physical characterization. *Strategic Highway Research Program, National Research Council, Report No. SHRP-A-369*.

Anderson, R. M., King, G. N., Hanson, D. I., & Blankenship, P. B. (2011). Evaluation of the relationship between asphalt binder properties and non-load related cracking. *Journal of the Association of Asphalt Paving Technologists*, *80*.

Apeagyei, A. K., Buttlar, W. G., & Reis, H. (2009). Assessment of low-temperature embrittlement of asphalt binders using an acoustic emission approach. *Insight-Non-Destructive Testing and Condition Monitoring*, *51*(3), 129-136.

ASTM, D7906 "Standard Practice for Recovery of Asphalt from Solution Using Toluene and the Rotary Evaporator," 2014.

Bahia, H. U., Teymourpour, P., Swiertz, D., Ling, C., Varma, R., Mandal, T. & Hanz, A. (2016). *Analysis and feasibility of asphalt pavement performance-based specifications for WisDOT* (No. 0092-15-04). Wisconsin Highway Research Program.

Bari, Javed, and Matthew Witczak. (2006). Development of a new revised version of the Witczak E* predictive model for hot mixture asphalt mixtures. *Journal of the Association of Asphalt Paving Technologists* Vol. 75.

Baumgaertel, M., & Winter, H. H. (1989). Determination of discrete relaxation and retardation time spectra from dynamic mechanical data. *Rheologica Acta*, *28*(6), 511-519.

Behnia, B., Dave, E., Ahmed, S., Buttlar, W., & Reis, H. (2011). Effects of recycled asphalt pavement amounts on low-temperature cracking performance of asphalt mixtures using acoustic emissions. *Transportation Research Record: Journal of the Transportation Research Board*, (2208), 64-71.

Bonnaure, F., Gest, G., Gravois, A., & Uge, P. (1977). New method of predicting the stiffness of asphalt paving mixtures. In *Association of Asphalt Paving Technologists Proc* (Vol. 46).

Booij, H. C., & Thoone, G. P. J. M. (1982). Generalization of Kramers-Kronig transforms and some approximations of relations between viscoelastic quantities. *Rheologica Acta*, *21*(1), 15-24.

Bozkurt, D., & Buttlar, W. G. (2002). Three-dimensional finite element modeling to evaluate benefits of interlayer stress absorbing composite for reflective crack mitigation. *Urbana*, *51*, 61801.

Braham, A., Buttlar, W., & Marasteanu, M. (2007). Effect of binder type, aggregate, and mixture composition on fracture energy of hot-mix asphalt in cold climates. *Transportation Research Record: Journal of the Transportation Research Board*, (2001), 102-109.

Chehab, G. R., Kim, Y. R., Schapery, R. A., Witczak, M. W., & Bonaquist, R. (2002). Time-temperature superposition principle for asphalt concrete with growing damage in tension state. *Journal of the Association of Asphalt Paving Technologists, 71*.

Christensen, D. W., & Anderson, D. A. (1992). Interpretation of dynamic mechanical test data for paving grade asphalt cements (with discussion). *Journal of the Association of Asphalt Paving Technologists, 61*.

Christensen Jr, D. W., Pellinen, T., & Bonaquist, R. F. (2003). Hirsch model for estimating the modulus of asphalt concrete. *Journal of the Association of Asphalt Paving Technologists*, *72*.

Christensen, Richard M. "Theory of viscoelasticity [M]," 1982: 158-239.

Clark, R. C. (1958). Practical results of asphalt hardening on pavement life. *Journal of the Association of Asphalt Paving Technologists*, *27*, 196-208.

Clendennen, C. R., & Romero, P. (2013). Evaluating the representative volume element of asphalt concrete mixture beams for testing in the bending beam rheometer. In *Multi-Scale modeling and characterization of infrastructure materials*(pp. 13-30). Springer, Dordrecht.

Daniel, J. S., & Kim, Y. R. (2002). Development of a simplified fatigue test and analysis procedure using a viscoelastic, continuum damage model (with discussion). *Journal of the Association of Asphalt Paving Technologists*, *71*.

Darabi, M. K., Al-Rub, R. K. A., Masad, E. A., Huang, C. W., & Little, D. N. (2011). A thermo-viscoelastic–viscoplastic–viscodamage constitutive model for asphaltic materials. *International Journal of Solids and Structures*, *48*(1), 191-207.

Dave, E. V., Behnia, B., Ahmed, S., Buttlar, W. G., & Reis, H. (2011a). Low temperature fracture evaluation of asphalt mixtures using mechanical testing and acoustic emissions techniques. *Journal of the Association of Asphalt Paving Technologists*, *80*.

Dave, E. V., Leon, S., & Park, K. (2011b). Thermal cracking prediction model and software for asphalt pavements. In *Transportation and Development Institute Congress 2011: Integrated Transportation and Development for a Better Tomorrow* (pp. 667-676).

Denby, E. F. (1975). A note on the interconversion of creep, relaxation and recovery. *Rheologica Acta*, *14*(7), 591-593.

Derewecki, K. E. (2013). *Applications of the 4 mm dynamic shear rheometer geometry for the forensic evaluation of bituminous materials*. Rutgers The State University of New Jersey-New Brunswick.

Doyle, P. C. (1958). Cracking characteristics of asphalt cement. *Proc of Assoc of Asphalt Paving Technologists*, *27*, 581-597.

Drescher, A., Kim, J. R., & Newcomb, D. E. (1993). Permanent deformation in asphalt concrete. *Journal of Materials in Civil Engineering*, *5*(1), 112-128.

Elseifi, M. A., Al-Qadi, I. L., & Yoo, P. J. (2006). Viscoelastic modeling and field validation of flexible pavements. *Journal of engineering mechanics*, *132*(2), 172-178.

Eslaminia, M., Thirunavukkarasu, S., Guddati, M. N., & Kim, Y. R. (2012). Accelerated pavement performance modeling using layered viscoelastic analysis. In *7th RILEM International Conference on Cracking in Pavements* (pp. 497-506). Springer, Dordrecht.

Farrar, M., Sui, C., Salmans, S., & Qin, Q. (2015). Determining the low temperature rheological properties of asphalt binder using a dynamic shear rheometer (DSR). Technical White Paper FP08 Prepared by Western Research Institute for the Federal Highway Administration. *Contract No. DTFH61-07-D-00005*.

Ferry, J. D., & Ferry, J. D. (1980). *Viscoelastic properties of polymers*. John Wiley & Sons.

Findley, W. N., Lai, J. S., & Onaran, K. Creep and Relaxation of Nonlinear Viscoelastic Materials. 1976.

Gardner, L. J., & Skok, E. L. (1967). Use of viscoelastic concepts to evaluate laboratory test results and field performance of some Minnesota asphalt mixtures. In *Intl Conf Struct Design Asphalt Pvmts*.

Gaw, W.J. (1981) Design Techniques to Minimize Low-Temperature Asphalt Pavement Transverse Cracking. Asphalt Institute. Research Report, No. 81-1.

Gibson, N. H. (2006). *A viscoelastoplastic continuum damage model for the compressive behavior of asphalt concrete* (Doctoral dissertation).

Glover, C. J., Davison, R. R., Domke, C. H., Ruan, Y., Juristyarini, P., Knorr, D. B., & Jung, S. H. (2005). Development of a new method for assessing asphalt binder durability with field validation. *Texas Dept Transport, 1872*.

Gordon, G. V., & Shaw, M. T. (1994). Computer Programs for Rheologists Hanser. *New York*.

Graziani, A., Di Benedetto, H., Perraton, D., Sauzéat, C., Hofko, B., Poulikakos, L. D., & Pouget, S. (2017). Recommendation of RILEM TC 237-SIB on complex Poisson's ratio characterization of bituminous mixtures. *Materials and Structures*, *50*(2), 142.

Haas, R., F. Meyer, G. Assaf, and H. Lee. (1987). A Comprehensive Study of Cold Climate Airport Pavement Cracking. *Journal of the Association of Asphalt Paving Technologists*, 56, pp 198-245.

Hardin, J. C. (1995). *Physical properties of asphalt cement binders* (Vol. 1241). ASTM International.

Heukelom, W., & Klomp, A. J. (1964). Road design and dynamic loading. In *Assoc Asphalt Paving Technol Proc*.

Johanneck, L., Geib, J., Van Deusen, D., Garrity, J., Hanson, C., & Dave, E. V. (2015). *DCT low temperature fracture testing pilot project* (No. MN/RC 2015-20).

Jung, D. H., & Vinson, T. S. (1994). *Low-temperature cracking: test selection* (No. SHRP-A-400).

Kaelble, D. H. (1985). *Computer aided design of polymers and composites* (Vol. 7). CRC Press.

Kallas, B. F. (1982). *Low-temperature mechanical properties of asphalt concrete* (No. RR-82-3).

Kandhal, P. S. (1977). Low-temperature ductility in relation to pavement performance. In *Low-Temperature Properties of Bituminous Materials and Compacted Bituminous Paving Mixtures*. ASTM International.

Kandhal, P. S., Foo, K. Y., & Mallick, R. B. (1988). *A critical review of VMA requirements in Superpave*. National Center for Asphalt Technology.

Kaseer, F., Yin, F., Arámbula-Mercado, E., & Epps Martin, A. (2017). Stiffness Characterization of Asphalt Mixtures with High Recycled Material Content and Recycling Agents. *Transportation Research Record: Journal of the Transportation Research Board*, (2633), 58-68.

King, G., Anderson, M., Hanson, D., & Blankenship, P. (2012). Using black space diagrams to predict age-induced cracking. In *7th RILEM international conference on cracking in pavements* (pp. 453-463). Springer, Dordrecht.

Lacroix, A. T. (2013). *Performance prediction of the NCAT test track pavements using mechanistic models*. North Carolina State University.

Lakes, R. S., & Vanderby, R. (1999). Interrelation of creep and relaxation: a modeling approach for ligaments. *Journal of biomechanical engineering*, *121*(6), 612-615.

Lakes, R. S., & Wineman, A. (2006). On Poisson's ratio in linearly viscoelastic solids. *Journal of Elasticity*, *85*(1), 45-63.

Lee, N. K., & Hesp, S. A. (1994). Low-temperature fracture toughness of polyethylene-modified asphalt binders. *Transportation Research Record*, (1436).

Li, X., & Marasteanu, M. (2004). Evaluation of the low temperature fracture resistance of asphalt mixtures using the semi circular bend test (with discussion). *Journal of the Association of Asphalt Paving Technologists*, *73*.

Li, X., Braham, A. F., Marasteanu, M. O., Buttlar, W. G., & Williams, R. C. (2008). Effect of factors affecting fracture energy of asphalt concrete at low temperature. *Road materials and pavement design*, *9*(sup1), 397-416.

Lu, H., Zhang, X., & Knauss, W. G. (1997). Uniaxial, shear, and Poisson relaxation and their conversion to bulk relaxation: studies on poly (methyl methacrylate). *Polymer Engineering & Science*, *37*(6), 1053-1064.

Lu, X., Uhlback, P., & Soenen, H. (2017). Investigation of bitumen low temperature properties using a dynamic shear rheometer with 4 mm parallel plates. *International Journal of Pavement Research and Technology*, *10*(1), 15-22.

Marasteanu, M. O., & Anderson, D. A. (1999). Improved Model for Bitumen Rheological Characterization, Eurobitume. Paper 133. In *Workshop on Performance Related Properties for Bituminous Binders, Luxembourg, Luxembourg*.

Marasteanu, M., Dai, S., Labuz, J., & Li, X. (2002). Determining the low-temperature fracture toughness of asphalt mixtures. *Transportation Research Record: Journal of the Transportation Research Board*, (1789), 191-199.

Marasteanu, M., Zofka, A., Turos, M., Li, X., Velasquez, R., Li, X., Buttlar, W., Paulino, G., Braham, A., Dave, E. and Ojo, J. (2007) Investigation of low temperature cracking in asphalt pavements national pooled fund study, Report No. 776.

Marasteanu, M., Buttlar, W., Bahia, H., Williams, C., Moon, K. H., Teshale, E. Z. & Ahmed, S. (2012). Investigation of low temperature cracking in asphalt pavements national pooled fund study–phase II.

McCarthy, L. M., Callans, J., & Scott, S. (2016). Performance specifications for asphalt mixtures. Synthe-sis topic 46-03. Washington, DC: *National Cooperative Highway Research Board*, National Research Council.

McLeod, J. M., Atkin, C. K., & Chaffee, S. H. (1972). Adolescents, parents, and television use: Self-report and other-report measures from the Wisconsin sample. *Television and social behavior*, *3*, 239-313.

Mensching, D. J., Rowe, G. M., Daniel, J. S., & Bennert, T. (2015). Exploring low-temperature performance in Black Space. *Road Materials and Pavement Design*, *16*(sup2), 230-253.

Mensching, D. J., Rowe, G. M., and Sias Daniel, J. A mixture-based Black Space parameter for low-temperature performance of hot mix asphalt. *Road Materials and Pavement Design*, 18, 2017, pp. 404-425.

Morrison, G. R., Lee, J. K., & Hesp, S. A. (1994). Chlorinated polyolefins for asphalt binder modification. *Journal of Applied Polymer Science*, *54*(2), 231-240.

Nemati, R., & Dave, E. V. (2018). Nominal property based predictive models for asphalt mixture complex modulus (dynamic modulus and phase angle). *Construction and Building Materials*, *158*, 308-319.

Olard, F., Di Benedetto, H., Eckmann, B., & Vaniscote, J. (2004). Failure behavior of bituminous binders and mixes at low temperatures. In *Proceedings of the 3rd Eurasphalt and Eurobitume Congress Hels Vienna, May 2004* (Vol. 2).

Oshone, M., Elshaer M, Dave E., Daniel J. (2017). Evolution of Asphalt Modulus from Falling Weight Deflectometer Tests and Challenges Associated with its Interpretation and Applications: A Case Study using LTPP Data. *The 10th International Conference on the Bearing Capacity of Roads, Railways and Airfields*.

Oshone, M., Dave, E., Daniel, J. S., & Rowe, G. M. (2017). Prediction of phase angles from dynamic modulus data and implications for cracking performance evaluation. *Road Materials and Pavement Design*, 1-23.

Oshone, M., Ghosh, D., Dave, E. V., Daniel, J. S., Voels, J. M., & Dai, S. (2018). *Effect of Mix Design Variables on Thermal Cracking Performance Parameters of Asphalt Mixtures* (No. 18-05397).

Park, S. W., & Kim, Y. R. (1999). Interconversion between relaxation modulus and creep compliance for viscoelastic solids. *Journal of materials in Civil Engineering*, *11*(1), 76-82.

Pavement Interactive. (2011). Rotational viscometer. *Pavement Interactive*.

Reinke, G., & Glidden, S. (2004). Development of mixture creep performance tests using a dynamic shear rheometer. *Performance Tests for Asphalt Mixes*, 1.

Romero, P., & Jones, Z. L. (2013). Implementation of low temperature tests for asphalt mixtures to improve the longevity of road surfaces. *Rep. MPC-13-260, North Dakota State Univ., Upper Great Plains Transportation Institute, Fargo, ND.*

Rowe, G., & Sharrock, M. (2001). Development of standard techniques for the calculation of master curves for linear-visco elastic materials. *Journal of Applied Asphalt Binder Technology*, *1*(1).

Rowe, G. M., & Pellinen, T. K. (2004). Consideration of elastic and viscous components of rheology relating to the permanent deformation of hot mix asphalt pavements. In *Recent Advances in Materials Characterization and Modeling of Pavement Systems* (pp. 65-82).

Rowe, G. (2009a). Phase angle determination and interrelationships within bituminous materials. In *Advanced Testing and Characterization of Bituminous Materials, Two Volume Set* (pp. 59-68). CRC Press.

Rowe, G., Baumgardner, G., & Sharrock, M. (2009b). Functional forms for master curve analysis of bituminous materials. In *Advanced testing and characterization of bituminous materials, two volume set* (pp. 97-108). CRC Press.

Rowe, G. M., King, G., & Anderson, M. (2014a). The influence of binder rheology on the cracking of asphalt mixes in airport and highway projects. *Journal of Testing and Evaluation*, *42*(5), 1063-1072.

Rowe, G. M. (2014b). Interrelationships in rheology for asphalt binder specifications. In *Proceedings of the Fifty-Ninth Annual Conference of the Canadian Technical Asphalt Association (CTAA): Winnipeg, Manitoba*.

Sabouri, M., & Kim, Y. (2014). Development of a failure criterion for asphalt mixtures under different modes of fatigue loading. *Transportation Research Record: Journal of the Transportation Research Board*, (2447), 117-125.

Sayegh, G. (1967). Determination of the viscoelastic properties of bituminous concrete by longitudinal vibrations. In *Conference of the British Rheology Society*.

Schapery, R. A. (1990). A theory of mechanical behavior of elastic media with growing damage and other changes in structure. *Journal of the Mechanics and Physics of Solids*, *38*(2), 215-253.

Schröter, K., Hutcheson, S. A., Shi, X., Mandanici, A., & McKenna, G. B. (2006). Dynamic shear modulus of glycerol: Corrections due to instrument compliance. *The Journal of chemical physics*, *125*(21), 214507.

Sui, C., Farrar, M., Tuminello, W., & Turner, T. (2010). New technique for measuring low-temperature properties of asphalt binders with small amounts of material. *Transportation Research Record: Journal of the Transportation Research Board*, (2179), 23-28.

Sui, C., Farrar, M., Harnsberger, P., Tuminello, W., & Turner, T. (2011). New low-temperature performance-grading method: Using 4-mm parallel plates on a dynamic shear rheometer. *Transportation Research Record: Journal of the Transportation Research Board*, (2207), 43-48.

Tarefder, R. A., & Rahman, A. S. M. (2016). Interconversion of Dynamic Modulus to Creep Compliance and Relaxation Modulus: Numerical Modeling and Laboratory Validation-Final Report.

Tayebali, A. A., Tsai, B. W., & Monismith, C. L. (1994). *Stiffness of asphalt-aggregate mixes* (No. SHRP-A-388). Washington DC: Strategic Highway Research Program, National Research Council.

Tschoegl, N. W., Knauss, W. G., & Emri, I. (2002). Poisson's ratio in linear viscoelasticity–a critical review. *Mechanics of Time-Dependent Materials*, *6*(1), 3-51.

Underwood, B. S., Kim, Y. R., & Guddati, M. N. (2010). Improved calculation method of damage parameter in viscoelastic continuum damage model. *International Journal of Pavement Engineering*, *11*(6), 459-476.

Underwood, B., Baek, C., & Kim, Y. (2012). Simplified viscoelastic continuum damage model as platform for asphalt concrete fatigue analysis. *Transportation Research Record: Journal of the Transportation Research Board*, (2296), 36-45.

Van der Poel, C. (1955). Time and temperature effects on the deformation of asphaltic bitumens and bitumen-mineral mixtures. *Society of Petroleum Engineers Journal*, *11*, 47-53.

Van Deusen, D., Johanneck, L., Geib, J., Garrity, J., Hanson, C., & Dave, E. V. (2015).DCT low temperaturefracture testing pilot project (report No. MN/RC 2015-20). St. Paul, MN: Minnesota Department ofTransportation, Research Services & Library.

Velasquez, L. M., Boellaard, R., Kollia, G., Hayes, W., Hoekstra, O. S., Lammertsma, A. A., & Galbraith, S. M. (2009). Repeatability of 18F-FDG PET in a multicenter phase I study of patients with advanced gastrointestinal malignancies. *Journal of Nuclear Medicine*, *50*(10), 1646-1654.

Wagoner, M., Buttlar, W., Paulino, G., & Blankenship, P. (2005a). Investigation of the fracture resistance of hot-mix asphalt concrete using a disk-shaped compact tension test. *Transportation Research Record: Journal of the Transportation Research Board*, (1929), 183-192.

Wagoner, M. P., Buttlar, W. G., & Paulino, G. H. (2005b). Development of a single-edge notched beam test for asphalt concrete mixtures. *Journal of Testing and Evaluation*, *33*(6), 452-460.

Wagoner, M.P., W.G. Buttlar, and G.H. Paulino, "Disk-Shaped Compact Tension Test for Asphalt Concrete Fracture," *Experimental Mechanics*, Vol. 45, pp. 270-277, 2005c.

Wang, Y. C., & Lakes, R. S. (2005). Composites with inclusions of negative bulk modulus: extreme damping and negative Poisson's ratio. *Journal of composite materials*, *39*(18), 1645-1657.

Yee, P., Aida, B., Hesp, S., Marks, P., & Tam, K. (2006). Analysis of premature low-temperature cracking in three Ontario, Canada, pavements. *Transportation Research Record: Journal of the Transportation Research Board*, (1962), 44-51.